

**Gas-Phase Chemistry of
Organotransition Metal Ions**

Thesis by

Karl K. Irikura

In Partial Fulfillment of the Requirements

for the Degree of

Doctor of Philosophy

California Institute of Technology

Pasadena, California

1991

(Submitted December 13, 1990)

(Slightly revised February 19, 1991)

TO MY FATHER

who did the hard part

Acknowledgments and Preface

Jack Beauchamp is my foremost intellectual creditor during my time at Caltech. I hope that his investment proves sound! Bill Goddard also provided me with guidance here, especially during the first year.

The most difficult time preceded the work of Chapter I. Seung Koo Shin and I were faced with a new FTICR and a lack of senior students who knew much about it. We spent a lot of time working together in those days and I am happy to acknowledge his help, both in experiments and theory, and especially his friendship.

This thesis really got started when Erich Uffelman told me about osmium tetroxide. I was interested, and he and Terry Collins sent me off with warnings and some compound. Erich kindly continued to check up on me until his untimely displacement to Carnegie-Mellon; everyone was sorry to see him and Louise leave. Eventually, after a long and painful gestation, Chapter I was finally delivered (to *JACS*, 1988, 110, 24).

It happened that Joel Blum, a graduate student in Geology, was working on rhenium-osmium dating techniques at about that time. He was amazed that some one else at Caltech was working with Os and gave us a seminar about the sophisticated REMPI scheme he was using to ionize Os selectively in the presence of Re. Jack suggested that it might be possible to separate the two based upon chemistry (rather than spectroscopy), leading eventually to Chapter II.

Edmund Fowles is the only real, preparative chemist who has been in the group during my stay. It has been a pleasure to work with him on the metal

oxides and, finally, on the Re-Os project of Chapter II. As a result, I learned many interesting techniques (and also some first-rate hiking and camping spots). It was his idea to examine Re_2O_7 that led to the chemistry of Re^+ and Chapter II (Irikura, Fowles, and Beauchamp, submitted).

All the poking around among the third-row transition metals led to the survey described in Chapter III (*JACS*, in press; *JPC*, submitted). The interpretation of much of the chemistry relies heavily upon the copious work from the research groups of Peter Armentrout and Ben Freiser.

The metalloporphyrins project of Chapter IV is largely a hybrid born of my interest in transition metal oxo ions and Jack's push toward the chemistry of biological molecules (*JACS*, in press). I am grateful to Prof. F. R. Longo (Drexel University) for his advice on the procedure for brewing porphine.

I had an urge to take some courses some time around my fourth year, and one of them was a new course in cosmochemistry taught by Wes Huntress and Geoff Blake. I had a good time in that course. The term paper topic that I picked from their list grew into Chapter V (almost the same as *Int. J. Mass Spec. Ion Proc.* 1990, 99, 213), so their contribution is basic. Geoff was particularly helpful and supportive of this work. I also thank Ewine van Dishoeck for her meticulous and lengthy comments on the manuscript, as well as for her delightful gypsy fiddling. Bruce Schilling's theoretical work provided some of the calculational methods. Jean-Marc Langlois wrote the program for the transition moment calculations for me; I am grateful for his extravagant helpfulness.

Chapter VI (to be submitted to *JACS*) appears somewhat misplaced in this thesis, but its evolution seemed natural at the time. I was interested in electronic excitation energies in regard to the study of the previous chapter, and

had noticed that calculations on the atomic transition metal ions sometimes gave poor excitation energies. It seemed possible that basis sets could be developed that were optimized for energy level differences, rather than total energies. (Although the resulting wavefunctions would of course have high total energies, total energy is not chemically relevant in most cases.) I wrote a program to optimize basis sets and wanted to test it on something simpler than transition metals. Since Seung Koo had been doing a lot of careful calculations of excitation energies in substituted carbenes, I decided to test the idea on the carbon atom and carbenes. For comparison, I checked the carbene singlet-triplet gaps obtained using the unmodified basis set for carbon. There were two surprises. First, the basis set modification worked, and gave more accurate energy gaps. Second, the unmodified basis set gave more *precise* energy gaps. The end result was that the modified basis sets ended up as a research proposition and the results with the unmodified basis were written up as a paper.

Many people who are not mentioned above helped me to get through Caltech, helping with the work, the relief from work, or even both. Among the Goddard group, Mark Brusich and Gilles Ohanessian were especially helpful. Bruce Schilling, actually in the Beauchamp group, showed me that the popular myth is wrong, and that it is indeed possible to do both good experiments and good theory.

Martin Schär and Mitchio Okumura both offered good advice when it came to getting experiments actually to work. Tom Dunn, Guy Duremberg, Ray Garcia, and especially Tony Stark contributed expertly and generously to the design and construction of essential pieces of equipment. Fran Bennett is tirelessly gracious in dealing with the many details associated with obtaining

necessary equipment and materials. Rick Hunter (of IonSpec) has been very generous with his time and help, especially in the initial FT-period.

Heonin Kang gave me my first ICR lesson, back before we went FT, and was always ready with helpful (if sleepy) advice. I shared many Chem 1 powwows with Bob Sweeney and also Erica Harvey, in those younger days when I was permitted a teaching assistantship. I certainly must acknowledge Gary Kruppa for his friendship and his dubious influence. Maggie Tolbert, Srihari Murthy, Catalina Fernandez, David Dearden, Mike Yamada, Roger Tang, Sherrie Walsh/Campbell/Walsh-Campbell, Elaine Marzluff, and Manuel Minas da Piedade all contributed irreparably to the important group ethos.

Music has been an important part of my life at Caltech. Delores Bing organized all the chamber music on campus and set me up with many groups. Her cheerful patience has always amazed me; she provided countless hours of critical listening as well as dealing with matters ranging from student feeding to pig-headed personalities. The Caltech-Occidental orchestra is managed and directed by Allen Gross; I am indebted to him for generous advice and in particular for providing the setting in which I met my wife Beth.

Julian Pranata and Paula Watnick were always ready for marathon sessions of good chamber music, for which I am grateful, although I am still sorry that they had the good taste to reject "The Noyes Quartet" as the name for our group. I am also indebted to Julian for his friendship and our many late-night discussions about science, music, and the world.

I appreciate the indulgence and attention of the members of my examining committee, which includes John Bercaw and Aron Kuppermann in addition to Jack and Bill. Fellowship support from the National Science Foundation and from the Department of Education is also acknowledged.

Finally, I owe the most to Beth for her love, support, patience, encouragement and coaxing during this peculiar time. I am deeply grateful for her companionship in my life.

Abstract

The gas-phase chemistry of many transition metal ions has been investigated by Fourier transform ion cyclotron resonance spectrometry (FTICR). Emphasis is on organometallic chemistry, including an application to geochronology, but inorganic and bio-inorganic systems have also been investigated. Quantum chemical calculations have been performed to address problems in interstellar chemistry and also traditional physical organic chemistry.

Chapter I is concerned with the chemistry of ions OsO_n^+ ($n = 0-4$) with several small molecules, including methane. A wide variety of reactions are observed, including many that are archetypes for fundamental mechanistic processes in organometallic chemistry. In Chapter II, the differences in the gas-phase chemistry of Os^+ and Re^+ are applied to analytical problems associated with the ^{187}Re - ^{187}Os dating method, which is important in geology.

Chapter III is a survey of the reactivity of third-row transition metal ions, with emphasis on the unusual reactions involving methane. Fundamental concepts that have proven useful in the interpretation of chemistry in the first and second transition series are also applicable in the third row.

Chapter IV describes the gas-phase synthesis of positive and negative metalloporphyrin ions by reactions of metal-containing ions with porphine vapor. Chapter V presents some possibilities for transition metal catalysis in interstellar clouds. A very low value is calculated for the rate of radiative association of Fe^+ and hydrogen atoms, suggesting that transition metal chemistry is not important in these systems.

Chapter VI involves scaling the results of *ab initio* calculations in order to predict accurate singlet-triplet energy gaps in many substituted carbenes.

Observed trends are rationalized using a synergistic bonding model. A simple relationship based upon electronegativity is presented to permit carbene singlet-triplet gaps to be computed using minimal resources, such as a hand calculator.

Chapter VII deals with five different experimental issues that have arisen during FTICR studies of reactive transition metal ions. Difficulties, helpful techniques, and data analysis are discussed.

x
Contents

Dedication.....	ii
Acknowledgments and Preface.....	iii
Abstract	viii
List of Tables	xi
List of Figures.....	xii
Chapter I. Osmium Tetroxide and Its Fragment Ions in the Gas Phase: Reactivity with Hydrocarbons and Small Molecules	1
Chapter II. Post-Ionization Chemical Separation: Application to ^{187}Re - ^{187}Os Dating	13
Chapter III. Third-Row Transition Metal Ions in the Gas Phase: Reactivity with Methane.....	21
Chapter IV. Gas-Phase Synthesis of Metalloporphyrin Ions	55
Chapter V. Prospects for the Involvement of Transition Metals in the Chemistry of Diffuse Interstellar Clouds: Formation of FeH^+ by Radiative Association	66
Chapter VI. Singlet-Triplet Gaps in Substituted Carbenes CXY ($\text{X}, \text{Y} = \text{H}, \text{F}, \text{Cl}, \text{Br}, \text{I}, \text{SiH}_3$)	84
Chapter VII. Some Experimental Considerations for Fourier-Transform Ion Cyclotron Resonance Spectrometry.....	104
Appendix. Energy Levels of Transition Metals: Atoms and Atomic Ions.....	122

List of Tables

Chapter I.	Summary of Thermochemical Limits	3
	Measured Rates and Efficiencies	3
	Self-Reactions in Osmium Tetroxide	4
	Proton-Transfer Reactions.....	8
	Primary Thermochemical Values.....	8
	Derived Bond Energies and Heats of Formation	9
Chapter III.	Electron Configurations and Reactivity with Methane of	
	Third-Row M^+	26
	Rates of Dehydrogenation of Methane	27
	Rates of Reactions Not Involving Methane	28
	Ligand Binding Energies Required	45
	Transition Metal Bond Strengths	
	$D(M^+-CH_2)$, $D(M^+-H)$, and $D(M^+-O)$	50
Chapter IV.	Metal-Porphine Ions Generated	62
	Oxygen Atom Affinities	65
Chapter V.	Selected Relative Abundances in a Typical Diffuse Cloud	70
Chapter VI.	Optimized Bond Angles and Predicted	
	Singlet-Triplet Gaps in CXY	90
	Orbital Ionization Energies in Carbon.....	94
	Charges on Carbon and Degree of π -donation in CXY.....	95
Appendix.	Selected Energy Levels of Neutral and Ionic Transition	
	Metal Atoms.....	124
	<i>Ab Initio</i> Energy Levels of Ta, Ta^+ , and Ta^{2+}	143
	<i>Ab Initio</i> Orbital Sizes $\langle r^2 \rangle^{1/2}$ of Ta, Ta^+ , and Ta^{2+}	143

List of Figures

Chapter I.	Degenerate reaction between $^{190}\text{OsO}_3^+$ and OsO_4	4
	Mass spectrum of OsO_4 ; terminal ions	5
	Primary and secondary reactions of OsO_3^+ with H_2	5
	Sequential double bond metathesis of $^{192}\text{OsO}_2^+$ with NH_3	6
	Osmium silicide formation from $^{192}\text{Os}^+$ and SiH_4	7
	Kinetic efficiency of proton transfer from OsO_4H^+	8
	Proposed transition states for reduction with CO and SO_2	9
Chapter II.	Re^+ and Os^+ after 100 ms in a mixture of CH_4 and H_2	16
Chapter III.	Reaction of $^{186}\text{W}^+$ with CH_4	24
	Reaction of Ta^+ with CH_4 , with CD_4 , and with a mixture	30
	Collision-induced dissociation of $^{186}\text{WC}_4\text{H}_8^+$ generated from methane and from cyclopentanone	32
	Reaction of $^{193}\text{Ir}^+$ with methane: kinetic models	36
	Bond strengths $D(\text{M}^+-\text{CH}_2)$ and $D(\text{M}^+-\text{H})$	41
	Energetics of metal-oxo and metal-methylene bonds	51
Chapter IV.	Primary and secondary reactions of Fe^+ with porphine	58
	Formation of $\text{Ni}(\text{P})^-$ from $\text{Ni}(\text{CO})_4$ and porphine	61
Chapter V.	Calculated potential energy curves for FeH^+	74
	Calculated electric dipole moment functions for FeH^+	76
	State contributions to the rate of radiative association of Fe^+ and H	79
Chapter VI.	Directly calculated singlet-triplet gaps vs. accurate values	91
	Predicted energy gaps vs. charge on the carbenic carbon	96
	Predicted energy gaps vs. calculated bond angles	100
	Predicted energy gaps vs. π -donation to the central carbon ...	101

Chapter VII. Reaction of Ir^+ with CD_4 with and without the ion pump	106
FeO_n^- , $n = 0-3$, generated by laser ablation of Fe_2O_3	110
Ir_2O_n^+ ($n = 0-4$) and Ir_3O_n^+ ($n = 0-2$) from laser ablation of IrO_2	111
Os^+ isolated in CH_4 with and without z-axis rf ejection.....	114
Tuning curve for chirp excitation of $\text{Ni}(\text{CO})_3^-$	116
Tuning curve for impulse excitation of $\text{Ni}(\text{CO})_3^-$	118
Tuning curve for shaped excitation ($2\pi RC = 800$ kHz) of $\text{Ni}(\text{CO})_3^-$ and $\text{Ni}_2(\text{CO})_6^-$	119

Chapter I

Osmium Tetroxide and Its Fragment Ions in the Gas Phase: Reactivity with Hydrocarbons and Small Molecules

Karl K. Irikura and J. L. Beauchamp

*Contribution No. 7797 from the
Arthur Amos Noyes Laboratory of Chemical Physics,
California Institute of Technology, Pasadena, California 91125*

Reprinted from the Journal of the American Chemical Society, 1989, 111, 75.
Copyright © 1989 by the American Chemical Society and reprinted by permission of the copyright owner.

Osmium Tetroxide and Its Fragment Ions in the Gas Phase: Reactivity with Hydrocarbons and Small Molecules

Karl K. Irikura and J. L. Beauchamp*

Contribution No. 7797 from the Arthur Amos Noyes Laboratory of Chemical Physics, California Institute of Technology, Pasadena, California 91125. Received June 13, 1988

Abstract: Gas-phase ion-molecule reactions of OsO_n^+ ($n = 0-4$) with a number of hydrocarbons and small molecules, including CH_4 , C_2H_4 , C_2H_6 , C_3H_8 , C_4H_{10} , H_2 , CO , NH_3 , and SiH_4 , have been investigated by Fourier transform ion cyclotron resonance spectrometry. Anion chemistry was briefly investigated. Thermochemical quantities derived include $D(\text{Os}^+-\text{O}) = 100 \pm 12$, $D(\text{OsO}^+-\text{O}) = 105 \pm 12$, $D(\text{OsO}_2^+-\text{O}) = 105 \pm 12$, $D(\text{OsO}_3^+-\text{O}) = 71 \pm 12$, $D(\text{OsO}_3-\text{O}) = 78 \pm 14$, $D(\text{OsO}_4^+-\text{H}) = 132 \pm 3$ kcal/mol, $D(\text{OsO}_3^+-\text{OH}) = 101 \pm 16$ kcal/mol, and $\text{PA}(\text{OsO}_4) = 161 \pm 2$ kcal/mol. Many diverse and novel reactions are observed. Among them are $[2, + 2]$ cycloaddition with H_2 , bond metathesis, oxo transfer, and hydrogen atom abstraction. These ions are also extraordinarily active dehydrogenation reagents; the most dramatic example is the sequential, complete dehydrogenation of SiH_4 to mono-, di-, and trisilicides. Another intriguing process is the double bond metathesis with NH_3 , in which one or two oxo ligands are exchanged for imido groups. The number of oxo ligands is found to have a striking effect on the chemistry; mechanisms are discussed for the reactions observed. For example, the relative inertness of OsO_3^+ is attributed to a failure of the $\text{Os}(+7)$ center to undergo oxidative addition. OsO_2^+ emerges as a potential model catalyst for the conversion of methane and dioxygen to aldehydes.

Gas-phase transition-metal ions have been the focus of much attention in recent years, with the library of reactions and the thermochemical base growing rapidly. The bulk of the early work emphasized the chemistry of naked, unligated metal ions. Although progress is being made in the investigation of ligand effects on reactivity, including some systematic studies by Freiser and co-workers,¹ much remains to be done in order to provide enough specific information for useful generalizations to be drawn.

Previous work on gas-phase transition-metal oxide ions includes studies of FeO^+ and CrO^+ , among others. In early work, Kappes and Staley² determined that the relatively weak bond in FeO^+ permitted this species to catalyze the oxidation of small organic molecules by N_2O . Jackson et al.³ subsequently found the oxo ligand to increase the reactivity of Fe^+ as well as appearing to favor C-H over C-C insertion in alkanes. The enhanced reactivity is ascribed to the exothermicity of H_2O elimination. In addition to chemistry typical of unligated metal ions, FeO^+ was found to react with hydrocarbons by radical loss processes. Neither FeO^+ nor Fe^+ , however, is reactive with methane. In ion beam studies,⁴ CrO^+ was found to react readily with hydrocarbons, while Cr^+ is unreactive. For example, CrO^+ oxidizes ethylene to acetaldehyde^{4a} and ethane to ethanol.^{4b} In another investigation,⁵ MnO^+ has been observed to react with ethylene to yield both $\text{C}_2\text{H}_4\text{O}$ and MnCH_2^+ , the double bond metathesis products. This metathesis has also been identified as the minor channel in the

reaction of ethylene with ClCrO_2^+ .⁶ The major products in this case correspond to oxygen transfer.

Despite the number of cases in which an oxo ligand increases reactivity, it is hazardous to generalize too freely. In the case of VO^+ , reactivity is reduced relative to unligated V^+ .⁷ Since the V^+-O bond is very strong, it is not cleaved during reactions, and the oxygen is thought to have little effect other than to occupy a coordination site on the metal.

Aside from the basic interest in ligand effects, motivation for studying the oxo ligand comes partly from condensed phase studies of metal oxides. In particular, hydrocarbon oxidation is a field of great scope and economic volume. A corresponding amount of effort and ingenuity has been directed to this area of research, and transformations mediated by metals and their oxides are increasingly prominent.⁸ From an economic viewpoint, methane is a uniquely attractive target for controlled oxidation; its high abundance and low cost make it an ideal feedstock. For example, direct conversion to methanol would permit natural gas to be transported in a convenient and inexpensive liquid form.⁹ Unfortunately, this particular process has not yet materialized on a commercial scale. There is also heavy demand for other potential products of direct methane oxidation, such as formaldehyde.¹⁰

For the present study, we have chosen to compare reactivity among the series of oxo ions derived from OsO_4 . This compound

(1) E. g., Jackson, T. C.; Carlin, T. J.; Freiser, B. S. *Int. J. Mass Spec. Ion Proc.* **1986**, *72*, 169. Jacobson, D. B.; Freiser, B. S. *J. Am. Chem. Soc.* **1985**, *107*, 4373.

(2) (a) Kappes, M. M.; Staley, R. H. *J. Am. Chem. Soc.* **1981**, *103*, 1286.

(b) Kappes, M. M.; Staley, R. H. *J. Phys. Chem.* **1981**, *85*, 942.

(3) Jackson, T. C.; Jacobson, D. B.; Freiser, B. S. *J. Am. Chem. Soc.* **1984**, *106*, 1252.

(4) (a) Kang, H.; Beauchamp, J. L. *J. Am. Chem. Soc.* **1986**, *108*, 5663.

(b) Kang, H.; Beauchamp, J. L. *J. Am. Chem. Soc.* **1986**, *108*, 7502.

(5) Stevens, A. E.; Beauchamp, J. L. *J. Am. Chem. Soc.* **1979**, *101*, 6449.

(6) Walba, D. M.; DePuy, C. H.; Grabowski, J. J.; Bierbaum, V. M. *Organometallics* **1984**, *3*, 498.

(7) Jackson, T. C.; Carlin, T. J.; Freiser, B. S. *J. Am. Chem. Soc.* **1986**, *108*, 1120.

(8) Sheldon, R. A.; Kochi, J. K. *Metal-Catalyzed Oxidations of Organic Compounds*; Academic: New York, 1981.

(9) (a) Foster, N. R. *Appl. Catal.* **1985**, *19*, 1. (b) Gesser, H. D.; Hunter, N. R.; Prakash, C. B. *Chem. Rev.* **1985**, *85*, 235. (c) Zhen, K. J.; Khan, M. M.; Mak, C. H.; Lewis, K. B.; Somorjai, G. A. *J. Catal.* **1985**, *94*, 501.

(10) (a) Spencer, N. D. *J. Catal.* **1988**, *109*, 187. (b) Otsuka, K.; Hatano, M. *J. Catal.* **1987**, *108*, 252.

Table I. Summary of Thermochemical Limits

bond	limit ^a	reaction	bond	limit ^a	reaction
Os ⁺ -NH	92 ± 2.5	15	OsC ₃ H ₄ ⁺ -C ₃ H ₄	69	42
OsO ⁺ -NH	92 ± 2.5	16a	Os ⁺ -C ₄ H ₆	56	43b
OsNH ⁺ -NH	92 ± 2.5	19	OsO ⁺ -C ₄ H ₆	56	44b
Os ⁺ -CH ₂	110 ± 1	21	Os ⁺ -C ₄ H ₄	109 ± 1	43a
OsO ⁺ -CH ₂	110 ± 1	22	OsO ⁺ -C ₄ H ₄	109 ± 1	44a
OsCH ₂ ⁺ -CH ₂	110 ± 1	25	OsO ⁺ -SiC	179 ± 8	62
OsOCH ₂ ⁺ -CH ₂	110 ± 1	26a	Os ⁺ -SiH ₂	61 ± 4	50b
OsOC ₂ H ₄ ⁺ -CH ₂	110 ± 1	30	OsOSi ⁺ -O	78 ± 14	60
OsOCH ₂ ⁺ -O	78 ± 14	27	OsO ₂ Si ⁺ -O	78 ± 14	69
OsOC ₂ H ₄ ⁺ -O	78 ± 14	29	Os ⁺ -Si	99.5 ± 2	50a
Os ⁺ -C ₃ H ₄	48	21, 25	OsO ⁺ -Si	99.5 ± 2	51a
OsO ⁺ -C ₃ H ₄	48	22, 26a	OsO ₂ ⁺ -Si	99.5 ± 2	52
OsOCH ₂ ⁺ -C ₂ H ₄	48	26a, 30	OsSi ⁺ -Si	99.5 ± 2	54
OsO ⁺ -C ₃ H ₆	58	22, 26a, 30	OsSi ₂ ⁺ -Si	99.5 ± 2	55
OsO ₂ ⁺ -H ₂	42	47	OsOSi ⁺ -Si	99.5 ± 2	56
Os ⁺ -C ₂ H ₂	74	32b	OsOSi ₂ ⁺ -Si	99.5 ± 2	57
OsO ⁺ -C ₂ H ₂	74	33b	OsO ₂ Si ⁺ -Si	99.5 ± 2	59
OsC ₂ H ₂ ⁺ -O	78 ± 14	49	OsO ₂ Si ₂ ⁺ -Si	99.5 ± 2	60
Os ⁺ -C ₃ H ₄	69	37a	OsO ₂ -O	105 ± 12	b
OsO ⁺ -C ₃ H ₄	69	38a			

^a Lower limit in kcal/mol. ^b Inferred from lack of OsO₂⁺ product from Os⁺ + OsO₄; see Discussion.

is of interest for its common use as an oxidizing agent in solution, usually for the *cis* vicinal dihydroxylation of olefins.¹¹ It is also well-suited for gas-phase studies; it is volatile, and electron impact gives rise to a complete series of oxo ions, OsO_{*n*}⁺ (*n* = 0–4). This represents the first study of the effects of successive oxo ligation on the reactivity of transition-metal ions with hydrocarbons and other small molecules.

Experimental Section

Reactions were investigated with Fourier transform ion cyclotron resonance spectrometry (FT-ICR), of which a number of reviews are available.¹² The 1-in., cubic, trapped-ion cell was built by Bio-Med Tech¹³ and driven with an IonSpec data system. Software was extensively modified for use in our laboratory. A Varian 15-in. electromagnet supplied the magnetic field, typically 2.0 Tesla. Pressures were generally in the range 10⁻⁸–10⁻⁶ Torr and were measured with a Schulz-Phelps ion gauge calibrated against a Baratron 390 HA-0001 capacitance manometer. Uncertainties in the absolute pressure are considered to limit rate constants to an accuracy of ca. 20%. Neutral compounds were obtained commercially and purified by freeze-pump-thaw cycling. Ionization was by electron impact, typically at a nominal energy of 50 eV. It is possible that electronically and vibrationally excited ions are produced by this method. Such excited ions may be manifested by upwardly curving kinetic plots.

Unwanted ions were ejected from the cell with the standard fixed-frequency and chirped double resonance pulses, in addition to gated rf excitation applied to the trapping well.¹⁴ In ambiguous cases, reaction sequences were confirmed with standard double resonance techniques, in which suppression of the daughter ion is sought by ejection of the supposed parent. In addition, isotopically labeled ions were generally employed, for increased confidence in peak assignment and precursor identification. The most abundant isotope, ¹⁹²Os, was used in most cases. Isotopically labeled ions, prepared by selective ejection, were also used to study degenerate reactions. Ion ejections cause translational heating of remaining ions at nearby masses.¹⁵ In order to determine if such translational heating would interfere unduly with kinetics measurements, some control reactions were studied in the pure OsO₄ system. Apparent rates of oxo transfer (vide infra) were measured with both unlabeled OsO_{*n*}⁺ and isolated ¹⁹²OsO_{*n*}⁺. Translational heating would be expected to be more problematic in the isotopic case, since other isotopomers must be ejected at nearby masses. No significant differences were found, however, suggesting that translational heating is not a problem, at least in these particular reactions.

Proton affinity bracketing experiments were done by following the reactions of OsO₄H⁺ with reference bases B and also the reverse reactions of OsO₄ with protonated reference bases BH⁺. Methane was used as the chemical ionization reagent for formation of BH⁺ and OsO₄H⁺ and was

Table II. Measured Rates and Efficiencies

reaction(s)	k ^a	k/k _{ADO} ^b
OsO ⁺ + H ₂ → Os ⁺ + H ₂ O	7 × 10 ⁻¹²	0.005
OsO ₂ ⁺ + H ₂ → OsO ⁺ + H ₂ O	3 × 10 ⁻¹⁰	0.2
OsO ₃ ⁺ + H ₂ → OsO ₂ ⁺ + H ₂ O	1 × 10 ⁻¹²	0.0007
OsO ₄ ⁺ + H ₂ → OsO ₄ H ⁺ + H	3 × 10 ⁻¹⁰	0.2
OsO ₄ ⁺ + HD → OsO ₄ (H,D) ⁺ + (H,D)	1 × 10 ⁻¹⁰	0.08
OsO ₄ ⁺ + D ₂ → OsO ₄ D ⁺ + D	6 × 10 ⁻¹¹	0.06
OsO ⁺ + CO → Os ⁺ + CO ₂	6 × 10 ⁻¹³	0.0009
OsO ₂ ⁺ + CO → OsO ⁺ + CO ₂	2 × 10 ⁻¹¹	0.03
OsO ₃ ⁺ + CO → OsO ₂ ⁺ + CO ₂	9 × 10 ⁻¹²	0.01
OsO ₄ ⁺ + CO → OsO ₃ ⁺ + CO ₂	1 × 10 ⁻¹⁰	0.2
OsO ₄ ⁺ + SO ₂ → OsO ₃ ⁺ + SO ₃	6 × 10 ⁻¹⁰	0.6
Os ⁺ + CH ₂ O (9)	2 × 10 ⁻¹⁰	0.1
OsO ⁺ + CH ₂ O (10)	2 × 10 ⁻¹⁰	0.1
OsO ₂ ⁺ + CH ₂ O (11)	1 × 10 ⁻¹⁰	0.07
OsO ₃ ⁺ + CH ₂ O (12)	2 × 10 ⁻¹⁰	0.1
OsO ₄ ⁺ + CH ₂ O (13)	4 × 10 ⁻¹⁰	0.2
Os ⁺ + NH ₃ → OsNH ⁺ + H ₂	2 × 10 ⁻¹⁰	0.1
OsO ⁺ + NH ₃ (16)	4 × 10 ⁻¹⁰	0.3
OsO ₂ ⁺ + NH ₃ → OsONH ⁺ + H ₂ O	5 × 10 ⁻¹⁰	0.3
OsO ₃ ⁺ + NH ₃ → OsO ₃ H ⁺ + NH ₂	6 × 10 ⁻¹⁰	0.3
Os ⁺ + CH ₄ → OsCH ₂ ⁺ + H ₂	3 × 10 ⁻¹⁰	0.3
OsO ⁺ + CH ₄ → OsOCH ₂ ⁺ + H ₂	6 × 10 ⁻¹⁰	0.6
OsO ₂ ⁺ + CH ₄ → OsOCH ₂ ⁺ + H ₂ O	5 × 10 ⁻¹⁰	0.5
OsOCH ₂ ⁺ + CH ₄ → OsOC ₂ H ₄ ⁺ + H ₂	2 × 10 ⁻¹⁰	0.2
OsO ₄ ⁺ + CH ₄ → OsO ₄ H ⁺ + CH ₃	6 × 10 ⁻¹⁰	0.7
OsO ₄ ⁺ + CH ₂ D ₂ → OsO ₄ (H,D) ⁺ + CHD(H,D)	4 × 10 ⁻¹⁰	0.4
OsO ₄ ⁺ + CD ₄ → OsO ₄ D ⁺ + CD ₃	2 × 10 ⁻¹⁰	0.2

^a Rate constant in cm³ s⁻¹. ^b Reaction efficiency; see ref 23.

present during the subsequent reactions. Low-mass ions due to methane were ejected from the cell with rf excitation of their trapping well motion.

The extreme reactivity of neutral OsO₄ caused some problems due to apparent degradation of organic residues (such as vacuum grease), as has been reported by other workers.¹⁶ Apparent products include H₂O, CO₂, and CO. Water was the most problematic contaminant, interfering with proton affinity measurements, but was conveniently controlled by packing the OsO₄ finger with Linde 4A molecular sieves. No effective methods for reducing CO or CO₂ contamination were found, and these gases were always present in variable amounts. As a result, the pressure of OsO₄ could not be measured accurately, and absolute rates of ion-molecule reactions involving neutral OsO₄ could not be determined with confidence.

Rate constants were generally determined in a straightforward manner, from the slope of a semilog plot of the decay of reactant over time and from the pressure of the neutral reactant. In the case of degenerate reactions of isotopically labeled ions, the treatment was equivalent to a semilog plot of the approach to equilibrium. The slope of such a plot

(11) Schröder, M. *Chem. Rev.* **1980**, *80*, 187.

(12) (a) Marshall, A. G. *Acc. Chem. Res.* **1985**, *18*, 316. (b) Comisarow, M. B. *Anal. Chim. Acta* **1985**, *178*, 1.

(13) Bio-Med Tech, 2001 E. Galbreth, Pasadena, CA 91104.

(14) Beauchamp, J. L.; Armstrong, J. T. *Rev. Sci. Instrum.* **1969**, *40*, 123

(15) Buttrill, S. E. *J. Chem. Phys.* **1969**, *50*, 4125.

(16) Evans, S.; Hamnett, A.; Orchard, A. F. *J. Am. Chem. Soc.* **1974**, *96*, 6221.

Table III. Self-Reactions in Osmium Tetroxide

reaction	relative rate ^a
$\text{Os}^+ + \text{OsO}_4 \rightarrow \text{OsO}^+ + \text{OsO}_3$	1.0
$\text{OsO}^+ + \text{OsO}_4 \rightarrow \text{OsO}_2^+ + \text{OsO}_3$	1.3
$\text{OsO}_2^+ + \text{OsO}_4 \rightarrow \text{OsO}_3^+ + \text{OsO}_3$	1.1
$^*\text{OsO}_3^+ + \text{OsO}_4 \rightarrow \text{OsO}_3^+ + ^*\text{OsO}_4$	0.6
$^*\text{OsO}_4^+ + \text{OsO}_4 \rightarrow \text{OsO}_4^+ + ^*\text{OsO}_4$	0.8
$^*\text{OsO}_3^- + \text{OsO}_4 \rightarrow \text{OsO}_3^- + ^*\text{OsO}_4$	0.2
$^*\text{OsO}_4^- + \text{OsO}_4 \rightarrow \text{OsO}_4^- + ^*\text{OsO}_4$	0.4
$\text{OsO}_3^- + \text{OsO}_4 \rightarrow \text{OsO}_4^- + \text{OsO}_3$	<0.1 ^b

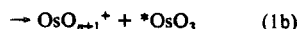
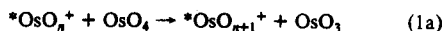
^aA relative rate of 1.0 corresponds approximately to $1 \times 10^{-9} \text{ cm}^3 \text{ s}^{-1}$. ^bUpward curvature of the kinetic plot prevents accurate rate determination and indicates the presence of translationally or internally excited OsO_3^- .

yields the desired pseudo-first-order rate constant (involving the total pressure of neutral reactant).

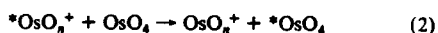
Results

A number of thermochemical limits and rate constants were determined for the reactions observed. These are summarized in Tables I and II, respectively. Minor products have been ignored when calculating product distributions. Auxiliary thermochemical data are from references 17 and 18 unless otherwise noted.

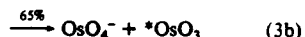
Reactions with OsO_4 . The OsO_4 system exhibits somewhat limited reactions, with formal O-atom transfer dominating. The reactions noted, and their relative rates, are listed in Table III. OsO_4^- and OsO_3^- are the only anions formed in measurable yield by electron impact (from ca. 1.5 to 70 eV). Collision-induced dissociation (CID) of these anions was unsuccessful. Among the cations, the general reaction is given by eq 1, where the asterisk



denotes isotopically labeled Os and $n = 0-2$. These reactions imply that $D(\text{OsO}_3-\text{O}) < D(\text{OsO}_n^+-\text{O})$. It should be noted that product ions containing both labeled and unlabeled osmium are obtained. The branching ratios between paths (1a) and (1b) are 55:45 ($n = 0$), 40:60 ($n = 1$), and 25:75 ($n = 2$). The values for the various branching ratios in this work are only approximate. For $n = 3-4$, only the degenerate reaction 2 is observed. Figure 1 illustrates the course and method of analysis of these reactions. Double resonance experiments indicated that this reaction does not occur for $n = 2$.



Reactions of the negative ions are relatively slow. Both electron transfer and formal O^+ transfer are observed. In reaction 3, the



extra electron may reside on either of the separating product fragments. This suggests that the two sets of products (3a and 3b) are of approximately equal energy and that the corresponding electron affinities are about the same, $EA(\text{OsO}_3) \approx EA(\text{OsO}_4)$.

No clustering was observed for either positive or negative ions. At long delay times (seconds), the terminal ion among the positive ions is OsO_3^+ (see Figure 2). Formation of this species from the lower oxo ions is by O-atom abstraction, as described above, and formation from OsO_4^+ is presumably by reaction with the CO impurity that was always present. The reaction with CO is discussed below.

(17) Cox, J. D.; Pilcher, G. *Thermochemistry of Organic and Organometallic Compounds*; Academic: London, 1970.

(18) Stull, D. R.; Prophet, H. *JANAF Thermochemical Tables*, 2nd ed. National Standard Reference Data Series, National Bureau of Standards (U.S.) 37; U.S. Government Printing Office: Washington, DC, 1971

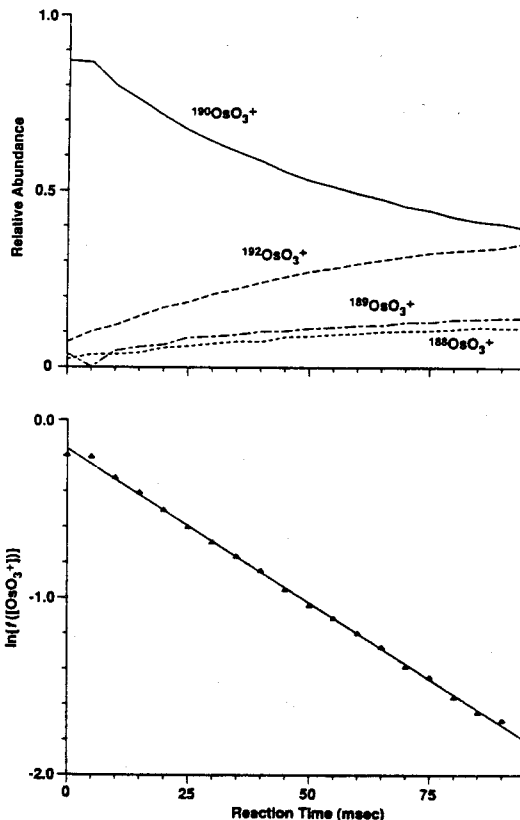
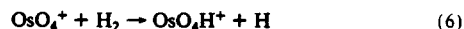
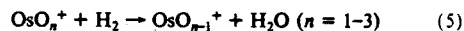


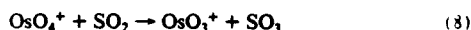
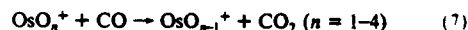
Figure 1. Degenerate reaction between $^{190}\text{OsO}_3^+$ (isolated) and OsO_4 ; formal O⁻ transfer, eq 2, $n = 3$. Top: Relative abundances of isotopomers of OsO_3^+ . Bottom: Pseudo-first-order plot of concentration vs time; solid line is least-squares fit. The function $f([\text{OsO}_3^+]) = [^{190}\text{OsO}_3^+] - 0.375([^{192}\text{OsO}_3^+] + [^{189}\text{OsO}_3^+] + [^{188}\text{OsO}_3^+])$ is plotted to correct for the reverse reaction. The lack of curvature suggests that translational heating is not important.

Reactions with Hydrogen. Although Os^+ and the anions (OsO_3^- and OsO_4^-) are unreactive with H_2 on the ICR time scale, the cations OsO_n^+ ($n = 1-4$) react as shown in eq 5 and 6. The



sequential reactions 5 are displayed in Figure 3; relative rates are also generally indicated by the extent of the reactions. OsO_4H^+ is unreactive with H_2 . If we assume that observed reactions are exothermic, then occurrence of these reactions leads us to infer that $D(\text{OsO}_{n-1}^+-\text{O}) < 117.4 \text{ kcal/mol}$ ($n = 1-3$) and that $D(\text{OsO}_4^+-\text{H}) > 104.2 \text{ kcal/mol}$. To ascertain that impurities were not responsible for OsO_4H^+ formation, the experiment was repeated with D_2 . OsO_4D^+ was formed, confirming the reaction as shown. Further confirmation comes from the observation that $^{192}\text{OsO}_4^+$ yields only $^{192}\text{OsO}_4\text{H}^+$ product, subject to uncertainties due to degenerate electron- and proton-transfer reactions. Reaction of OsO_4^+ with HD gives a roughly 2:1 ratio of OsO_4H^+ to OsO_4D^+ . Table II includes the rates and efficiencies of reactions 5 and 6.

Reactions with CO and SO_2 . The reactions of OsO_n^+ ($n = 1-4$) with CO and of OsO_4^+ with SO_2 proceed as shown in eq 7 and 8. Os^+ and OsO_4H^+ are unreactive with CO. Rates and effi-



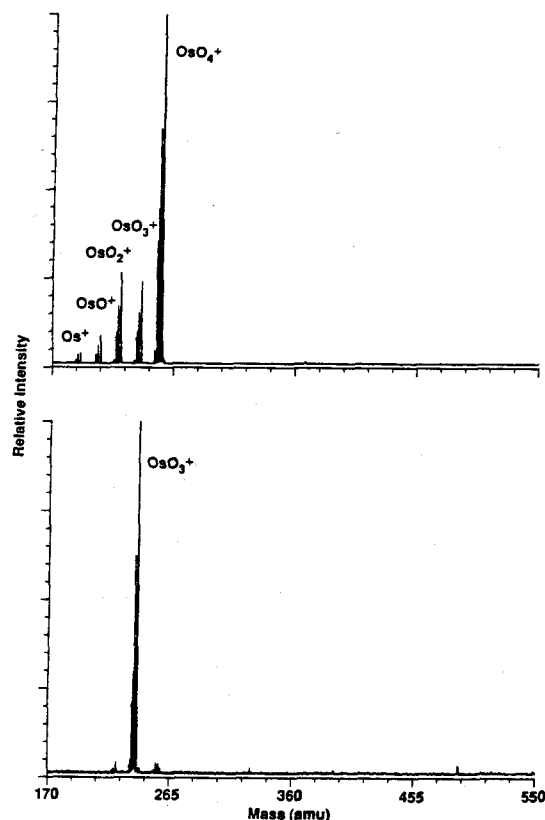


Figure 2. Top: Mass spectrum of OsO_4 under 50-eV electron impact. Bottom: After extensive reaction with neutral OsO_4 , no clustering is observed. The terminal ion is OsO_3^+ ; see text for discussion.

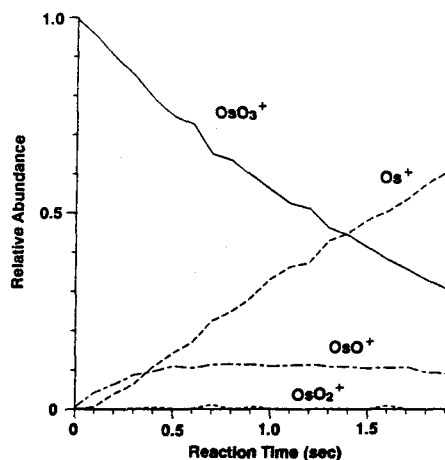
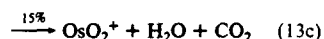
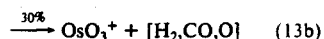
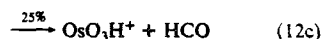
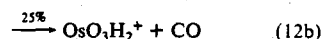
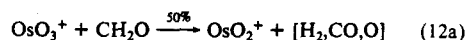
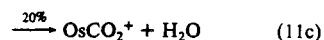
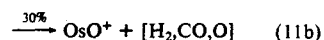
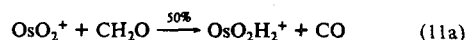
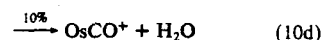
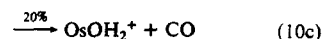
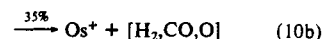


Figure 3. Primary and secondary reactions of OsO_3^+ with H_2 , reactions 5; $p(\text{H}_2) = 1.6 \times 10^{-3}$ Torr. OsO_2^+ is too reactive to accumulate in any substantial amount.

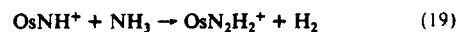
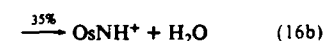
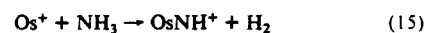
iciencies for these reactions are included in Table II. The CO_2 eliminations are not thermochemically helpful (they imply bond energies less than 127.3 kcal/mol), but the SO_3 elimination indicates that $D(\text{OsO}_3^+-\text{O}) < 83.3 \pm 0.2$ kcal/mol. In other attempts to bracket the strength of this bond, O-atom transfer was sought with NO (to give NO_2) and with N_2O (to give $\text{N}_2 + \text{O}_2$). There was no reaction in either case, but this cannot be taken to

imply reaction endothermicity; the reverse transfer from NO_2 to OsO_3^+ was not observed either. Likewise, although OsO_4H^+ is unreactive with CO, it does not follow that $D(\text{OsO}_3\text{H}^+-\text{O})$ is necessarily greater than 127.3 kcal/mol.

Reactions with CH_2O . More possibilities arise for CH_2O than for the molecules considered above, and the chemistry, given by eq 9–14, is correspondingly richer. Reaction rates and efficiencies are included in Table II. Since the endothermicity for decomposition of CH_2O to CO and H_2 is only 0.5 ± 1.5 kcal/mol, these reactions provide no useful lower limits to metal–ligand bond energies.



Reactions with NH_3 . As shown in eq 15–18, all the oxo ions except for OsO_3^+ are reactive with ammonia. Extrusion of H_2 or H_2O is the principal process, although OsO_4^+ abstracts a hydrogen atom from NH_3 , as from H_2 . Secondary reactions are also prominent, eq 19 and 20 and Figure 4. Again, rates and efficiencies are included in Table II. Buckner et al. have recently shown ammonia dehydrogenation to be facile for the group 3–5, early transition-metal ions.¹⁹ The dehydrogenation reactions indicate that $D([\text{Os}^+-\text{NH}]) > 92 \pm 2.5$ kcal/mol.



(19) Buckner, S. W.; Gord, J. R.; Freiser, B. S. *J. Am. Chem. Soc.* submitted for publication.

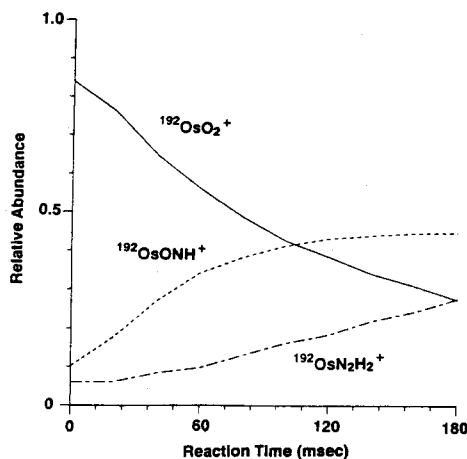
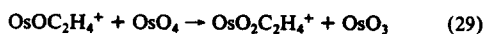
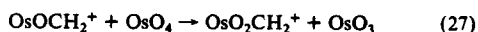
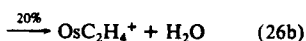
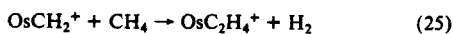
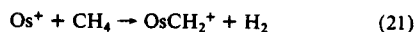


Figure 4. Sequential double bond metathesis of $^{192}\text{OsO}_2^+$ with NH_3 , reactions 17 and 20. $p(\text{NH}_3) = 4 \times 10^{-7}$ Torr.

Reactions with Methane. As with ammonia, all the oxo ions except OsO_3^+ are reactive under our conditions, reactions 21–24. A number of secondary reactions, 25–30, are observed in this



system as well. Measured rates and efficiencies are included in Table II. The primary and peculiar secondary reactions of OsO_4^+ were confirmed with CD_4 . Reaction of OsO_4^+ with CH_2D_2 gives the statistical 1:1 ratio of OsO_4H^+ to OsO_4D^+ . Occurrence of the secondary reaction 30 implies that $\Delta H_f(\text{OsO}_3\text{H}_2^+) < 111.7 \pm 7.5$ kcal/mol.²⁰ (Assuming CH_3O^+ to be the neutral product yields $\Delta H_f(\text{OsO}_3\text{H}_2^+) < 105.2 \pm 5.5$ kcal/mol.²¹)

Other thermochemical limits derived are $D([\text{Os}^+]-\text{CH}_2) > 109.9 \pm 1$ kcal/mol, $D([\text{Os}^+]-\text{C}_2\text{H}_4) > 48.3 \pm 0.2$ kcal/mol; $D(\text{OsO}^+-\text{C}_3\text{H}_6) > 58.6 \pm 0.4$ kcal/mol, $D(\text{OsO}_4^+-\text{H}) > 104.8 \pm 0.3$ kcal/mol, and $D([\text{OsOCH}_2^+]-\text{O}) > D(\text{OsO}_3-\text{O})$. The methane dehydrogenation reaction implies facile α -elimination. Although exothermic methane dehydrogenation is unusual, it has previously been observed with Ta^+ .²² Reaction of Os^+ with CH_2D_2 yields OsCH_2^+ , OsCHD^+ , and OsCD_2^+ in a roughly statistical 1.5:4:1 ratio.

The sole product of the reaction between Os^+ and acetaldehyde is the osmium methylenide complex indicated in eq 31. This is a fast reaction, with a kinetic efficiency of $k_{\text{obsd}}/k_{\text{ADO}} \approx 0.3$.²³

(20) $\Delta H_f(\text{CH}_2\text{OH}) = -5.8 \pm 3.0$ kcal/mol; Dyke, J. M.; Ellis, R.; Jonathan, N.; Keddar, N.; Morris, A. *Chem. Phys. Lett.* 1984, 111, 207.

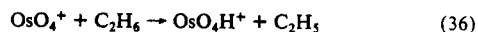
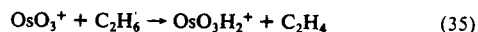
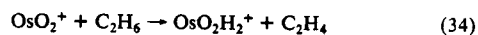
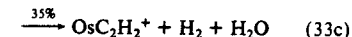
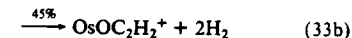
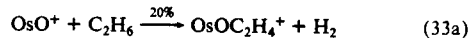
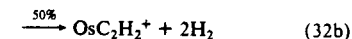
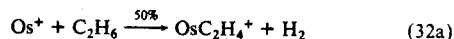
(21) $\Delta H_f(\text{CH}_3\text{O}^+) = 0.7 \pm 1.0$ kcal/mol; Engelking, P. C.; Ellison, G. B.; Lineberger, W. C. *J. Chem. Phys.* 1978, 69, 1826.

(22) Freiser, B. S. and co-workers, manuscript in preparation.

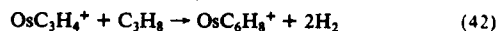
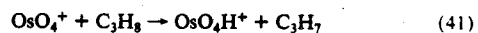
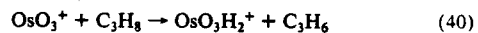
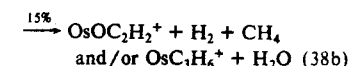
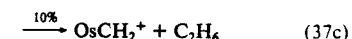
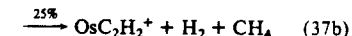
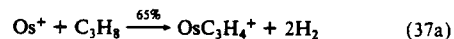
The reaction was confirmed with acetaldehyde- d_4 . Singly labeled CH_3CDO gives a statistical $\text{OsCH}_2^+:\text{OsCHD}^+$ ratio of 1:1.



Ethane. Both single and double dehydrogenation occur with Os^+ and OsO^+ ; OsO_2^+ and OsO_3^+ effect single dehydrogenation but at lower rates. OsO_4^+ exhibits only H atom abstraction. Results are detailed in eq 32–36. OsO_4H_2^+ was also observed from OsO_4^+ , but its origin was unclear. These processes imply that $D([\text{Os}^+]-\text{C}_2\text{H}_4) > 32.7 \pm 0.2$ kcal/mol and $D([\text{Os}^+]-\text{C}_2\text{H}_2) > 74.4 \pm 0.3$ kcal/mol.

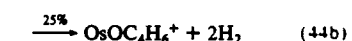
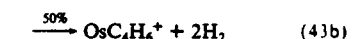


n-Propane. Reactions in this system are shown in eq 37–42. Double dehydrogenation is common. Note that products of C–C



bond cleavage are apparent with Os^+ and probably with OsO^+ . (OsC_3H_6^+ is isobaric with $\text{OsOC}_2\text{H}_2^+$ and so represents an alternative product assignment.) Dehydrogenation implies that $D([\text{Os}^+]-\text{C}_3\text{H}_4) > 69.2 \pm 0.4$ kcal/mol, in addition to other limits consistent with those established above.

n-Butane. The experiments with butane were not as clean as those with the simpler molecules. Nonetheless, reactions 43 and 44, double and triple dehydrogenation, were unambiguously identified. Implications are that $D([\text{Os}^+]-\text{C}_4\text{H}_6) > 56.5 \pm 0.4$ kcal/mol (1,3-butadiene) and $D([\text{Os}^+]-\text{C}_4\text{H}_4) > 109 \pm 1$ kcal/mol (butatriene).



(23) Collision rates are calculated by using ADO theory: Su, T.; Bowers, M. T. *Int. J. Mass Spec. Ion Phys.* 1973, 12, 347.

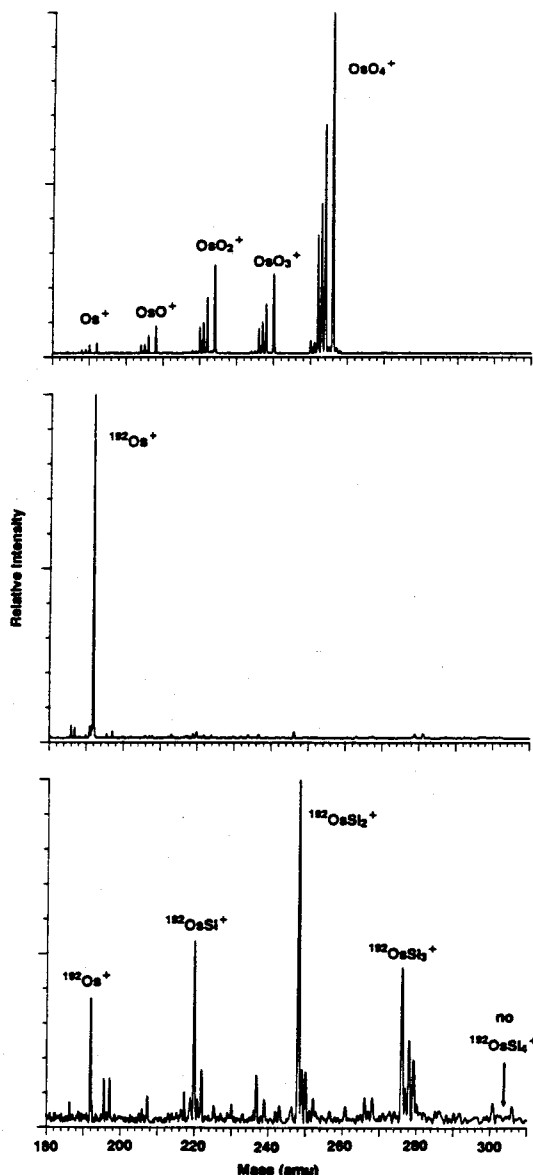
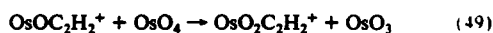
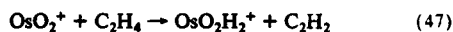
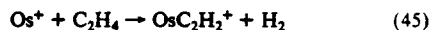


Figure 5. Osmium silicide formation from $^{182}\text{Os}^+$ and SiH_4 , reactions 50a, 54, and 55. Top: Ions generated by 50-eV electron impact on OsO_4 . Center: $^{182}\text{Os}^+$ isolated by ejections of all other ions, including those of mass less than 180 amu. Bottom: After 800 ms of reaction with $\approx 4 \times 10^{-7}$ Torr of SiH_4 .

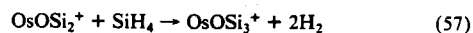
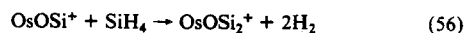
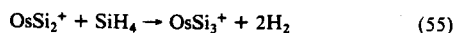
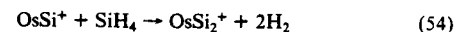
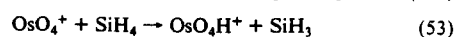
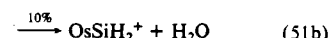
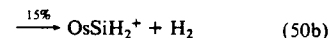
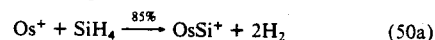
Ethylene. Os^+ effects sequential dehydrogenation, reactions 45 and 48. A weak signal corresponding to OsC_6H_6^+ is also



observed. These reactions establish that $D(\text{OsO}_2^+-\text{H}_2)$ and D -

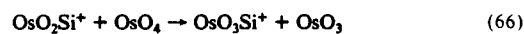
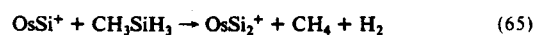
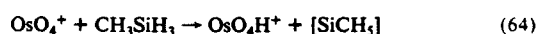
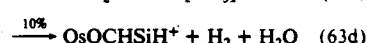
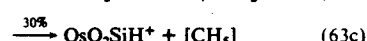
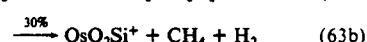
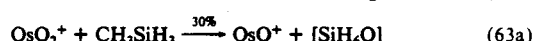
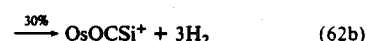
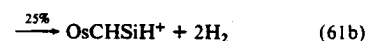
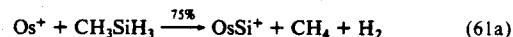
$(\text{OsC}_2\text{H}_2^+-\text{C}_2\text{H}_2) > 41.7 \pm 0.3$ kcal/mol. Reduction of OsO^+ , reaction 46, implies that $D(\text{Os}^+-\text{O}) < 111.8 \pm 0.2$ kcal/mol. OsO_2^+ reacts only slowly, eq 47, and OsO_4^+ and OsO_3^+ appear unreactive with C_2H_4 .

Reactions with SiH_4 . Complete dehydrogenation of SiH_4 is the dominant reaction, eq 50–60, and was observed to occur se-



quentially up to three times (see Figure 5). OsO_3^+ is unreactive, and OsO_4^+ reacts by H atom abstraction. No Si_4 products are formed. Silicide formation indicates that the strength of each additional bond to Si exceeds 99.5 ± 2 kcal/mol. Reactions 50b and 58 indicate that $D(\text{Os}^+-\text{SiH}_2) > 61 \pm 3$ kcal/mol²⁴ and $D(\text{OsOSi}^+-\text{O}) > D(\text{OsO}_3-\text{O})$, respectively. Reaction 52b implies $D(\text{OsO}^+-\text{O}) < 130 \pm 5$ kcal/mol. Note that the products of reaction 52b may be $\text{SiO} + 2\text{H}_2$, simply a loss of SiO subsequent to reaction 52a. This process would indicate $D(\text{OsO}^+-\text{O}) < 91.8 \pm 3$ kcal/mol.²⁵

Reactions with Methylsilane. Many reactions were seen with CH_3SiH_3 , eq 61–65, some of them quite novel. Results with



(24) Shin, S. K.; Beauchamp, J. L. *J. Phys. Chem.* 1986, 90, 1507.

(25) (a) H_2SiOH implies an upper limit of 130 ± 5 kcal/mol, based upon the following: Luke, B. T.; Pople, J. A.; Krogh-Jespersen, M.-B.; Apeloig, Y.; Chandrasekhar, J.; Schleyer, P. v. R. *J. Am. Chem. Soc.* 1986, 108, 260. (b) $\text{H}_2\text{SiO} + \text{H}_2$ implies an upper limit of 86 ± 7 kcal/mol, based upon the following: Luke, B. T.; Pople, J. A.; Krogh-Jespersen, M.-B.; Apeloig, Y.; Chandrasekhar, J.; Schleyer, P. v. R. *J. Am. Chem. Soc.* 1986, 108, 270. (c) $\text{SiH}_2 + \text{H}_2\text{O}$ implies an upper limit of 57 ± 4 kcal/mol; see ref 26a.

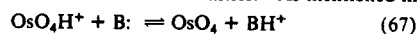
Table IV. Proton-Transfer Reactions

base	PA ^a	BH ⁺ xfer?	OsO ₄ H ⁺ xfer?	k ^b	k/k _{ADO} ^c
CS ₂	166.1 ^d	no	yes	9 ± 3	1.0 ± 0.3
CH ₃ Br	165.7 ^e	no	yes	10 ± 3	0.9 ± 0.3
C ₂ H ₄	162.6 ^d	no	yes	4 ± 3	0.4 ± 0.3
CF ₃ COCl	161.2 ^d	yes ^f	yes	1.2 ± 0.2	0.12 ± 0.05
SO ₂	155.3 ^d	yes	no		
(CF ₃) ₂ CO	153.8 ^d	yes	no		

^aProton affinity of base in kcal/mol. ^bRate constant for proton transfer from OsO₄H⁺ to the base, in units of 10⁻¹⁰ cm³ s⁻¹. ^cReaction efficiency; see ref 23. ^dValue from ref 27. ^eValue from ref 28. ^fProton transfer from CF₃COClH⁺ appears slower than transfer from OsO₄H⁺.

labeled CH₃SiD₃ are consistent with those listed below. OsO₃⁺ is again unreactive, and OsO₄⁺ abstracts a hydrogen atom as indicated in eq 64. Reaction 62b implies that $D(\text{OsO}^+-\text{SiC}) > 179 \pm 8$ kcal/mol.²⁶

Proton Affinity Measurement. The proton affinity of OsO₄ was bracketed with a ladder of reference bases of known proton affinity. Reference proton affinity values were taken from the recent work of McMahon and Kebarle when available.²⁷ Other values were obtained from the compilation by Lias et al.²⁸ Proton transfer was sought in both directions, reaction 67, in order to increase confidence in the relative affinities. As mentioned in

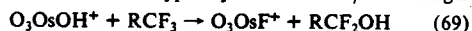


the Experimental Section, the pressure of OsO₄ could not be determined reliably, precluding quantitative interpretation of equilibria. Results of the various proton-transfer experiments are summarized in Table IV. The kinetic efficiencies of the proton transfers from OsO₄H⁺ are displayed graphically in Figure 6 as well as in Table IV. Bracketing alone leads to PA(OsO₄) = 159 ± 4 kcal/mol. Although competing reactions prevent attainment of equilibrium, proton transfer is seen in both directions for CF₃COCl, so that PA(OsO₄) must be quite close to PA-(CF₃COCl). Our recommended value is therefore 161 ± 2 kcal/mol. Observed reactions other than simple proton transfer are described below.

OsO₄H⁺ reacts with isobutane to yield a butyl cation, assumed to be the tertiary isomer. This process implies PA(OsO₄) < 166 ± 2 kcal/mol.²⁹



Both fluorine-containing bases, (CF₃)₂CO and CF₃COCl, react with OsO₄H⁺ to give the products of the novel metathesis reaction 69. Since C-F bonds are typically about 15 kcal/mol stronger



than C-OH bonds,³⁰ the OsO₃⁺-F bond energy must be greater than roughly 116 ± 16 kcal/mol if reaction 69 is to be exothermic.

Discussion

Bond Energies in the OsO₄ System. Only one study of the bond energies $D(\text{OsO}_4^+-\text{O})$ has been reported to date, that by Dillard and Kiser based on electron impact appearance potential measurements.³¹ The authors were aware of the limitations of their technique, noting that their derived value for $\Delta H_f(\text{Os}^+)$ was too high by 32 kcal/mol. Nonetheless, their results, listed in Table VI, do indicate an interesting alternation in bond strengths $D(\text{OsO}_3^+-\text{O}) \approx D(\text{OsO}^+-\text{O}) < D(\text{OsO}_2^+-\text{O}) \approx D(\text{Os}^+-\text{O})$. An earlier Knudsen cell/mass spectrometric study of the gas-phase

(26) Auxiliary thermochemical information from the following: (a) Walsh, R. *Acc. Chem. Res.* 1981, 14, 246. (b) Shin, S. K.; Irikura, K. K.; Beauchamp, J. L.; Goddard, W. A., III *J. Am. Chem. Soc.* 1988, 110, 24.

(27) McMahon, T. B.; Kebarle, P. J. *Am. Chem. Soc.* 1985, 107, 2612.

(28) Lias, S. G.; Liebman, J.; Levin, R. D. *J. Phys. Chem. Ref. Data* 1984, 13, 695.

(29) Auxiliary thermochemical information from the following: (a) Tsang, W. J. *Am. Chem. Soc.* 1985, 107, 2872. (b) Houle, F. A.; Beauchamp, J. L. *J. Am. Chem. Soc.* 1979, 101, 4067.

(30) Benson, S. W. *Thermochemical Kinetics*, 2nd ed.; Wiley: New York, 1976; p 309.

(31) Dillard, J. G.; Kiser, R. W. *J. Phys. Chem.* 1965, 69, 3893.

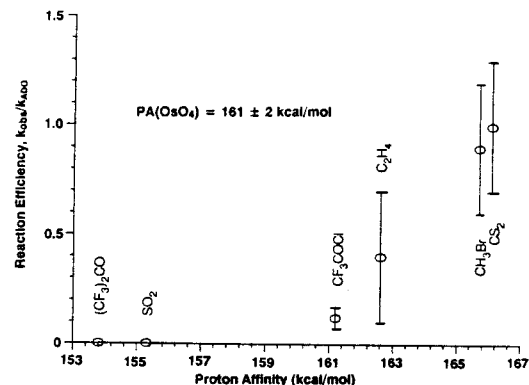


Figure 6. Kinetic efficiency of proton transfer from OsO₄H⁺ to reference bases, reaction 67, plotted against the proton affinity of the reference bases.

Table V. Primary Thermochemical Values^a

quantity	value
$\Delta H_f(\text{OsO}_4(g))$	-80.9 ± 2.4 kcal/mol
$\Delta H_f(\text{Os}(g))$	188 ± 2 kcal/mol
$\Delta H_f(\text{O}(g))$	59.56 kcal/mol
IP(OsO ₄)	12.35 ± 0.04 eV
IP(OsO ₃)	12.1 ± 0.1 eV
IP(Os)	8.3 ± 0.1 eV

quantity	limit ^b	reaction
$D(\text{Os}^+-\text{O})$	<111.8 ± 0.2	46b
$D(\text{OsO}^+-\text{O})$	<117.4	5
$D(\text{OsO}_2^+-\text{O})$	<117.4	5
$D(\text{OsO}_3^+-\text{O})$	<83.3 ± 0.2	8

^aSee Appendix for discussion. ^bIn kcal/mol.

equilibrium between OsO₄ and OsO₃ had yielded a value for IP(OsO₃).³² By combining this with their appearance potentials, Dillard and Kiser calculated $D(\text{OsO}_3-\text{O}) = 108$ kcal/mol.³¹ This value and another, based on the equilibrium data from the Knudsen cell experiment³² (72.9 kcal/mol³³), are also included in Table VI.

Of the many thermochemical limits derived in the Results section, a few are very helpful in delimiting the bond energies just mentioned. These limits are collected in Table V, along with the auxiliary thermochemical quantities employed. A detailed discussion of these other quantities is provided in the Appendix.

Algebraic manipulation of the data in Table V yields an atomization energy for OsO₄⁺ of 413.7 ± 7.6 kcal/mol, and furthermore $D(\text{Os}^+-\text{O}) = 99.9 \pm 12.1$ kcal/mol, $D(\text{OsO}^+-\text{O}) = 105.3 \pm 12.1$ kcal/mol, $D(\text{OsO}_2^+-\text{O}) = 105.3 \pm 12.1$ kcal/mol, $D(\text{OsO}_3^+-\text{O}) = 71.4 \pm 12.1$ kcal/mol, and in the neutral molecule $D(\text{OsO}_3-\text{O}) = 78.3 \pm 14.4$ kcal/mol.³⁴ These values are included in Table VI for comparison with the earlier work. Note that the kinetics of the reactions of OsO₄⁺ with CO and H₂ is generally supportive of an alternation in bond energies. If the barriers are small and the mechanisms similar, then the relative reaction rates probably correlate with the strengths of the bonds being broken.³⁵ One then expects that $D(\text{OsO}_3^+-\text{O}) < D(\text{OsO}^+-\text{O}) \ll D(\text{Os}^+-\text{O}) \approx D(\text{OsO}_2^+-\text{O})$.

Additional bond energies may be derived. In particular, the proton affinity of 161 ± 2 kcal/mol implies an O-H bond energy $D(\text{OsO}_4^+-\text{H}) = 132 \pm 3$ kcal/mol. This is similar to $D(\text{CO}_2^+-\text{H})$

(32) Grimley, R. T.; Burns, R. P.; Inghram, M. J. *J. Chem. Phys.* 1960, 33, 308.

(33) Schäfer, H.; Tebben, A.; Gerhardt, W. *Z. Anorg. Allg. Chem.* 1963, 321, 41.

(34) If the neutral products of reaction (52b) are SiO + 2H₂, then the following bond energies are implied: $D(\text{Os}^+-\text{O}) = 112$, $D(\text{OsO}^+-\text{O}) = 94$, $D(\text{OsO}_2^+-\text{O}) = 117$, $D(\text{OsO}_3^+-\text{O}) = 83$, $D(\text{OsO}_3^+-\text{OH}) = 113$, and $D(\text{OsO}_3-\text{O}) = 91$ kcal/mol.

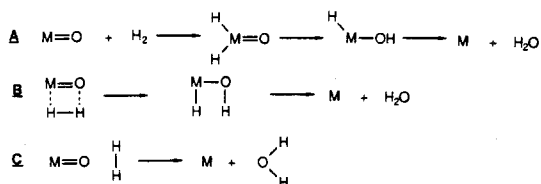
(35) Hammond, G. S. *J. Am. Chem. Soc.* 1955, 77, 334.

Table VI. Derived Bond Energies and Heats of Formation^a

M-X	previous $D(M-X)$	this work	$\Delta H_f(MX)^d$
Os ⁺			379.4 ± 4.3
Os ⁺ -O	130 ^b	99.9 ± 12.1	334.7 ± 12.1
OsO ⁺ -O	96 ^b	105.3 ± 12.1	276.9 ± 12.1
OsO ₂ ⁺ -O	121 ^b	105.3 ± 12.1	219.0 ± 12.1
OsO ₃ ⁺ -O	94 ^b	71.4 ± 12.1	203.9 ± 3.3
OsO ₃ -O	108, ^b 72.9 ^c	78.3 ± 14.4	-80.9 ± 2.4
OsO ₄ -H ⁺		161 ± 2	123.8 ± 4.4
OsO ₄ ⁺ -H		132 ± 3	123.8 ± 4.4
OsO ₃ ⁺ -OH		101 ± 16	123.8 ± 4.4

^aIn kcal/mol. ^bReference 31. ^cReference 33. ^dStationary electron convention.

Scheme I



= 135³⁶ but substantially greater than $D(FeO^+-H) = 106 \pm 4$, $D(CoO^+-H) = 107 \pm 4$, and $D(CrO^+-H) = 89 \pm 5$ kcal/mol.⁴ OsO₄⁺, like CO₂⁺, is an oxygen-centered cation radical,^{16,37} whereas the first-row diatomic MO⁺ probably are not. Another derived bond strength is $D(OsO_3^+-OH) = 101 \pm 16$ kcal/mol. $D(Fe^+-OH) = 73 \pm 3$, $D(Co^+-OH) = 71 \pm 3$, and $D(Cr^+-OH) = 73 \pm 5$ kcal/mol are all much less, reflecting the relatively weak bonds in the corresponding monoxides.⁴

Reactions with OsO₄. All the reactions of OsO_n⁺, including isotopic scrambling, may be explained by postulating the formation of an intermediate, [Os₂O_{4+n}]⁺, that subsequently dissociates. Dissociation might be expected to yield more ions than those shown in eq 1 and 2. Since $IP(OsO_n) < IP(OsO_{n+1})$,³⁸ however, only the smaller fragment will carry the charge. This restricts possibilities for multiple O-atom transfer to the reaction of Os⁺ to yield OsO₂⁺. Double resonance experiments established that this reaction does not occur, suggesting that it is thermodynamically unfavorable and that $D(OsO_2-O) > D(OsO^+-O)$.

As mentioned above, the absolute rates of reactions with neutral OsO₄ remain uncertain. A crude estimate has been obtained by making a few assumptions, the strongest of which is that the major impurity is carbon monoxide. From the measured rate of reaction of OsO₄⁺ with added CO, a pressure of CO impurity is inferred. This leads indirectly to an estimated rate of 1×10^{-9} cm³ s⁻¹ for the reaction of Os⁺ with OsO₄. For comparison, the collision rate between Os⁺ and OsO₄ is calculated to be 5.7×10^{-10} cm³ s⁻¹.³⁹

Reactions with H₂. Three possible mechanisms for reaction 5 are illustrated in Scheme I. Mechanism A involves initial oxidative addition of H₂ to the metal center, followed by hydrogen migration to the oxygen, and finally reductive elimination of H₂O. In B we suppose an initial [2_s + 2_s] addition of H₂ across the Os=O bond, with subsequent elimination of water. Finally, mechanism C depicts direct attack of H₂ on the oxygen, resulting

(36) Auxiliary thermochemical information from the following: Franklin, J. L.; Dillard, J. G.; Rosenstock, H. M.; Herron, J. T.; Draxl, K.; Field, F. H. *Ionization Potentials, Appearance Potentials, and Heats of Formation of Gaseous Positive Ions; National Standard Reference Data Series*, National Bureau of Standards (U.S.) 26; U.S. Government Printing Office: Washington, DC, 1969.

(37) This is the expectation based upon simple oxidation state arguments. See, also: (a) Diemann, E.; Müller, A. *Chem. Phys. Lett.* 1973, 19, 538. (b) Burroughs, P.; Evans, S.; Hammett, A.; Orchard, A. F.; Richardson, N. V. *J. Chem. Soc., Faraday Trans. 2* 1974, 70, 1895. (c) Our Hartree-Fock calculations place the T₂ level 1.1 eV below the T₁. For a different opinion, see: (d) Foster, S.; Felps, S.; Cusachs, L. C.; McGlynn, S. P. *J. Am. Chem. Soc.* 1973, 95, 5521.

(38) From estimated values in ref 31. This ordering is reasonable, based upon $IP(Os) = 8.3$ eV (see Appendix) and $IP(O) = 13.6$ eV.³⁶

(39) Using $\alpha(OsO_4) = 6.4 \times 10^{-24}$ cm³, based upon data in the following: Linke, R. Z. *Phys. Chem. B* 1941, 48, 193.

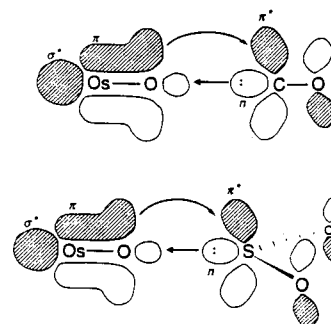


Figure 7. Orbital diagrams for proposed transition states for reactions 7 and 8, reduction with CO and SO₂. This model is directly analogous to the classical Dewar-Chart-Duncanson model for transition-metal/ π -acid bonding.

in a coordinated H₂O molecule which then departs.

In general, we will assume that all the oxo ions that react to give analogous products do so by analogous pathways. Although this assumption leads to mechanisms that are somewhat speculative, we feel that it is reasonable, lacking evidence to the contrary. Proceeding in this spirit, mechanism C in the reaction at hand may be eliminated because of its erroneous prediction that OsO₄⁺ will be reactive. For OsO₃⁺, route A involves Os in the unreasonable +9 oxidation state. The mechanism of choice is thus B, involving a four-centered electrocyclic rearrangement. Such rearrangements are symmetry-allowed for systems with substantial d-orbital character in the metal-ligand bond.⁴⁰ The net positive charge on the complexes may be important in rendering the osmium-oxo bond sufficiently covalent for it to have the requisite d-orbital participation.

The failure of OsO₄⁺ to react by H₂O elimination is consistent with this mechanism, which requires a vacant coordination site on the metal. The hydrogen atom abstraction, reaction 6, may be understood by noting that OsO₄⁺ is an oxygen-centered radical.³⁷ An organic analogue is hydrogen atom abstraction by CO₂⁺.⁴¹ The isotope effect observed with HD, OsO₄H⁺:OsO₄D⁺ ≈ 2:1, suggests that the reaction proceeds by a direct mechanism,⁴² rather than by a long-lived intermediate, in accord with expectations for a radical abstraction reaction. H atom abstraction has been observed in reactions of CrO⁺ and of electronically excited VO⁺.^{4,26}

The high kinetic efficiencies of the reactions with H₂ indicate low barriers. For comparison, it may be noted that a related reaction, [2_s + 2_s] addition of H₂ to Cl₂Ti=CH₂, has been calculated to have a small activation barrier of 6.7 kcal/mol.⁴³

Reactions with CO and SO₂. Mechanisms analogous to those of Scheme I may be drawn for reactions 7 and 8 of CO and SO₂. Unlike H₂, these molecules are reactive with OsO₄⁺; no vacant coordination site is required. This suggests a direct attack on oxygen, analogous to mechanism C in Scheme I. Frontier orbital diagrams for the CO and SO₂ reactions are given in Figure 7 and depict $n(C \text{ or } S) \rightarrow \sigma^*(MO^+)$ and $\pi(MO^+) \rightarrow \pi^*(CO \text{ or } SO_2)$ dative interactions.

Reactions with CH₂O. These reactions are much like those with H₂, with the added possibility of retaining CO in the product ion. With Os⁺, H₂ retention is also observed, to form the dihydride OsH₂⁺. A similar reaction has been reported between Gd⁺ and CH₂O.⁴⁴

There is a conspicuous lack of products corresponding to loss of CO₂. Since CO oxidation is 10 kcal/mol more exothermic than

(40) Steigerwald, M. L.; Goddard, W. A., III *J. Am. Chem. Soc.* 1984, 106, 308.

(41) Copp, N. W.; Hamdan, M.; Jones, J. D. C.; Birkinshaw, K.; Twiddy, N. D. *Chem. Phys. Lett.* 1982, 88, 508.

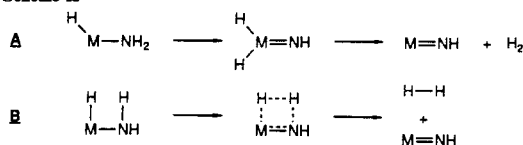
(42) Armentrout, P. B. In *Structure/Reactivity and Thermochemistry of Ions*; Ausloos, P., Lias, S. G., Eds.; Reidel: Dordrecht, 1987; pp 97-164.

(43) Rappé, A. K. *Organometallics* 1987, 6, 354.

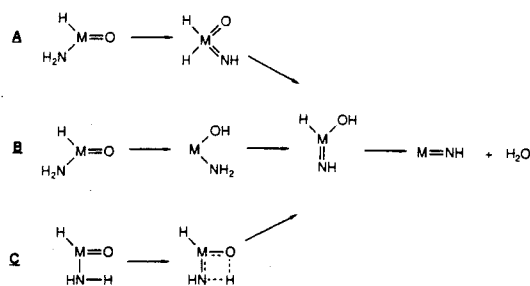
(44) Schilling, J. B.; Beauchamp, J. L. *J. Am. Chem. Soc.* 1988, 110, 15

Osmium Tetroxide and Its Fragment Ions

Scheme II



Scheme III

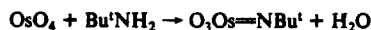


H_2 oxidation, the prevalence of H_2O loss is initially surprising. Mechanistic considerations, however, can easily rationalize this observation. From Figure 7, we see that CO reacts by attacking the oxygen atom directly, along the Os-O bond axis. In the reactions of CH_2O , however, any CO fragment formed is probably bound to the metal center and therefore unable to attain the required geometry for reaction with the oxo ligand. In contrast, H_2 can react starting from a hydroxy hydride (the intermediate in Scheme I, both A and B) and presumably also from a dihydride (α -migration can be reversible; see the discussion of CH_3CHO below), both of which are reasonable intermediates in CH_2O activation. On the basis of this argument, we believe that the $[\text{H}_2, \text{CO}, \text{O}]$ losses are actually losses of $\text{H}_2\text{O} + \text{CO}$.

Reactions with NH_3 . These reactions appear to occur with initial insertion of the osmium center into the N-H bond. This is inferred from the inertness of OsO_3^+ ; the required intermediate, $\text{OsO}_3(\text{H})(\text{NH}_2)^+$, places osmium in the unlikely +9 formal oxidation state. For the dehydrogenation reactions, two possibilities are detailed in Scheme II. In mechanism A, a dihydride intermediate is formed by α -hydrogen migration from N to Os, followed by reductive elimination of H_2 . Path B involves a $[2_e + 2_e]$ concerted elimination of H_2 . Note that route A is unavailable to OsO_2^+ because the dihydride would involve Os(+9). The failure of OsO_2^+ to yield OsO_2NH^+ therefore argues against pathway B, and we favor mechanism A.

If an oxo ligand is present, H_2O may be eliminated instead, a formal double-bond metathesis reaction. This reaction has also been observed with FeO^+ .¹⁹ Three possible mechanisms for this reaction are illustrated in Scheme III. In A, a dihydride intermediate is formed, followed by α -migration of hydrogen to oxygen and reductive elimination of H_2O . In B, the initial adduct rearranges to a hydroxy complex, finally leading to H_2O elimination. In mechanism C, a hydroxy hydride is formed from the adduct directly, through a four-centered transition state. Reactions 17 and 20 of OsO_2^+ and OsONH^+ cannot reasonably proceed by mechanism A because of oxidation state restrictions. Since the very directional orbitals of non-hydrogenic atoms are expected to slow $[2_e + 2_e]$ cycloadditions, we favor mechanism B, involving reductive elimination of H_2O from a hydroxy hydride intermediate.

This double-bond metathesis reaction has also been observed in condensed phases. In solution, neutral OsO_4 reacts with bulky amines only once to yield imido complexes. The product complexes are effective in stoichiometric or catalytic cis vicinal oxyamination of olefins.⁴⁵ Diimidomolybdenum centers have been implicated



(45) Chong, A. O.; Oshima, K.; Sharpless, K. B. *J. Am. Chem. Soc.* **1977**, *99*, 3420.

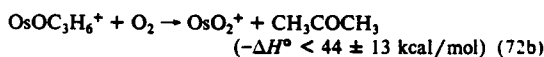
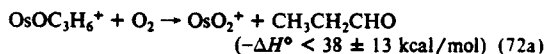
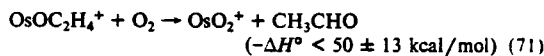
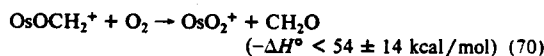
as the active sites in heterogeneous bismuth molybdate ammoxidation catalysts. These centers are thought to arise from the metathetical transformation of dioxo centers by ammonia,⁴⁶ presumably by processes analogous to the sequential reactions 17 and 20.

Reactions with Methane. These reactions exhibit a variety of mechanisms, in which the carbon-containing ligands can have a strong effect on the chemistry. One of the most curious is the secondary reaction 30, to yield $^*\text{CH}_2\text{OH}$ (or CH_3O^*). The corresponding limit on $\Delta H_f^\circ(\text{OsO}_3\text{H}_2^+)$ implies $D(\text{OsO}_3^+-\text{H}_2) > 113.8 \pm 7.6$ kcal/mol. This is far too strong for a dihydrogen complex; assuming the hydrogens to be bonded separately lead to an average bond energy of at least 109.0 ± 8.8 kcal/mol. This high value suggests O-H bonds, rather than Os-H bonds, since typical metal-hydride bond strengths are only 30-60 kcal/mol.⁴⁷ Likewise, the inference $D(\text{OsO}_2^+-\text{H}_2\text{O}) > 113.9 \pm 17.6$ kcal/mol appears unreasonable for an aquo complex. We therefore conclude that OsO_3H_2^+ has the dihydroxy structure $\text{OsO}(\text{OH})_2^+$, with an average $[\text{OsO}^*]-\text{OH}$ bond strength of at least 124.2 ± 9.1 kcal/mol. This may be compared with $D(\text{OsO}_3^+-\text{OH}) = 101 \pm 16$ kcal/mol, derived above.

As with NH_3 , OsO_3^+ is unreactive with CH_4 , again suggesting that initial oxidative addition is required. CH_4 apparently reacts with Os^+ by a route as in Scheme II, to yield the corresponding dehydrogenation products. No isotope effect was found with CH_2D_2 , which yields products $\text{OsCH}_2^+:\text{OsCHD}^+:\text{OsCD}_2^+$ in nearly the statistical 1:4:1 ratio. The same mechanism is probably operative in the reaction of OsO^+ , although CH_4 differs from NH_3 in that it does not yield any H_2O loss. The reaction of OsO_2^+ with CH_4 is analogous to that with NH_3 , but the secondary reaction 26 results in predominant loss of H_2 , in contrast to the analogous reaction 20, in which only H_2O loss is observed. No H_2O loss is seen in the secondary reaction 28. Possible mechanisms for the reactions of OsO_2^+ , OsOCH_2^+ , and $\text{OsOC}_2\text{H}_4^+$ are illustrated in Scheme IV.

There is a clear trend away from H_2O loss as the extent of hydrocarbon ligation increases. OsO_2^+ reacts only to lose H_2O ; OsOCH_2^+ yields H_2O in the minor pathway; $\text{OsOC}_2\text{H}_4^+$ yields little or no H_2O . The simplest explanation is that hydrocarbon ligands donate electron density to the metal. Electron donation will increase the ionicity of the metal-oxygen bond, making it stronger.⁴⁸ Another contribution to the OsO_2^+ reactivity may be the "spectator oxo" effect, in which a "spectator" oxo or imido ligand compensates for loss of metal-ligand bonds by forming a triple bond to the metal center.⁴⁹

Regardless of the particulars of the reaction mechanisms, the thermochemistry raises some intriguing possibilities for gas-phase catalysis. Especially interesting is the apparent formation of C_2H_4 and C_3H_6 complexes. (The failure to form C_4 complexes suggests an especially stable structure for $\text{OsOC}_3\text{H}_6^+$, such as an allyl hydride.) Derived thermodynamic limits leave ample leeway for reactions 70-72 to be exothermic (i.e., $-\Delta H^\circ > 0$), and catalytic



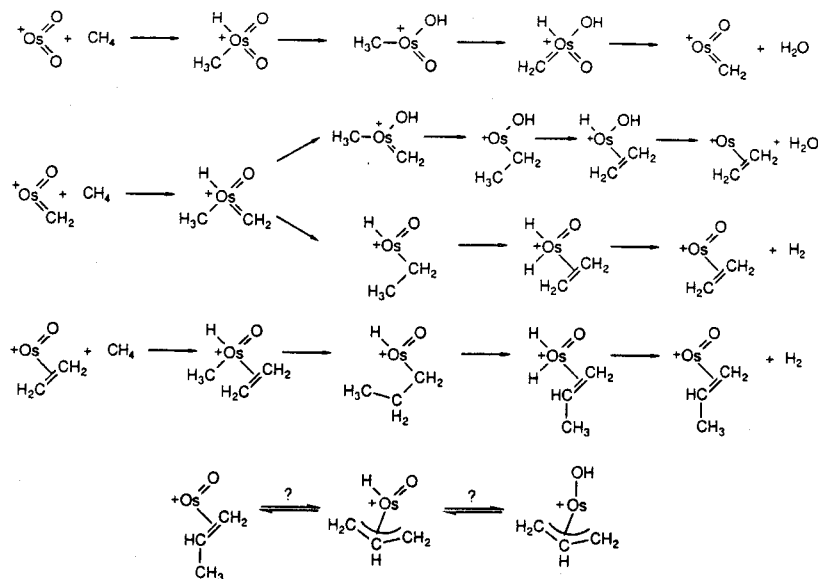
(46) Graselli, R. K. *Appl. Catal.* **1985**, *15*, 127.

(47) (a) Schilling, J. B.; Goddard, W. A., III; Beauchamp, J. L. *J. Phys. Chem.* **1987**, *91*, 5616. (b) Schilling, J. B.; Goddard, W. A., III; Beauchamp, J. L. *J. Am. Chem. Soc.* **1987**, *109*, 5565.

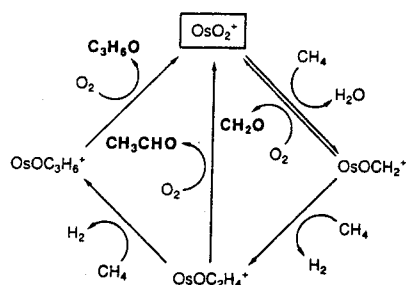
(48) Preliminary results of our Hartree-Fock calculations indicate that the Os-O bond is substantially ionic in OsO_3^+ as well as in neutral OsO_2 .

(49) Rappé, A. K.; Goddard, W. A., III *J. Am. Chem. Soc.* **1982**, *104*, 3287.

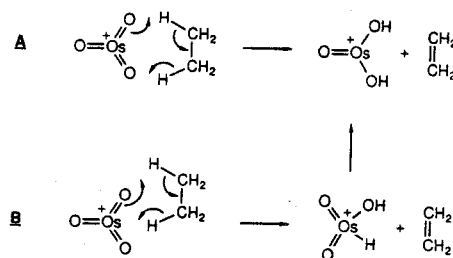
Scheme IV



Scheme V



Scheme VI



cycles converting CH_4 to a number of partially oxidized compounds may be possible, as illustrated in eq 70–72 and Scheme V. Work is currently in progress to explore the viability of these cycles. We are encouraged by reports by Squires et al. that O_2 can oxidize the ligands in gas-phase organometallic anions.⁵⁰

Reaction with CH_3CHO . As mentioned in the Results section, CH_3CHO reacts with Os^+ to give OsCH_2^+ as the only product. With acetaldehyde- d_1 , CH_3CDO , the product methylenide complexes are formed in a statistical 1:1 ratio of $\text{OsCH}_2^+ \cdot \text{OsCHD}^+$. This suggests the intermediacy of a methylenide dihydride species in which α -hydrogen shifts are reversible, allowing scrambling.

This reaction constitutes clear evidence for reversible α -migrations to and from carbon; preliminary results with H_2^{18}O suggest that such reversibility is also possible to and from oxygen.

Reactions with Heavier Hydrocarbons. With some exceptions, reactivity is very similar among the heavier hydrocarbons examined: ethylene, ethane, propane, and butane. Os^+ and OsO^+ both react by extensive dehydrogenation. With propane, C–C bond cleavage is also observed. Unfortunately, the limited detail available precludes any confidence in choosing from among the many possible mechanisms.

With minor exceptions, a single oxo ligand has little effect on Os^+ chemistry. As mentioned previously, this is also the case with V^+ , and, as with V^+ , the lack of qualitative change is probably due to the strength of the metal–oxo bond. Subsequent oxygens, however, completely change the reactivity.

In reactions with C_2H_4 , C_2H_6 , and C_3H_8 , only single dehydrogenation generally occurs with OsO_2^+ and OsO_3^+ , with loss of hydrocarbon rather than H_2 . Two possible mechanisms are outlined in Scheme VI, using the reaction between OsO_3^+ and C_2H_6 as an example. The reactivity of OsO_3^+ argues against oxidative addition to the metal center. Reaction 39, in which OsO_2^+ and propane yield $\text{OsOC}_3\text{H}_7^+$, H_2 , and H_2O , does not appear to follow either mechanism. As usual, OsO_4^+ reacts only by hydrogen atom abstraction.

Reactions with Silane. These reactions are dominated by complete dehydrogenation of SiH_4 to yield the corresponding silicides. This is in marked contrast to reactions of first-row transition-metal atomic ions with SiH_4 .⁵¹ Single dehydrogenation is the only exothermic reaction observed with these metals, and some ions, including the osmium congener Fe^+ , are unreactive.

OsO_3^+ is again unreactive, consistent with a requirement for initial oxidative addition, and OsO_4^+ again reacts only by hydrogen atom abstraction. Among the other ions, however, the ligands have no effect on the chemistry; all the $\text{OsO}_m\text{Si}_n^+$ ($n = 0-2$, $m = 0-2$) react by double dehydrogenation to the corresponding silicides. One exception is reaction 52b of OsO_2^+ to form silanol (or $2 \text{H}_2 + \text{SiO}$). The formation of the higher $\text{OsO}_m\text{Si}_n^+$ suggests that the SiO moiety may be present as a ligand, as an electropositive analogue of CO. More knowledge of the structures of reactants and products is needed to devise mechanisms for the dehydrogenation. The only real clue is that the reactive $\text{OsO}_m\text{Si}_n^+$

(50) (a) Wang, D.; Squires, R. R. *Organometallics* 1987, 6, 905. (b) Squires, R. R. *Chem. Rev.* 1987, 87, 623.

(51) Kang, H.; Jacobson, D. B.; Shin, S. K.; Beauchamp, J. L.; Bowers, M. T. *J. Am. Chem. Soc.* 1986, 108, 5668.

must have the metal in an oxidation state less than +7 in order for oxidative addition of SiH_4 to be reasonable.

Formation of metal silicides is of heightened interest because of the applications of these materials in the electronics industry.⁵² MSi_x layers with $x > 2$ are particularly desirable in this context.

Reactions with Methylsilane. This system displays reactivity similar to silane in some cases and similar to ethane in others. As with the silane reactions, it is difficult to assign structures for the products in this system. In sharp contrast to the reactions of SiH_4 , however, the products formed from CH_3SiH_3 are very sensitive to the ligands present on osmium. OsO_3^+ is unreactive, suggesting that oxidative addition is an essential first step for CH_3SiH_3 , as with SiH_4 but not C_2H_6 . OsO_2^+ either demethanates or is reduced to the monoxide; OsO^+ gives double and triple dehydrogenation; Os^+ reacts both by demethanation and dehydrogenation; OsSi^+ reacts by loss of CH_4 and H_2 to give the disilicide. The 1,1-dehydrogenation product that would be expected based upon reactions of first-row transition-metal ions⁵¹ was not observed. The diversity of these reactions dramatically demonstrates the possible sensitivity of the chemistry of gas-phase, ionic metal complexes to the number and character of ligands.

Conclusions

Ion-molecule reactions of the osmium and oxo osmium ions OsO_n^+ ($n = 0-4$) with a variety of hydrocarbons and small molecules have been found to yield a wealth of chemical information. In many cases, mechanistic details have been inferred from the patterns of reactivity. Oxidative addition appears to be the initial step in many reactions, as suggested by the lack of reactivity of OsO_3^+ (formally Os^{7+}) in these systems. Isotopic labeling experiments provide strong evidence for rapidly reversible α -hydrogen shifts to and from carbon and possibly oxygen. OsO_4^+ is an oxygen-centered cation radical and exhibits H atom abstraction reactions closely analogous to the organic cation radical CO_2^+ .⁴¹

Reactions of OsO_n^+ ($n = 1-3$) with H_2 appear to be $[2_1 + 2_1]$ cycloadditions. High kinetic efficiencies indicate low barriers for this process, consonant with *ab initio* predictions for H_2 addition to metal methylidene complexes. *Ab initio* studies of metal oxo systems would be helpful in corroborating (or contradicting) this mechanism as well as clarifying the role of the net positive charge.

Reductions with CO and SO_2 are proposed to proceed through a transition state with Dewar-Chat-Duncanson bonding through a coordinated oxygen atom. An *ab initio* evaluation of this proposal would also be welcome.

Another intriguing process observed is facile formation of mono-, di-, and trisilicides from SiH_4 ; such a process may have

implications for silicide technology in the electronics industry. Oxo-silicide complexes may contain SiO coordinated to Os^+ in a manner similar to the archetypal CO ligand. Finally, there is the strong possibility that OsO_2^+ will catalytically oxidize methane to aldehydes in the presence of a terminal oxidant such as O_2 . Investigations into this process as well as other reactions of oxo-metal ions are currently underway.

Acknowledgment. We gratefully acknowledge the support of donors of the Petroleum Research Fund, administered by the American Chemical Society, and the National Science Foundation under Grant CHE-87-11567. K.K.I. thanks the National Science Foundation for graduate fellowship support during part of the term of this study. We also thank E. S. Uffelman for helpful suggestions.

Appendix

The following discussion is intended to clarify the reasoning behind the choice of literature values for the thermochemical quantities presented in the upper part of Table V.

The $\Delta H_f(\text{OsO}_4(g))$ value is based on von Wartenberg's measurement of $\Delta H_f(\text{OsO}_4(c)) = -93.4 \pm 1.4$ kcal/mol⁵³ and a value for $\Delta H_{vap}(\text{OsO}_4) = 12.5 \pm 1$ kcal/mol. The latter value is a simple average of those reported by von Wartenberg (13.5)⁵³ and by Ogawa (11.6).⁵⁴ $\Delta H_f(\text{Os}(g))$ was taken to be an average of the values reported by Parrish and Reif (187.4 ± 0.9 kcal/mol)⁵⁵ and by Carrera et al. (189.0 ± 1.4).⁵⁶ $\text{IP}(\text{OsO}_4)$ is the average of values reported from photoelectron studies by Diemann and Müller (12.39 eV),^{37a} Burroughs et al. (12.35),^{37b} and Foster et al. (12.32).^{37d}

$\text{IP}(\text{OsO}_3)$ is more problematic; the cited experimental value of 12.3 ± 1 eV comes from the electron impact measurement by Grimley et al.³² They also measured $\text{IP}(\text{OsO}_4)$ to be 12.6 ± 1 eV. If their error is assumed to be systematic, then their difference in ionization potentials is reliable. Estimating an error limit of 0.1 eV yields the listed value for $\text{IP}(\text{OsO}_3)$.

From spectroscopic data, Albertson has estimated $\text{IP}(\text{Os})$ to be roughly 8.7 eV.⁵⁷ Subsequently, van Kleef and Klinkenberg reviewed the available spectroscopic data to conclude that Albertson had based his estimate upon an erroneous assignment. They suggested $\text{IP}(\text{Os})$ to be "about" 8.5 ± 0.1 eV.⁵⁸ In a recent and more comprehensive study of metal ionization potentials, Rauh and Ackermann determined $\text{IP}(\text{Os}) = 8.28$ eV by electron impact, as corrected for excited states of the neutral atoms.⁵⁹ We have chosen a value of 8.3 ± 0.1 eV to reflect this apparently more accurate value.

(53) von Wartenberg, H. *Ann. Chem.* 1924, 440, 97.

(54) Ogawa, E. *Bull. Chem. Soc. Jpn.* 1931, 6, 302.

(55) Parrish, M. B.; Reif, L. *J. Chem. Phys.* 1962, 37, 128.

(56) Carrera, N. J.; Walker, R. F.; Plante, E. R. *J. Res. Nat. Bur. Stand.* 1964, 68A, 325.

(57) Albertson, W. *Phys. Rev.* 1934, 45, 304.

(58) van Kleef, Th. A. M.; Klinkenberg, P. F. A. *Physica* 1961, 27, 83.

(59) Rauh, E. J.; Ackermann, R. J. *J. Chem. Phys.* 1979, 70, 1004.

(52) (a) Murarka, S. P. *Solid State Technol.* 1985, 28, 181. (b) Brors, D. L.; Fair, J. A.; Monnig, K. A.; Saraswat, K. C. In *Proceedings of the 9th International Conference on Chemical Vapor Deposition*; Robinson, McD., Cullen, G. W., van den Brekel, C. H. J., Blocher, J. M., Jr., Rai-Choudhury, P., Eds.; The Electrochemical Society: Pennington, NJ, 1984; pp 275-286.

Chapter II

Post-Ionization Chemical Separation:

Application to ^{187}Re - ^{187}Os Dating

Karl K. Irikura, Edmund H. Fowles and J. L. Beauchamp

*Arthur Amos Noyes Laboratory of Chemical Physics,
California Institute of Technology, Pasadena, California 91125*

Rhenium-osmium dating, which relies on the beta decay of ^{187}Re to ^{187}Os (half-life = 4.23×10^{10} years¹) has generated considerable interest among geologists.^{2,3} Unfortunately, the technique has not been used extensively because it requires the difficult separation and pre-concentration of the two metals.⁴ *In situ* methods are hampered by lack of sensitivity and the difficulty in distinguishing ^{187}Re and ^{187}Os , which differ in mass by only 3×10^{-6} mass units.⁵ We wish to report a novel solution to the mass-spectrometric problem of resolving the two ions.

Although $^{187}\text{Re}^+$ and $^{187}\text{Os}^+$ have the same mass, they are different elements and exhibit different chemical reactivity. We have found that gas-phase Os^+ reacts readily with small molecules such as methane, whereas Re^+ is among the least reactive of the third-row transition metal ions.^{6,7} Gas-phase ion chemistry may therefore be exploited to effect post-ionization chemical separation (PICS) in a trapped-ion mass spectrometer. If an external ion source is employed, ions can be accumulated in the trap and sample pre-

¹Lindner, M.; Leich, D. A.; Russ, G. P.; Bazan, J. M.; Borg, R. J. *Geochim. Cosmochim. Acta* **1989**, *53*, 1597-1606.

²Luck, J.-M.; Allègre, C. J. *Nature* **1983**, *302*, 130-132.

³Luck, J.-M. In *Nuclear Methods of Dating*; Roth, E.; Poty, B., Eds.; Kluwer: Dordrecht, 1989; Chapter 4.

⁴Walker, R. J. *Anal. Chem.* **1988**, *60*, 1231-1234.

⁵Weast, R. C., Ed. *CRC Handbook of Chemistry and Physics*, 66th ed.; CRC Press: Boca Raton, Florida, 1985.

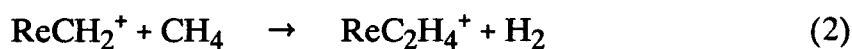
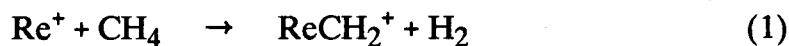
⁶Irikura, K. K.; Beauchamp, J. L. *J. Am. Chem. Soc.* **1989**, *111*, 75-85. (Chapter I in this thesis.)

⁷Irikura, K. K.; Beauchamp, J. L. *J. Am. Chem. Soc.*, in press; *J. Phys. Chem.*, submitted. (Also see Chapter III in this thesis.)

concentration may be avoided. The PICS technique may be applicable to other chronometric systems involving isobaric interferences.

In order to test the separation chemistry, a solid solution of rhenium and osmium in iron was prepared by fusion of compressed metal powders in an induction furnace. Electron microprobe analysis indicated 0.8 atom % Re and 1.9% Os, with reasonable homogeneity (Os/Re = 2.30, $\sigma = 0.06$). Ions were generated by excimer laser ablation (308 nm) of the sample in the cell of a Fourier-transform ion cyclotron resonance (FTICR) spectrometer. Since laser ablation produces translationally and electronically excited ions,⁸ some loss of chemical selectivity may occur. To forestall this, two techniques have proven effective. The reagent gas pulse may be delayed, providing sufficient time for collisional and radiative relaxation of the ions. Alternatively, reagents may be introduced in pairs. For example, CH₄ and H₂ may be introduced together. Excited Re⁺ reacts with CH₄ to form ReCH₂⁺, but the H₂ reduces this product⁷ back to Re⁺, preventing contamination of the ¹⁸⁷OsCH₂⁺ peak. This technique is illustrated in Figure 1.

Lacking the value for the bond energy $D(\text{Re}^+\text{-CH}_2)$, we can only place an upper limit on the amount of rhenium contamination of the ¹⁸⁷OsCH₂⁺ peak. Based upon our upper limit for the rate of reaction 1 ($k_1 < 1.6 \times 10^{-15} \text{ cm}^3 \text{ s}^{-1}$) and the rapid rate of reaction 2 ($k_2 = 1.6 \times 10^{-10} \text{ cm}^3 \text{ s}^{-1}$),



⁸ Kang, H.; Beauchamp, J. L. *J. Phys. Chem.* 1985, 89, 3364-3367.

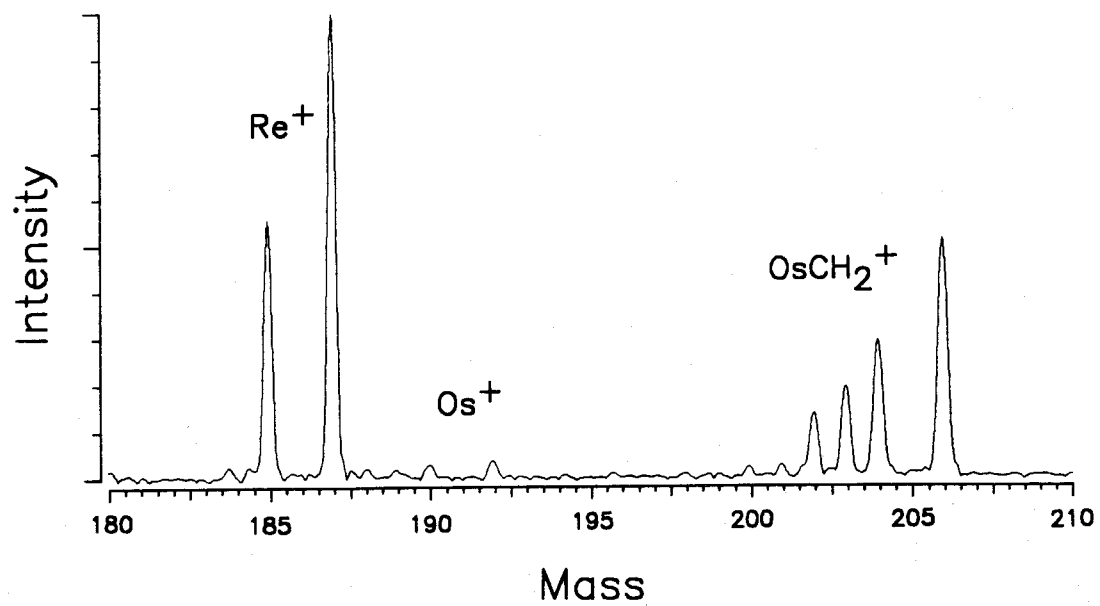


Figure 1. Re^+ and Os^+ after 100 ms in a mixture of methane ($1. \times 10^{-6}$ torr) and hydrogen (3.2×10^{-5} torr). OsCH_2^+ , but no ReCH_2^+ , is produced.

the amount of contaminating $^{187}\text{ReCH}_2^+$ is less than 9×10^{-6} times the amount of $^{187}\text{Re}^+$. Addition of hydrogen reduces the contamination even further. This is two orders of magnitude less contamination than is obtained using the alternative *in situ* techniques described below.

Fehn et al., using accelerator mass spectrometry, have reported the fortuitous separation of Re and Os when metal anions are generated by sample sputtering with an energetic Cs^+ beam.^{9,10} They found that very little Re^- was formed, so that contamination of $^{187}\text{Os}^-$ is $\sim 0.1\%$. They reported successful analysis at the 50 ppb level. However, $^{186}\text{W}^-$ is formed efficiently and interferes with the $^{186}\text{Os}^-$ measurement.⁹⁻¹¹ Although W^+ is reactive with CH_4 ,⁷ we have found that CO_2 (or a mixture of CO_2 and CO) is an appropriate PICS reagent since W^+ (and not ground-state Os^+ or Re^+) is reactive with this gas. Thus a pulse of CO_2 and CO followed by one of CH_4 and H_2 will separate Re^+ , Os^+ , and W^+ by forming OsCH_2^+ and heavier species $\text{WO}_n\text{C}_m\text{H}_{2m}^+$. Alternatively, CH_4 and CO_2 may be used without H_2 or CO if they are pulsed after a suitable delay.

Three-color resonant multiphoton ionization has been used to ionize osmium with a selectivity over rhenium of 10^3 .¹² Unfortunately, this technique

⁹ Fehn, U.; Teng, R.; Elmore, D.; Kubik, P. W. *Nature* **1986**, *323*, 707-710.

¹⁰ Teng, R. T. D.; Fehn, U.; Elmore, D.; Hemmick, T. K.; Kubik, P. W.; Gove, H. E. *Nucl. Instr. Meth. Phys. Res.* **1987**, *B29*, 281-285.

¹¹ Rasmussen, K. L. *Nucl. Instr. Meth. Phys. Res.* **1989**, *B43*, 256-258.

¹² Blum, J. D.; Pellin, M. J.; Calaway, W. F.; Young, C. E.; Gruen, D. M.; Hutcheon, I. D.; Wasserburg, G. J. *Anal. Chem.* **1989**, *62*, 209-214.

requires pre-concentration to ≥ 15 ppm Os,¹³ whereas crustal concentrations of osmium can be less than 0.05 ppb.³ In our experiment, the plasma resulting from each laser shot temporarily disrupts the electric fields necessary for ion trapping, preventing ions from being accumulated over many laser shots.¹⁴ External ion sources circumvent this problem, and can be used to store the ions from many laser shots.¹⁵ In addition, coarse mass selection by time-of-flight^{15,16} or quadrupole¹⁷ filtering can be combined with standard or tailored¹⁸ ion rejection to inject and store ions selectively at the masses of interest. This prevents the ion trap from becoming saturated with ions derived from the sample matrix. The capability to accumulate the ions from many ionization events will permit the analysis of trace elements without pre-concentration. The detection limit is expected to be determined only by the number of ions that can be trapped in the cell and the dynamic range.

¹³ Blum, J. D.; Pellin, M. J.; Calaway, W. F.; Young, C. E.; Gruen, D. M.; Hutcheon, I. D.; Wasserburg, G. J. *Geochim. Cosmochim. Acta* 1990, 54, 875-881.

¹⁴ A similar loss of trapping has been demonstrated for an rf ion trap: Kwong, V. H. S. *Phys. Rev. A* 1989, 39, 4451-4454.

¹⁵ Smalley, R. E. *Anal. Instrum.* 1988, 17, 1-21.

¹⁶ Alford, J. M.; Williams, P. E.; Trevor, D. J.; Smalley, R. E. *Int. J. Mass Spec. Ion Proc.* 1986, 72, 33-51.

¹⁷ Lebrilla, C. B.; Amster, I. J.; McIver, R. T., Jr. *Int. J. Mass Spec. Ion Proc.* 1989, 87, R7-R13.

¹⁸ Chen, L.; Wang, T.-C. L.; Ricca, T. L.; Marshall, A. G. *Anal. Chem.* 1987, 59, 449-454.

Since the ionization energies of rhenium and osmium are different (7.76 and 8.28 eV, respectively¹⁹), mass-discrimination in the laser ablation process may complicate measurement of the Re/Os ratio.²⁰ Much less discrimination occurs if a second laser is used to effect non-resonant, two-photon ionization of ablated neutral atoms.²¹

The method of ion detection is an important concern. Detection by Fourier-transform mass spectrometry currently suffers from unreliable peak intensities.^{22,23} A frequency-swept bridge detector²⁴ may be preferable for careful isotope abundance measurements.

The PICS technique can probably be extended to other isotope dating schemes, such as the Sr-Rb, Sm-Nd, Lu-Hf, and U-Pb methods. Generally, these dating techniques involve dissolution of the rock sample and tedious chemical separation.²⁵ A rare exception is an *in situ* U-Pb study of lunar zircons using high resolution ion microprobe mass spectrometry.²⁶ These

¹⁹ Rauh, E. G.; Ackermann, R. J. *J. Chem. Phys.* **1979**, *70*, 1004-1007.

²⁰ Simons, D. S. *Int. J. Mass Spec. Ion Proc.* **1983**, *55*, 15-30.

²¹ Odom, R. W.; Schueler, B. In *Lasers and Mass Spectrometry*; Lubman, D. M., Ed.; Oxford: New York, 1990; Chapter 5.

²² Mitchell, D. W.; DeLong, S. E. *Int. J. Mass Spec. Ion Proc.* **1990**, *96*, 1-16.

²³ de Koning, L. J.; Kort, C. W. F.; Pinske, F. A.; Nibbering, N. M. M. *Int. J. Mass Spec. Ion Proc.* **1989**, *95*, 71-92.

²⁴ Wronka, J.; Ridge, D. P. *Rev. Sci. Instrum.* **1982**, *53*, 491-498.

²⁵ Roth, E.; Poty, B., Eds. *Nuclear Methods of Dating*; Kluwer: Dordrecht, 1989.

²⁶ Compston, W.; Williams, I. S.; Meyer, C. J. *Geophys. Res.* **1984**, *89*, B525-B534.

workers considered several isobaric interferences including $^{208}\text{PbH}^+ / ^{209}\text{Bi}^+$ and $^{186}\text{W}^{18}\text{O}^+ / ^{204}\text{Pb}^+$. Such interferences, as well as $^{87}\text{Rb} / ^{87}\text{Sr}$ and $^{176}\text{Lu} / ^{176}\text{Hf}$, for example, could be resolved by PICS using suitable reagents. Moreover, samples are often dated using several isotope schemes and this would be facilitated in the trapped-ion mass spectrometer described above. Using a single sample, analyzing the different elements and isotope ratios would be a simple matter of changing the reactant gas mixture.

Acknowledgments. We thank G. J. Wasserburg for bringing this problem to our attention and for helpful discussions. This work is supported by the National Science Foundation (grant CHE 8711567), the Office of Naval Research (grant N00014-89-J-3198), the Caltech Consortium in Chemistry and Chemical Engineering (founding members: E. I. duPont de Nemours and Company, Inc.; Eastman Kodak Company; Minnesota Mining and Manufacturing Company; Shell Development Company), and the donors of the Petroleum Research Fund, administered by the American Chemical Society. KKI is grateful to the Department of Education for fellowship support.

Chapter III

Third-Row Transition Metal Ions in the Gas Phase: Reactivity with Methane

Karl K. Irikura and J. L. Beauchamp

*Arthur Amos Noyes Laboratory of Chemical Physics
California Institute of Technology, Pasadena, California 91125*

Abstract.

Methane is spontaneously dehydrogenated in the gas phase by many metal ions of the 5d transition series. In most cases, the product MCH_2^+ undergoes further reaction, leading eventually to products such as $WC_8H_{16}^+$, which must contain at least six carbon-carbon bonds. Reactivity patterns are rationalized in terms of electronic structure. Promotion energy, exchange energy, and orbital sizes all appear to be important for both bare and simply-ligated ions. Mechanistic and structural information is sought using isotopic labeling, reactivity, and kinetics studies. Thermochemistry relevant to the partial oxidation of methane is discussed.

Introduction.

Alkane dehydrogenation is a common reaction in the gas-phase chemistry of bare transition-metal ions.¹ Reaction with methane, however, is unusual; exothermic formation of MCH_2^+ requires a metal-carbene bond strength of at least 111 kcal/mol. None of the first-row transition metal ions meets this requirement,² and in the second row, only Zr^+ has so far been found to react with methane.³ In the third row, however, both Os^+ and Ta^+ dehydrogenate more than one molecule of methane.^{4,5} We have used Fourier-transform ion cyclotron resonance spectrometry (FTICR) to investigate the

¹ Russell, D. H., Ed. *Gas Phase Inorganic Chemistry*; Plenum: New York, 1989.

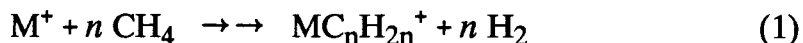
² Martinho Simões, J. A.; Beauchamp, J. L. *Chem. Rev.* **1990**, *90*, 629-688.

³ MacMahon, T. J.; Ranasinghe, Y. A.; Freiser, B. S. *J. Phys. Chem.*, submitted.

⁴ Irikura, K. K.; Beauchamp, J. L. *J. Am. Chem. Soc.* **1989**, *111*, 75-85. (Chapter I in this thesis.)

⁵ Buckner, S. W.; MacMahon, T. J.; Byrd, G. D.; Freiser, B. S. *Inorg. Chem.* **1989**, *28*, 3511-3518.

reactions of the third row ions from Hf⁺ through Au⁺ and found rapid, sequential reaction with methane to be common (eq. 1 and Figure 1). The rapid reactions are often followed by slower steps that involve extensive ligand coupling. For example, WC₈H₁₆⁺, which is formed at long reaction times, must



contain at least six carbon-carbon bonds. We believe that these reactions carry significant implications for fundamental processes in C₁ chemistry. In particular, it is clear that Fischer-Tropsch type methylene coupling need *not* require several metal centers.

Experimental.

Ions are generated in the cell of an FTICR spectrometer by ablation of metal targets with the focused output of an excimer laser (308 nm).⁶ Rapid reactions of ions containing the early metals (La,⁷ Hf, Ta, W) with oxygen-containing impurities such as H₂O and O₂ are problematic, especially at high pressures or long reaction times. Mass ambiguities are resolved using isotopically labeled methane and single, mass-selected metal isotopes. Since the laser ablation process often produces ions that are translationally and electronically excited,⁸ one must be careful to distinguish ground-state and

⁶ The use of metal oxides as sources of metal ions is discussed in Chapter VII of this thesis.

⁷ Huang, Y.; Wise, M. B.; Jacobson, D. B.; Freiser, B. S. *Organometallics* 1987, 6, 346-354.

⁸ Kang, H.; Beauchamp, J. L. *J. Phys. Chem.* 1985, 89, 3364-3367.

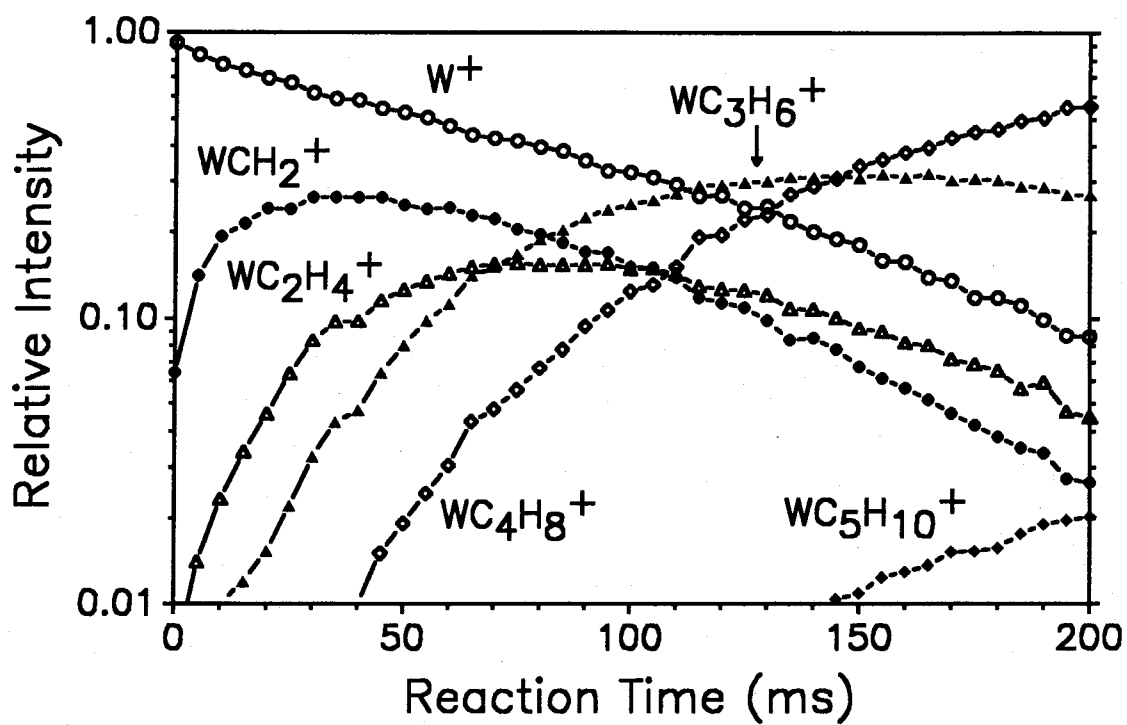


Figure 1. Reaction of labeled $^{186}W^+$ with 3.5×10^{-6} torr of methane. Successive condensation steps have relative rates of 1 : 3 : 3 : 1 : 0.05.

excited-state chemistry. In many cases, reactants other than methane were also investigated, but not in a systematic way across the period.

Results.

Both the number of rapid sequential reactions and the heaviest products observed are summarized in Table 1. Table 2 contains rate constants for reactions of various species with methane. Rate constants for reactions involving other neutral molecules are listed in Table 3.

Lanthanum. La^+ was not included in this study because its reactivity with hydrocarbons has already been investigated.^{7,9} The only available third-row $D(\text{M}^+-\text{CH}_2)$ value is $D(\text{La}^+-\text{CH}_2) = 98.2 \pm 1.4$ kcal/mol.⁹ Since the dissociation of methane to CH_2 and H_2 requires 111 kcal/mol,¹⁰ reaction of La^+ with methane is endothermic. Both single and double dehydrogenation of ethane are however exothermic. Reactions of LaCH_2^+ were not reported, since secondary products are not observed under the single-collision conditions of the ion-beam experiment.⁹

Hafnium. Although a portion of laser-ablated Hf^+ reacts with methane, thermal Hf^+ does not react spontaneously. Furthermore, HfCH_2^+ (generated by collisional activation) is readily reduced by hydrogen back to Hf^+ , confirming that the reaction with methane is endothermic. HfCH_2^+ undergoes no reaction with methane. Reaction of Hf^+ with cyclopropane yields HfCH_2^+ (as well as HfC_3H_4^+ , HfC_3H_2^+ , and HfC_2H_2^+). We therefore obtain $D(\text{Hf}^+-\text{CH}_2) = 102 \pm 9$ kcal/mol.

⁹ Sunderlin, L. S.; Armentrout, P. B. *J. Am. Chem. Soc.* **1989**, *111*, 3845-3855.

¹⁰ Unless noted, auxiliary thermochemical data are from: Lias, S. G.; Bartmess, J. E.; Liebman, J. F.; Holmes, J. L.; Levin, R. D.; Mallard, W. G. *J. Phys. Chem. Ref. Data* **1988**, *17*, Supplement No. 1.

Table 1. Electron configurations and reactivity with methane of third-row M⁺.

M ⁺	G. S. ^a	E. S. ^b	Energy ^c	(k ₁ /k _c) ^d	facile extent ^e	max. extent ^f
La ⁺	d ²	d ¹ s ¹	4.0	-	0 ^g	1 ^{h,i}
Hf ⁺	d ¹ s ²	d ² s ¹	10.4	-	0	1 ⁱ
Ta ⁺	d ³ s ¹	d ² s ²	9.1	0.3	4	4
W ⁺	d ⁴ s ¹	d ⁵	21.2	0.1	4	8
Re ⁺	d ⁵ s ¹	d ⁴ s ²	39.4	-	0	4 ^{i,j}
Os ⁺	d ⁶ s ¹	d ⁷	21.2 ^k	0.3	1	4
Ir ⁺	d ⁷ s ¹	d ⁸	6.5 ^k	0.7	2	3
Pt ⁺	d ⁹	d ⁸ s ¹	13.7	0.4	1	5
Au ⁺	d ¹⁰	d ⁹ s ¹	43.0	-	0	0

^aElectron configuration of the ground state. All atomic data are from ref. 23 unless noted. ^bElectron configuration of the lowest excited state. ^cEnergy required to reach the lowest *J*-level of the excited state (kcal/mol). ^dReaction efficiency for first CH₄ molecule (ref. 25). ^eNumber of fast, sequential reactions. ^fMaximum number of CH₄ molecules to react. ^gRef. 7. ^hRef. 9. ⁱFirst reaction induced by translational excitation. ^jReC₄H₆⁺. ^kvan Kleef, Th. A. M.; Metsch, B. C. *Physica C* 1978, 95, 251-265.

Table 2. Rates of Dehydrogenation of Methane. ^a

Ion	CH ₄	CD ₄ ^b	Ion	CH ₄	CD ₄ ^b
Ta ⁺	3.4	2.4	ReCH ₂ ⁺	1.6	1.3
TaCH ₂ ⁺	2.0	0.6	ReC ₃ H ₄ ⁺	0.4	0.5
TaC ₂ H ₄ ⁺	2.0	1.4	Os ⁺	3.4	
TaC ₃ H ₆ ⁺	1.4	1.3	OsO ⁺	6. ^c	
W ⁺	1.2	< 0.1	OsO ₂ ⁺	5. ^{c,d}	
WCH ₂ ⁺	3.0	3.4	OsOCH ₂ ⁺	2. ^{c,e}	
WC ₂ H ₄ ⁺	2.4	2.2	Ir ⁺	7.0	7.0
WC ₃ H ₆ ⁺	1.0	0.7	IrCH ₂ ⁺	1.7 ^f	3.0 ^f
Re ⁺	< 0.000014		IrC ₂ H ₄ ⁺	0.6 ^g	0.6
ReO ₂ ⁺	1.6		Pt ⁺	3.9	3.1
ReO ₂ CH ₂ ⁺	2.8		PtCH ₂ ⁺	0.09	
ReCH ⁺	4.1		PtC ₂ H ₄ ⁺	0.05	

^aRates in units of $10^{-10} \text{ cm}^3 \text{ s}^{-1}$, estimated to be accurate to $\pm 25\%$. Collision rates are $9.8 \times 10^{-10} \text{ cm}^3 \text{ s}^{-1}$ for CH₄ and $8.8 \times 10^{-10} \text{ cm}^3 \text{ s}^{-1}$ for CD₄ (ref. 25).

^bRate in the fully deuterated system. ^cRef. 4. ^dProduct is OsOCH₂⁺. ^eIncludes $\sim 20\%$ OsC₂H₄⁺ product. ^fAfter apparent relaxation that occurs at the same rate. ^gFor initially-formed IrC₂H₄⁺, which appears to become inert at the same rate (see text).

Table 3. Rates of Reactions Not Involving Methane. ^a

Ion	Neutral	Product	Rate	k _{ADO} ^b
Hf ⁺	O ₂	HfO ⁺	4.5	5.6
Hf ⁺	H ₂ O	<i>c</i>	3.8	17.7
HfO ⁺	H ₂ O	HfO ₂ H ⁺	1.6	17.7
HfOH ⁺	H ₂ O	HfO ₂ H ⁺	3.4	17.7
HfO ₂ H ⁺	H ₂ O	HfO ₃ H ₃ ⁺	0.5	17.6
Hf ⁺	C ₂ H ₆	HfC ₂ H _{2,4} ⁺	1.4	9.8
W ⁺	O ₂	WO ⁺	1.5	5.6
WO ⁺	O ₂	WO ₂ ⁺	1.0	5.6
W ⁺	CO ₂	WO ⁺	0.6	6.7
WO ⁺	CO ₂	WO ₂ ⁺	0.2	6.7
ReO ⁺	O ₂	ReO ₂ ⁺	2.2	5.6
ReO ₂ ⁺	O ₂	ReO ₃ ⁺	0.2	5.6
ReC ₂ H ₂ ⁺	C ₂ H ₆	<i>d</i>	2.9	9.7
ReC ₂ H ₄ ⁺	C ₂ H ₆	<i>d</i>	2.4	9.7
ReC ₄ H ₄ ⁺	C ₂ H ₆	<i>d</i>	2.0	9.6
ReC ₄ H ₆ ⁺	C ₂ H ₆	<i>d</i>	0.9	9.6
Re ⁺	C ₃ H ₈	[ReC ₆ H ₆ ⁺]	0.028	9.8
Ir ⁺	C ₂ H ₆	IrC ₂ H ₂ ⁺	4.4	9.7
Ir ⁺	C ₂ H ₆	IrC ₂ H ₄ ⁺	7.1	9.7
Ir ⁺	CH ₃ OH	<i>e</i>	18.	14.7

^aRates in units of 10⁻¹⁰ cm³ s⁻¹. Rates are estimated to be accurate to ± 25%.

^bCollision rate: Su, T.; Bowers, M. T. *Int. J. Mass Spec. Ion Proc.* **1973**, *12*, 347.

^cHfO⁺ and HfOH⁺ in ~ 1.6:1 ratio. ^dUndetermined dehydrogenation products.

^eReaction sequence not determined; see text.

Ethane undergoes single and double dehydrogenation to HfC_2H_4^+ and HfC_2H_2^+ (in a 2:1 ratio). These reactions imply $D(\text{Hf}^+-\text{C}_2\text{H}_4) > 32.6$ kcal/mol and $D(\text{Hf}^+-\text{C}_2\text{H}_2) > 74.6$ kcal/mol. CH_3CD_3 yields HfC_2H_4^+ , $\text{HfC}_2\text{H}_3\text{D}^+$, and $\text{HfC}_2\text{H}_2\text{D}_2^+$ in the statistical 1:3:1 ratio. Under collisional activation conditions, a product isotope ratio of 1:5:1 was obtained. HfHD^+ but not HfD_2^+ is formed by collisional activation. HfH_2^+ can not be definitively excluded because of its mass coincidence with HfD^+ .

Formaldehyde yields an increase in the HfO^+ signal as well as a peak due to HfH_2^+ . This dihydride undergoes sequential H/D exchange with added D_2 .

Tantalum. The qualitative chemistry with hydrocarbons has already been reported.⁵ Four sequential reactions with methane lead to TaC_4H_8^+ . Rate constants were not reported in ref. 5; the values from our study are included in Table 2. Reactions with residual air lead to products containing oxygen, including $\text{TaOC}_n\text{H}_{2n}^+$ ($n = 0-4$) and $\text{TaO}_2\text{C}_2\text{H}_4^+$.

Results of our own cursory collision-induced dissociation (CID) studies of TaCH_2^+ , TaC_2H_4^+ , and TaC_4H_8^+ are in accord with those reported in ref. 5. In particular, CID of TaC_4H_8^+ does not lead to any TaC_2H_4^+ . We also note that CID of the TaC_2H_2^+ fragment from TaC_2H_4^+ yields principally Ta^+ , suggesting a $\text{Ta}(\text{HC}\equiv\text{CH})^+$ structure.

Crossover experiments involving both CH_4 and CD_4 lead to H/D scrambling even in the primary product, as shown in Figure 2. This indicates that the addition of methane is reversible.

*Tungsten.*¹¹ W^+ also reacts rapidly four times with methane. Subsequent reactions occur much more slowly, but lead as far as $\text{WC}_8\text{H}_{16}^+$. There is a

¹¹ Work done in collaboration with Edmund H. Fowles.

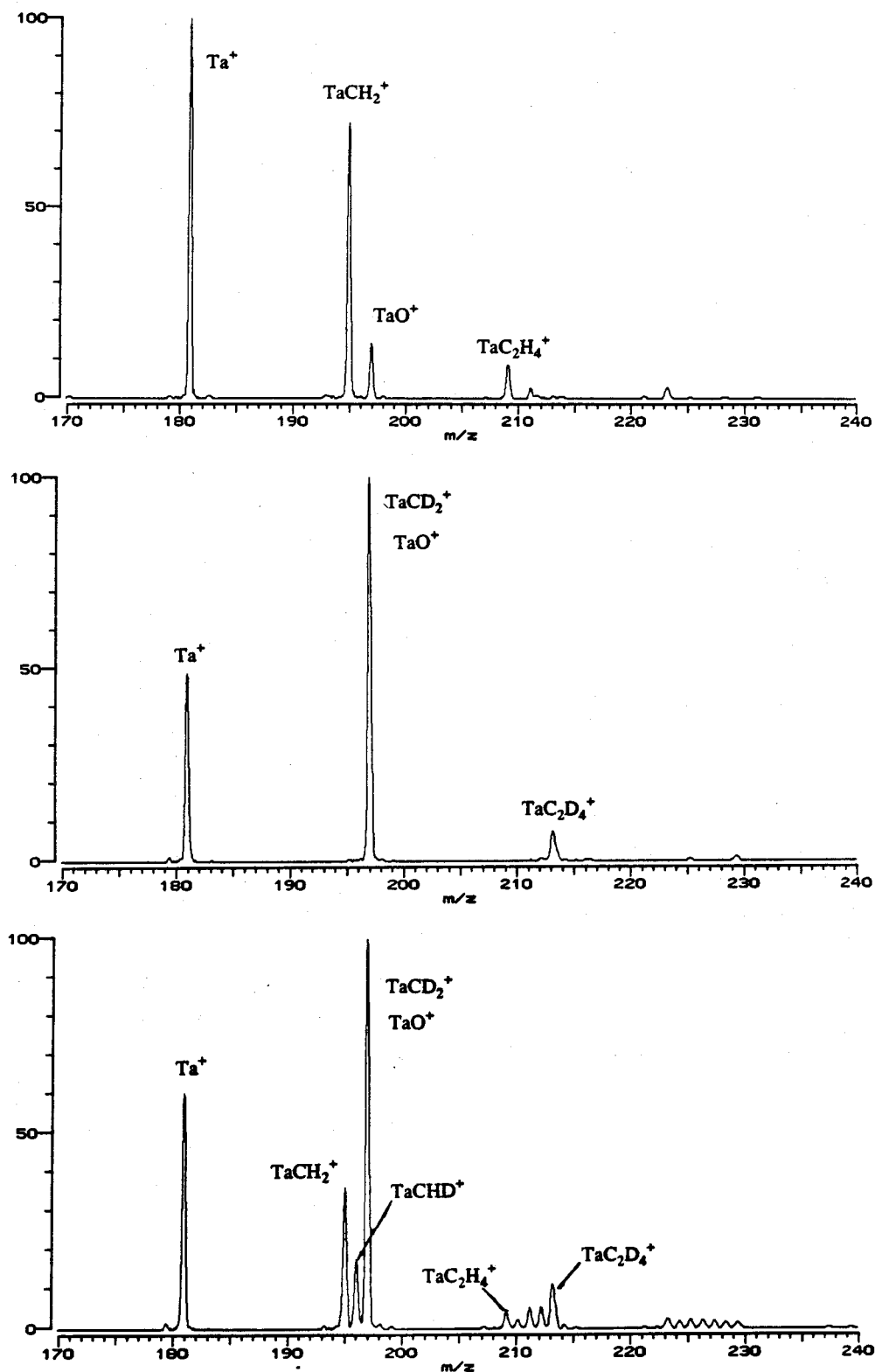


Figure 2. Reaction of Ta^+ for 20 ms. Top: With 3.3×10^{-6} torr of CH_4 . Middle: With 6.2×10^{-6} torr of CD_4 . Bottom: With both gases.

strong deuterium isotope effect; $^{13}\text{CD}_4$ (used because of the mass equality of $\text{W}^{12}\text{CD}_2^+$ and WO^+) appears to react only with excited W^+ . Subsequent reactions of $\text{W}^{13}\text{CD}_2^+$ are however spontaneous and lead to $\text{W}^{13}\text{C}_4\text{D}_8^+$. Reactions with residual air are prominent, but slower and less problematic than in the Ta^+ system.

Some attempts were made to determine the structure of the relatively stable product WC_4H_8^+ . No displacement of ethylene by CH_3CN or pulsed C_2D_4 is observed. No H/D exchange occurs with C_2D_4 . Although the spectra show substantial contamination with air, no H/D exchange with pulsed D_2 is evident for WC_4H_8^+ or WC_2H_4^+ . At least four exchanges appear to occur for WC_3H_6^+ . C_2D_4 reacts sequentially with W^+ to lead eventually to $\text{WC}_{10}\text{D}_{10}^+$. This is similar to Nb^+ , which reacts with ethylene six times to yield $\text{NbC}_{12}\text{H}_{12}^+$, and probably also involves extensive ligand coupling.⁵

The CID spectrum of WC_4H_8^+ is shown in the upper part of Figure 3. The principal products are WC_4H_6^+ (loss of H_2) and WC_2H_2^+ (loss of C_2H_6 or the equivalent). An ion of composition WC_4H_8^+ can also be generated from W^+ and cyclopentanone. Its CID spectrum is shown in the lower part of Figure 3. The two spectra are quite similar, with the exception of the larger WO_2^+ peak in the upper spectrum. This difference is probably due to the much higher total pressure, and therefore greater amount of unwanted air, in the experiment with pulsed methane. We note also that the reactivity of WC_4H_8^+ (with pulsed methane and with residual air) does not depend upon whether the ion is generated from methane or from cyclopentanone. An attempt to generate $\text{W}(\text{C}_2\text{H}_4)_2^+$ from W^+ and ethane was unsuccessful; WC_2H_2^+ is the dominant initial product (implying $D(\text{W}^+-\text{C}_2\text{H}_2) > 74.6$ kcal/mol). Likewise, reaction of

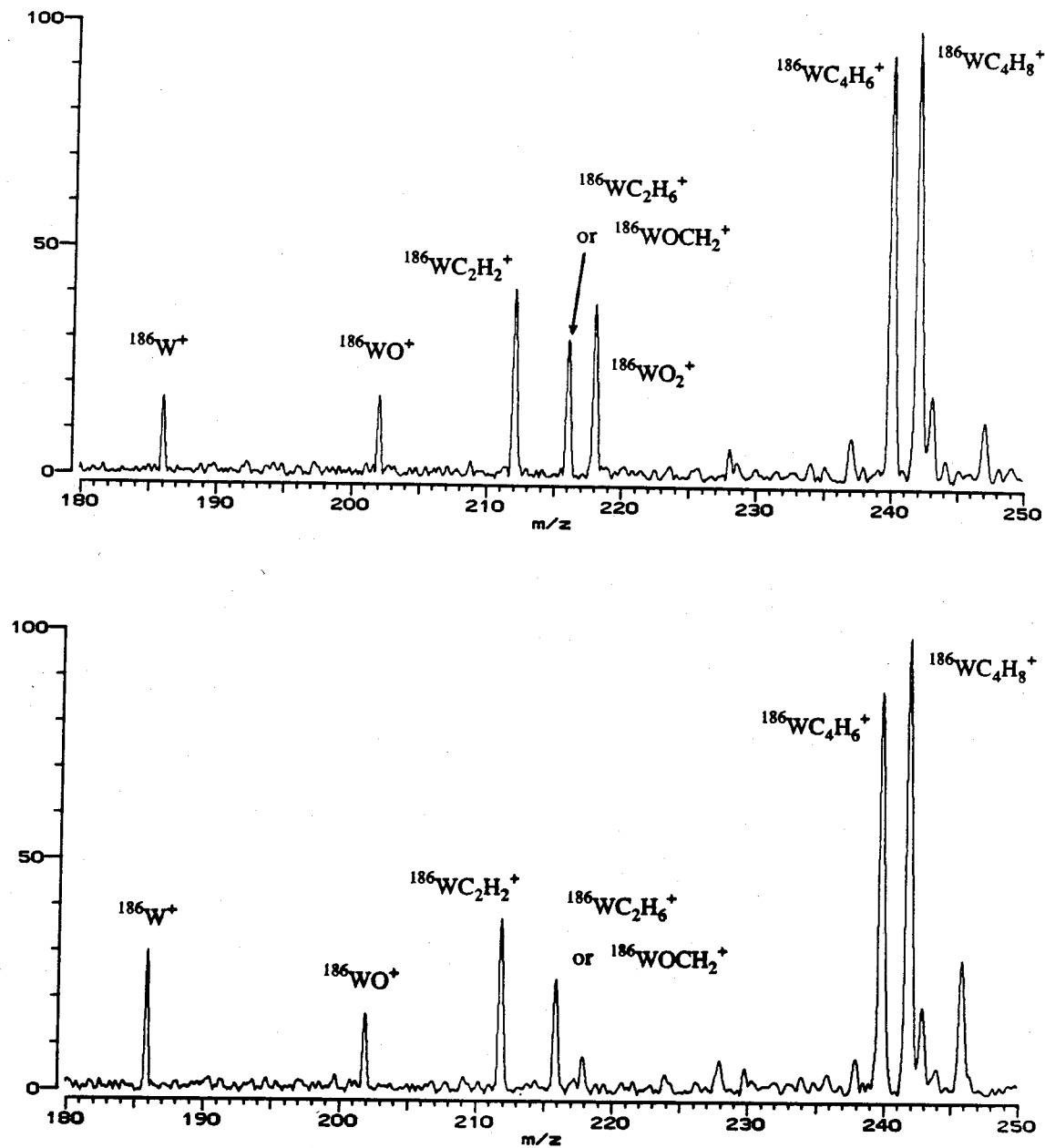


Figure 3. Collision-induced dissociation of $^{186}\text{WC}_4\text{H}_8^+$ in 9×10^{-6} torr of argon. Top: $^{186}\text{WC}_4\text{H}_8^+$ generated by reaction of $^{186}\text{W}^+$ with pulsed CH_4 . Bottom: $^{186}\text{WC}_4\text{H}_8^+$ generated by reaction of $^{186}\text{W}^+$ with cyclopentanone.

W^+ with acetone yields mainly $WC_3H_2O^+$, $WOCH_2^+$, and possibly WO^+ , but no $W(CH_2)_2^+$.

There is kinetic evidence for more than one isomer of $WC_4H_8^+$. After it forms rapidly in methane, half of the $^{186}WC_4H_8^+$ (242 amu) reacts to give a species at 244 amu (probably $WOC_3H_6^+$) which in turn reacts completely to give a peak at 246 amu (probably $WO_2C_2H_4^+$). The other half of the $WC_4H_8^+$ is unreactive. This partial reactivity is observed even when the $^{186}WC_4H_8^+$ is not subjected to isolation pulses, so it is not the result of inadvertent collisional activation. Likewise, preparing $^{186}WC_4H_8^+$ from isolated $^{186}WC_3H_6^+$ results in the same kinetic behavior. We note that the dual reactivity is easily explained if part of the peak at 242 amu is due to $WC_3H_4O^+$, possibly formed by reaction of $WC_3H_6^+$ with O_2 . Experiments using $^{13}CH_4$ would resolve this ambiguity.

In connection with the observation of oxygenated species, reactions with H_2O , O_2 , and CO_2 were briefly studied. WO^+ is the initial product in all cases; the rate constants that were measured are included in Table 3.

Rhenium. Like Hf^+ , Re^+ reacts endothermically with methane. The product can also be reduced with H_2 back to the atomic ion. $ReCH_2^+$ reacts quickly with methane to produce $ReC_2H_4^+$. Similarly, although Re^+ does not react spontaneously with ethane, $ReC_2H_2^+$ and $ReC_2H_4^+$ react sequentially. Reaction of Re^+ with propane is very slow, implying either a reaction barrier or slight endothermicity. The initial product is difficult to identify because it reacts at a much greater rate than it is formed. $ReC_6H_6^+$ is the most prominent and persistent product in both the ethane and propane sequences. Re^+ is unreactive with O_2 , but ReO^+ reacts twice to give ReO_3^+ . Since the failure of Re^+ to react with methane was shown to be thermodynamic rather than kinetic, it is reasonable to suppose the same for the failure to react with O_2 .

Cyclopropane reacts with Re^+ to give ReCH_2^+ (as well as ReC_3H_2^+ and ReC_3H_4^+). Ethylene oxide is also reactive, with products including both ReO^+ and ReCH_2^+ . The rate of this reaction decreases with increasing kinetic energy, resulting in an apparent increase in Re^+ reaction rate with time. In addition, the isotope isolation procedure imparts sufficient kinetic energy to the selected ion (such as $^{187}\text{Re}^+$) to cause a substantial drop in the reaction rate.

The reactions described above imply $D(\text{Re}^+-\text{CH}_2) = 102 \pm 9$ kcal/mol and also $D(\text{Re}^+-\text{O}) = 102 \pm 17$ kcal/mol (with the upper limit somewhat tentative). The lower bounds $D(\text{ReO}^+-\text{O}) > 119$ kcal/mol and $D(\text{ReO}_2^+-\text{O}) > 119$ kcal/mol are also established.

Evidence for partial oxidation of methane was sought in mixtures of methane and oxygen. Collisional activation is necessary to initiate reaction. The ReO^+ thus generated reacts with CH_4 exothermically to form ReOCH_2^+ , in analogy to OsO^+ .⁴ Another method for generating ReO_n^+ ions is by electron impact on the vapors above heated ReO_3 .^{6,11} ReO_2^+ thus formed reacts with methane twice to give $\text{ReO}_2\text{C}_2\text{H}_4^+$. This is unlike OsO_2^+ , which undergoes double bond metathesis to OsOCH_2^+ followed either by a second metathesis step (to OsC_2H_4^+) or simple dehydrogenation (to $\text{OsOC}_2\text{H}_4^+$).⁴ ReO_3^+ appeared to be reduced by methane to ReO_2^+ , but some reduction occurred in the absence of added methane and this reaction requires further study. ReO_2^+ and OsO_2^+ are similar in their reactions with ammonia; sequential metathesis occurs to form the corresponding MN_2H_2^+ species.

Osmium. The reactions of OsO_n^+ ($n = 0-4$) with methane have been studied previously;⁴ rate constants are included in Table 2. A solid solution of osmium and rhenium in iron was available from the study described in Chapter II of this thesis.¹¹ For the present study, Os^+ was generated by laser ablation of

this solution, since metallic osmium is commercially available only as a powder or sponge. The rate measured for the reaction with methane is in agreement with the value in ref. 4. Reaction with O_2 slowly generates OsO_n^+ ($n = 1-3$), but the reaction sequence was not determined with confidence and additional double-resonance experiments are needed.

Iridium. Ir^+ reacts three times with methane to give $IrC_3H_6^+$. Subsequent reactions involve residual oxygen and generate $IrC_2H_4O^+$, $IrC_3H_2O^+$, and $IrC_4H_4O^+$. Timeplots of the reaction of $IrCH_2^+$ with methane show an apparent increase in rate with time. This behavior persists even when the $IrCH_2^+$ is not subjected to isolation pulses that could affect its translational energy. As illustrated in Figure 4, a good fit to the data can be obtained using a kinetic model in which the initially-formed $IrCH_2^+$ must undergo a relaxation step before it can react further.¹² The rate of reaction of $IrCH_2^+$ (and to a lesser extent, of Ir^+) decreases with increasing ion kinetic energy. As a result, rates often appear lower when measured using a single isotope of iridium instead of the natural combination of isotopes. We also note that the reactivity of $IrCH_2^+$ with methane is enhanced when O_2 is added as a buffer gas.

At long reaction times, the reaction of $IrC_2H_4^+$ with methane appears to stop. This behavior can be modeled using a scheme in which the initially-formed $IrC_2H_4^+$ is slowly converted to an unreactive form.

Reactions with ethane were briefly investigated. Sequential single and double dehydrogenation are the principal processes (implying $D(Ir^+-C_2H_4) >$

¹² The procedure used for curve-fitting is described in Chapter VII of this thesis. In every fit, the excited $IrCH_2^+$, denoted $(IrCH_2^+)^*$, has been found to relax at a rate equal to the rate of the subsequent reaction of relaxed $IrCH_2^+$. The significance of this peculiar coincidence is unclear at this time, but may indicate that the kinetic model is oversimplified.

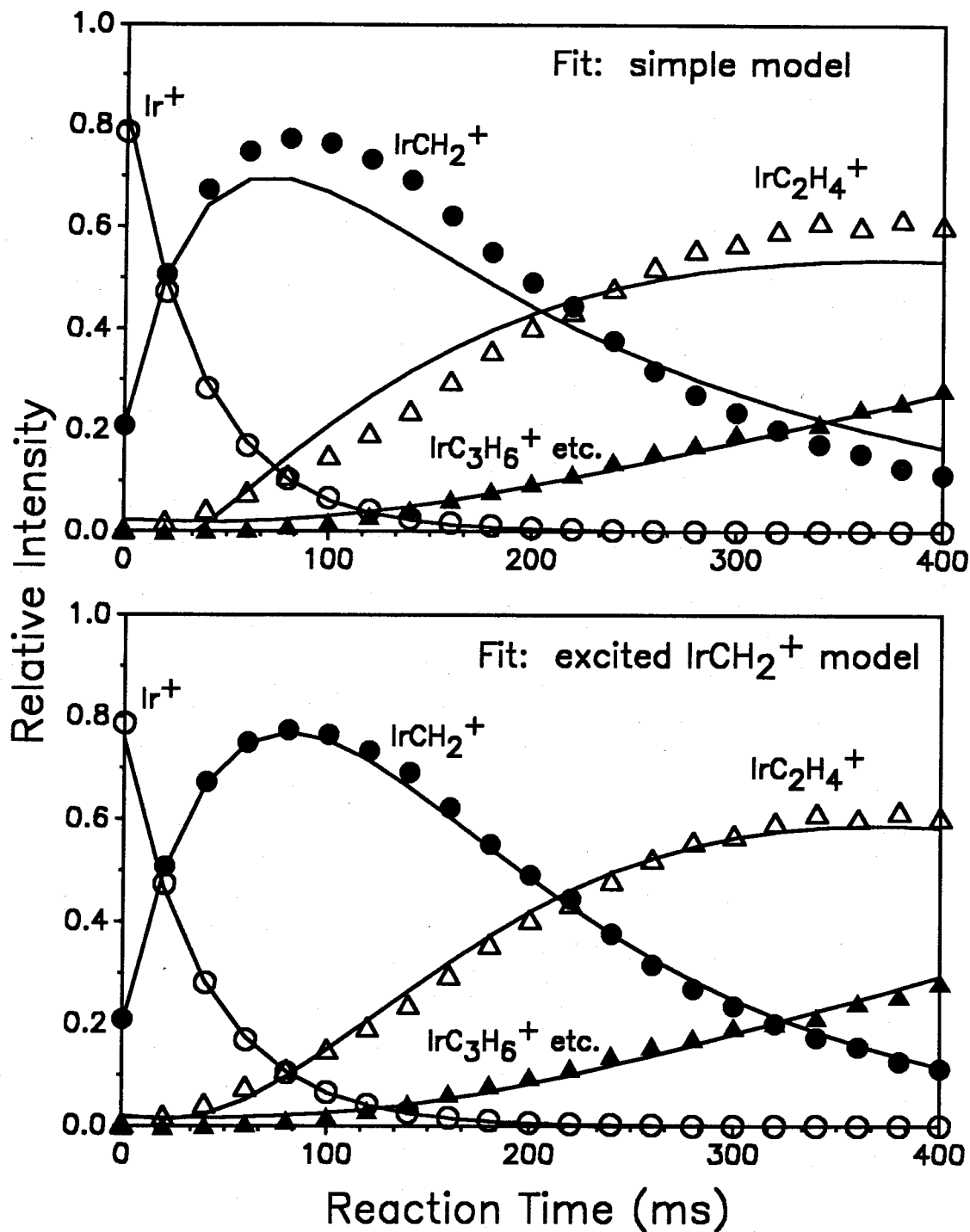


Figure 4. Reaction of $^{193}\text{Ir}^+$ with 1.3×10^{-6} torr of methane. Top: Least-squares fit using the simple kinetic model $\text{Ir}^+ \rightarrow \text{IrCH}_2^+ \rightarrow \text{IrC}_2\text{H}_4^+ \rightarrow$ subsequent products. Bottom: Fit assuming initially unreactive IrCH_2^+ , that is, $\text{Ir}^+ \rightarrow (\text{IrCH}_2^+)^* \rightarrow \text{IrCH}_2^+ \rightarrow \text{IrC}_2\text{H}_4^+ \rightarrow$ subsequent products.

32.6 kcal/mol and $D(\text{Ir}^+-\text{C}_2\text{H}_2) > 74.6$ kcal/mol), although there are minor products that appear to contain odd numbers of carbon atoms. In contrast to the abundant formation of ReC_6H_6^+ from Re^+ , no trace of IrC_6H_6^+ is evident in the Ir^+ system. Instead, IrC_6H_8^+ and $\text{IrC}_6\text{H}_{10}^+$ dominate at long reaction times.

In connection with the much-sought direct conversion of methane to methanol, reactions with methanol were examined briefly. As with methane, there is an apparent increase in rate over time when a single iridium isotope is selected. The reason is again thought to be a reaction cross section that decreases rapidly with increasing kinetic energy. Natural abundance Ir^+ yields clean, pseudo-first order kinetics. The products are IrCO^+ , IrCH_2O^+ , and a small amount of IrH_2^+ . No IrO^+ or IrCH_2^+ is formed. Exothermic formation of the dihydride requires that the average Ir-H bond strength be at least 63 kcal/mol. If IrH_2^+ is a dihydrogen complex, then $D(\text{Ir}^+-\text{H}_2) > 22$ kcal/mol.¹³ Substantial IrCH_3OH^+ is also formed, presumably by displacement of the CO ligand in IrCO^+ by CH_3OH . Dehydrogenation and ligand substitution continue to predominate in subsequent reaction steps. At long reaction times, the spectrum is dominated by a peak corresponding to $\text{IrC}_4\text{H}_8\text{O}_4^+$.

Platinum. Pt^+ reacts sequentially to give species as high as $\text{PtC}_5\text{H}_{10}^+$. Only the first step is efficient. These reactions have not yet been confirmed using CD_4 .¹⁴ An attempt to produce PtO^+ by collisional activation in O_2 was

¹³ For comparison, there is an estimate $D(\text{Cp}'\text{Cr}(\text{CO})_2-\text{H}_2) \sim 16.7 \pm 1.2$ kcal/mol: Howdle, S. M.; Healy, M. A.; Poliakoff, M. *J. Am. Chem. Soc.* **1990**, *112*, 4804-4813.

¹⁴ Our attempt was spoiled by major impurities which were produced by the ion pump; see Chapter VII in this thesis.

unsuccessful.

Gold. An extensive study of the gas-phase chemistry of Au^+ has been published.¹⁵ Although Au^+ will slowly dehydrogenate ethane, it is unreactive with methane. In the present work, Au^+ was inadvertently generated by laser ablation of a gold mesh that covered the laser target. In accord with the prior work, no reaction was observed with methane. A lower limit $D(\text{Au}^+-\text{CH}_2) > 95$ kcal/mol has been established.¹⁵

Mercury. Hg^+ was not included in this study. It is not expected to react with methane because its $d^{10}s^1$ electron configuration cannot form a double bond.

Discussion.

Reactivity. Dehydrogenation of methane was initially surprising. However, bonds to third-row transition metals are generally stronger than those to metals of the first and second rows.² This may be attributed to the lanthanide contraction and to relativistic effects.¹⁶ Changes in orbital size and stability lead to increased overlap and a reduced loss of exchange energy upon bonding.¹⁶⁻¹⁸ As a result, third-row metals are more reactive than their lighter

¹⁵ Chowdhury, A. K.; Wilkins, C. L. *J. Am. Chem. Soc.* **1987**, *109*, 5336-5343.

¹⁶ (a) Pyykkö, P. *Chem. Rev.* **1988**, *88*, 563-594. (b) Ziegler, T.; Snijders, J. G.; Baerends, E. J. In *The Challenge of d and f Electrons*; ACS Symposium Series 394; Salahub, D. R.; Zerner, M. C., Eds.; American Chemical Society: Washington, D. C., 1989; Chapter 23.

¹⁷ (a) Ohanessian, G.; Brusich, M. J.; Goddard, W. A., III *J. Am. Chem. Soc.* **1990**, *112*, 7179-7189. (b) Ohanessian, G.; Goddard, W. A., III *Acc. Chem. Res.* **1990**, *23*, 386-392.

¹⁸ Schilling, J. B.; Beauchamp, J. L. *Organometallics* **1988**, *7*, 194-199.

congeners. We note in this context that the transition metal dications Nb^{2+} , Ta^{2+} , and Zr^{2+} have also been found to undergo sequential reactions with methane.^{3,19} The high charge in the dications is expected to cause substantial orbital contraction, which may be responsible for the very strong bonds in these systems (e.g., $D(\text{Nb}^{2+}\text{-CH}_2) = 197 \pm 10 \text{ kcal/mol}^{19\text{a}}$). The double charge is also expected to lead to a deeper well for the initial ion-molecule complex, so that more energy is available for overcoming reaction barriers.

Variations in bond energies to transition metal ions have successfully been rationalized in terms of the energy required to promote the metal ion from its ground state to a state that is well-suited for bonding.^{2,17,20,21} For MH^+ species, the appropriate state often involves the $d^{n-1}s^1$ configuration, but in the second and third transition series the d^n configuration is sometimes more relevant. The actual bonding will always involve both s and d orbitals to varying degrees.^{17,22} We find that the reactivity of the third row transition metal ions with methane is well-explained using a simple model in which the $d^{n-1}s^1$ configuration is considered to be required for bonding to a methylene fragment.

¹⁹ (a) Buckner, S. W.; Freiser, B. S. *J. Am. Chem. Soc.* **1987**, *109*, 1247-1248.

(b) Gord, J. R.; Freiser, B. S.; Buckner, S. W. *J. Chem. Phys.* **1989**, *91*, 7530-7536.

²⁰ Carter, E. A.; Goddard, W. A., III *J. Phys. Chem.* **1988**, *92*, 5679-5683.

²¹ Armentrout, P. B.; Sunderlin, L. S.; Fisher, E. R. *Inorg. Chem.* **1989**, *28*, 4436-4437.

²² (a) Schilling, J. B.; Goddard, W. A., III; Beauchamp, J. L. *J. Phys. Chem.* **1987**, *91*, 5616-5623. (b) Schilling, J. B.; Goddard, W. A., III; Beauchamp, J. L. *J. Am. Chem. Soc.* **1987**, *109*, 5565-5573.

Each of the unreactive third row metals is discussed below using this model. Note that although $D(M^+-CH_2)$ and $D(M^+-H)$ are correlated, as illustrated in Figure 5, there is no clear relationship with predictive value.

J -averaged atomic energy levels are ordinarily used for comparison with non-relativistic *ab initio* calculations.^{17,22} The promotion energies quoted here are instead those between the lowest J -levels in the two terms involved. For the first two transition series there is little practical difference, but spin-orbit coupling is so strong in the third row that different terms often overlap substantially. For example, the levels of the ground state ($d^2, {}^3F$) of La^+ are at 0, 2.9, and 5.7 kcal/mol. The first excited state ($d^1s^1, {}^1D$), lies among the ground state levels at 4.0 kcal/mol.²³ For the present purposes it is therefore more appropriate to refer to the lowest level in each term.

La^+ is unique in the third row because it is not subject to the lanthanide contraction. As a result, its 6s orbital is unusually large and diffuse compared with the 5d orbital,¹⁷ reducing the bonding overlap with the CH_2 moiety. In addition, as mentioned above, the $d^2 ({}^3F_2)$ ground state requires 4.0 kcal/mol to attain the more favorable $d^1s^1 ({}^1D_2)$ configuration.

Hf^+ also suffers from an inappropriate electron configuration, $d^1s^2 ({}^2D_{3/2})$, and requires 10.4 kcal/mol to reach $d^2s^1 ({}^4F_{3/2})$. Ethane is the smallest alkane with which Hf^+ will react (with about 14% efficiency). The d^9s^1 configuration (3D_3) of Au^+ lies 43.0 kcal/mol above the ground state $d^{10} ({}^1S_0)$.

²³ Experimental atomic data are from: Moore, C. E. *Atomic Energy Levels*, NSRDS-NBS 35 (reprint of NBS circular 467); U. S. Govt. Printing Office: Washington, D. C., 1971; vol. 3. Selected values are summarized in the Appendix to this thesis.

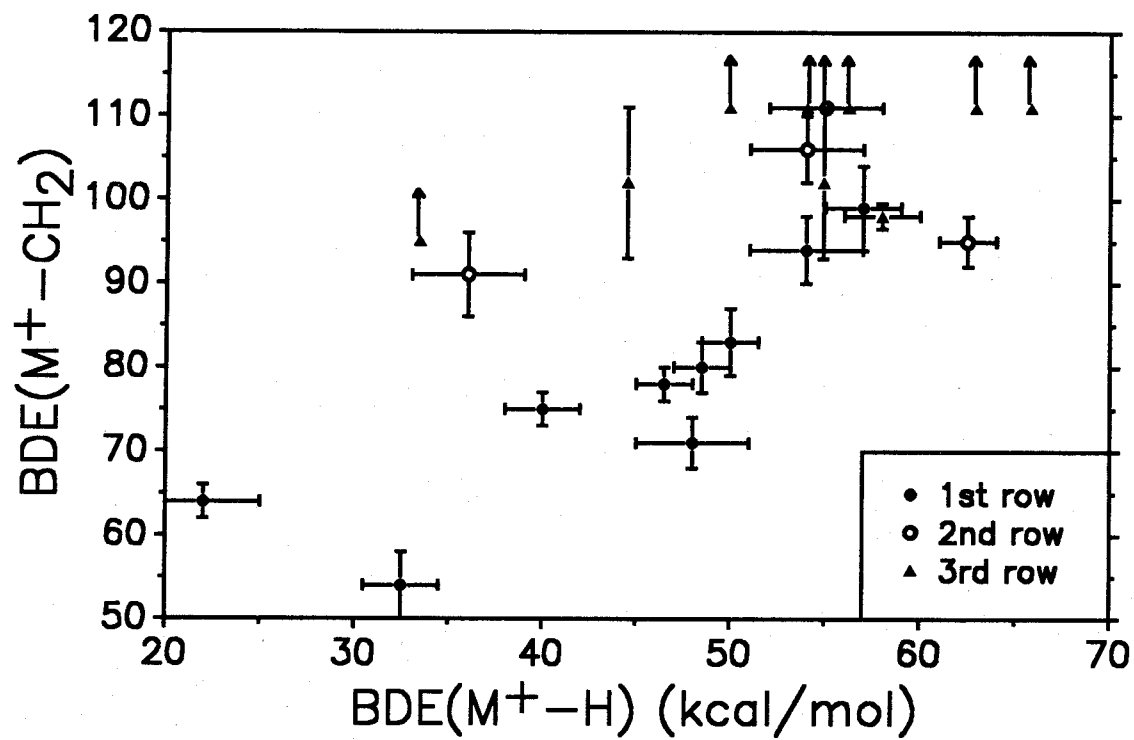


Figure 5. Bond strengths $D(M^+-CH_2)$ and $D(M^+-H)$ (from Table 5). Solid circles are for first row, open circles for second row, and triangles for third row transition metals.

Hg⁺, which was not included in this study, is not expected to react because its d¹⁰s¹ configuration cannot form a double bond.

Re⁺ has the d⁵s¹ ground state (⁷S) required for bonding, and is unreactive for a more subtle reason.^{17,20,22} Between every pair of parallel-spin electrons there exists an exchange interaction (the energy behind Hund's rule). The number of such interactions is a maximum for Re⁺, which has five s-d interactions (K_{sd}) and 10 d-d interactions (K_{dd}). Bonding results in loss of approximately 58 kcal/mol (2.5 K_{sd} + 2 K_{dd}).²⁴ This heavy penalty makes Re⁺ especially unreactive; propane is the smallest alkane with which it will react, and that reaction proceeds at only 0.3% of the collision rate.²⁵ ReCH₂⁺ loses only about 36 kcal/mol (2.5 K_{dd}) upon bonding to a second carbene fragment, and this reaction is indeed observed (15% efficiency).

Comparison Among Transition Series. The extraordinary dehydrogenation ability of the third row transition metal cations is consistent with the established differences between the first and second rows.^{18,26,27} Unlike first row metals, little loss of carbon-containing neutral molecules is observed in the second row. Instead, dehydrogenation is more common and

²⁴ Values of K_{sd} and K_{dd} for the first and second row M⁺ are available in ref. 19. Values for Re⁺ are in ref. 16a. We estimate the exchange energies for the remainder of the third row using the following simple scaling formula:

$$K(3rd) = K(2nd) + \Delta K(2nd-1st) [\Delta K(Re^+-Tc^+)/\Delta K(Tc^+-Mn^+)].$$

²⁵ Collision rate calculation: Gioumousis, G.; Stevenson, D. P. *J. Chem. Phys.* **1958**, *29*, 294-299.

²⁶ Byrd, G. D.; Freiser, B. S. *J. Am. Chem. Soc.* **1982**, *104*, 5944-5950.

²⁷ Tolbert, M. A.; Mandich, M. L.; Halle, L. F.; Beauchamp, J. L. *J. Am. Chem. Soc.* **1984**, *106*, 5675.

extensive. Thermochemistry cannot explain this difference. For example, demethanation of ethane by Ta⁺, W⁺, Os⁺, Ir⁺, and Zr⁺ is exothermic, yet only dehydrogenation is observed. The different reactivity has instead been interpreted as a kinetic effect, resulting from competition between β -hydrogen migration (leading to H₂ loss) and β -alkyl migration (leading to alkane loss).²⁷ The relevant orbital of a migrating alkyl group is much more directional than the spherical orbital of a migrating hydrogen atom. If the metal orbital is also directional, then it will be difficult to maintain overlap with the alkyl orbital during the migration process. In contrast, overlap with the hydrogen atomic orbital is easily maintained. The second and third row metals employ greater d character in their bonds.^{17,22} They are therefore expected to favor hydrogen migration and loss of H₂.²⁷ As experimental evidence for greater d orbital character in bonding, we note that the rotational barrier around a metal-ethylene bond is much greater for iridium than for rhodium.²⁸ Equivalently, there is more metallacyclopropane character in the [Ir]-C₂H₄ complex.

Structure and Mechanism. The exothermicity of reaction 1 implies very strong binding of the hydrocarbyl ligand to the metal (eq. 2). For example,

$$D(\text{M}^+-\text{C}_n\text{H}_{2n}) \geq 18n + \Delta H_f(\text{C}_n\text{H}_{2n}) \quad (\text{kcal/mol}) \quad (2)$$

considering $n = 4$, if the C₄H₈ ligand is 2-butene ($\Delta H_f = -3$ kcal/mol), the metal-olefin bond strength must be at least 69 kcal/mol. For a metallacyclopentane structure, each metal-carbon bond must also be at least 69 kcal/mol strong.²⁹ A

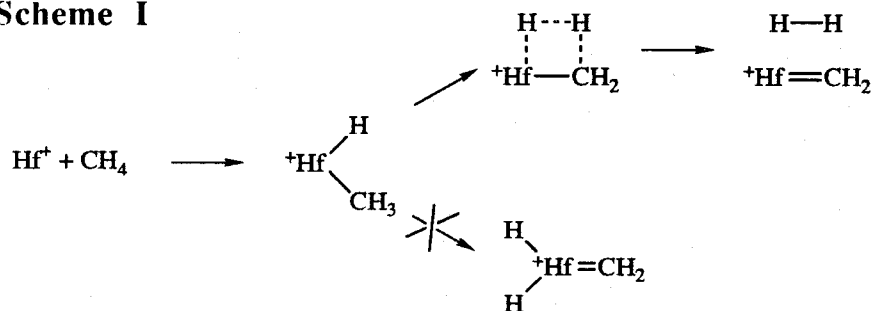
²⁸ Arthurs, M. A.; Nelson, S. M. *J. Coord. Chem.* **1983**, *13*, 29-40.

²⁹ Estimating $\Delta H_f(1,4\text{-butane-diy}) = 2 \Delta H_f(n\text{-C}_4\text{H}_9) - \Delta H_f(n\text{-C}_4\text{H}_{10})$.

bis-ethylene ($\Delta H_f = 25$ kcal/mol) structure requires the metal-olefin bond to exceed an average of 48 kcal/mol. Several possible structures are evaluated in Table 4. While the required metal-ligand bond strengths are all high, they are not sufficiently unreasonable to permit any structures to be excluded on thermodynamic grounds. Results of labeling, reactivity, and fragmentation studies must also be considered.

We suppose that oxidative addition is the initial step in all of the reactions with methane. This was a simple and successful working hypothesis in our earlier work with oxo-osmium cations.⁴ As has previously been argued for the reaction between La^+ and CH_4 ,⁹ the oxidative addition of methane to Hf^+ is probably followed by concerted $[2_s + 2_s]$ elimination of H_2 (Scheme I). The

Scheme I



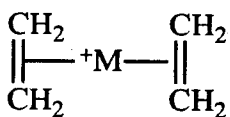
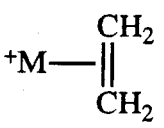
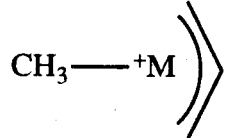
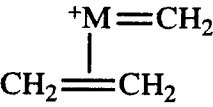
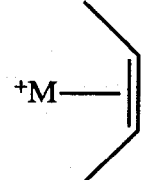
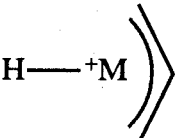
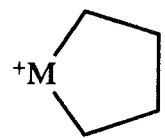

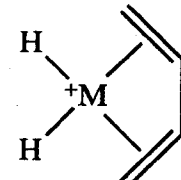
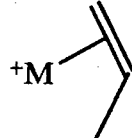
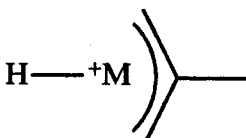
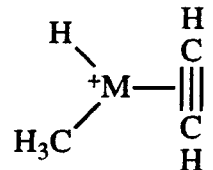
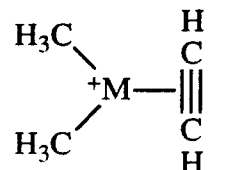
Hf(V) methylene dihydride intermediate is dismissed as involving an unreasonable oxidation state of hafnium. An analogous concerted mechanism is supposed for the H/D exchange of HfH_2^+ with D_2 . These Möbius-type reactions are symmetry-allowed when one of the bonds involves a d orbital.^{30,31}

The labeling pattern among the products of the reaction of Hf^+ with CH_3CD_3 suggests the competition illustrated in Scheme II. Initial oxidative addition is followed by a β -hydrogen migration. The ethylene dihydride

³⁰ Steigerwald, M. L.; Goddard, W. A., III *J. Am. Chem. Soc.* **1984**, *106*, 308-311.

³¹ Rappé, A. K. *Organometallics* **1987**, *6*, 354-357.

Table 4. Ligand Binding Energies Required.^a

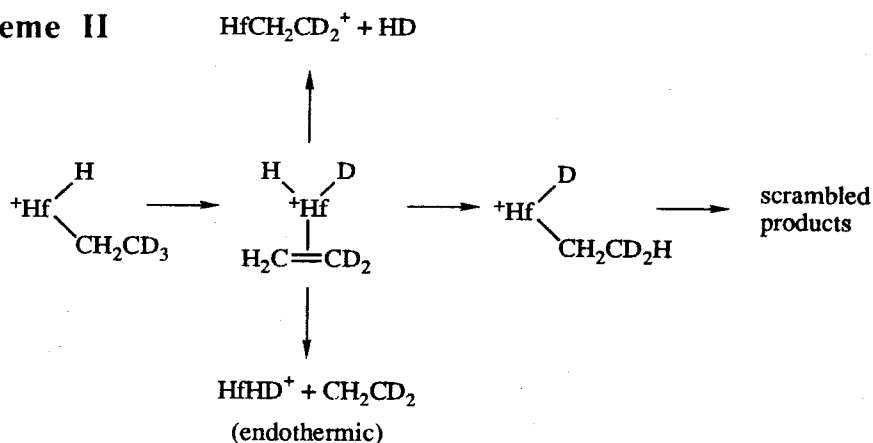
Structure	$D(M^+-C_nH_{2n})$	Structure	$D(M^+-C_nH_{2n})$
$+M=CH_2$	111		97
	49		146
	160		69
	145		138 ^c
	127 ^b		203
	59		153
	195		196

^aIn kcal/mol; calculated using eq. 2.

^bEstimating $\Delta H_f(1,3\text{-propane-diyl}) = 2\Delta H_f(1\text{-C}_3\text{H}_7) - \Delta H_f(\text{C}_3\text{H}_8)$.

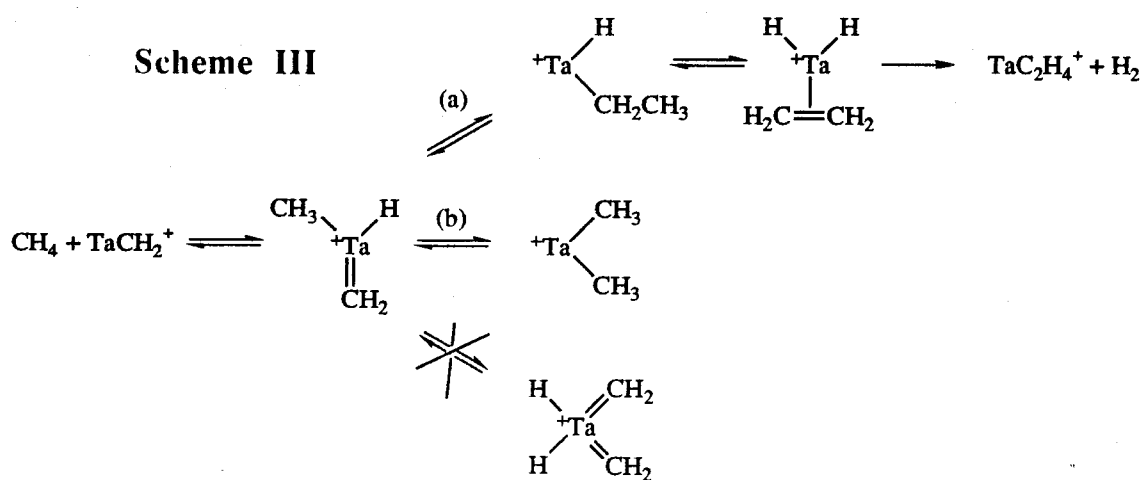
^cEstimating $\Delta H_f(1,4\text{-butane-diyl}) = 2\Delta H_f(n\text{-C}_4\text{H}_9) - \Delta H_f(\text{C}_4\text{H}_{10})$.

Scheme II



intermediate can either dissociate to products or revert to the ethyl hydride, leading to scrambling. As the internal energy of the complex is increased, dissociation appears to become more rapid and predominate. When the energy is sufficient to release the endothermic HfH_2^+ product, no scrambling occurs at all.

The results of the crossover experiment involving Ta^+ indicate that the second reaction with methane occurs by one or both of the paths outlined in Scheme III. Path *a* also leads to the TaC_2H_4^+ product, but could lead to crossover only by an unusual α -methyl migration.



Although one might hope that CID experiments would simply remove ligands, this is clearly not always the case. The most reasonable structure for

TaC_2H_4^+ is an ethylene complex. Fragmentation of this ion, however, results mainly in dehydrogenation to the acetylene complex. Loss of CH_2 and of C_2H_4 are also observed.⁵ Third row M^+ ions react with ethane to yield mostly $\text{M}(\text{C}_2\text{H}_2)^+$ and no MH_2^+ . Activation of $\text{M}(\text{C}_2\text{H}_4)^+$, the probable intermediate in the reaction with ethane, is therefore expected to give mostly $\text{M}(\text{C}_2\text{H}_2)^+$ and little M^+ , as observed.

Both C_2D_4 and CH_3CN fail to displace ethylene from WC_4H_8^+ . In addition, CID of TaC_4H_8^+ leads to loss of neither ethylene nor CH_2 .⁵ These results argue against a *bis*-ethylene structure. The lack of H/D exchange with C_2D_4 or D_2 implies that there are no hydride ligands in WC_4H_8^+ . The similar reactivity and CID patterns for the WC_4H_8^+ ions generated from methane and from cyclopentanone are consistent with similar structures. Since Ni^+ reacts with cyclopentanone to give a metallacyclopentane ion,³² it is reasonable to suppose that W^+ also forms a metallacycle. We therefore favor a metallacyclic structure for the MC_4H_8^+ ions from the sequential reactions with methane.

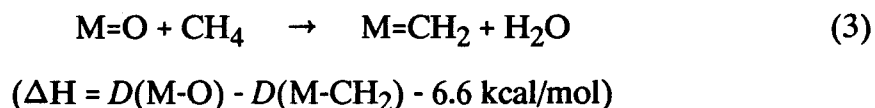
As discussed above, IrCH_2^+ appears to be reactive only after some relaxation process has occurred. Possible forms of initial excitation include translational, electronic, vibrational, and chemical (isomerization) energy. Translational excitation does indeed decrease the rate of reaction of IrCH_2^+ . It is however unreasonable to expect significant kinetic energy to be retained in the primary and secondary products, when none is apparent in the initial Ir^+ . Furthermore, the iridium-containing ions are much more massive than methane, so that little of the kinetic energy would actually be available in the center of mass. Electronic excitation is plausible if IrCH_2^+ and IrC_2H_4^+ are

³² Jacobson, D. B.; Freiser, B. S. *J. Am. Chem. Soc.* **1983**, *105*, 736-742.

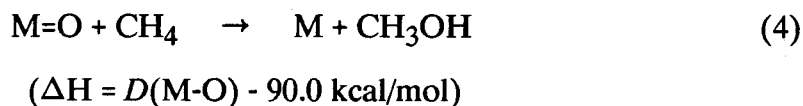
formed in unreactive spin-excited states, since changes of spin could easily be slow enough to be observable on the ICR time scale. Radiative and collisional relaxation of a vibrationally hot product would probably also be slow. Vibrationally hot products, however, suggest a very tight transition state, which is probably incompatible with the high kinetic efficiency. A chemical isomerization is less likely; it is difficult to construct reasonable pairs of isomers, to explain why unstable isomers would be formed, and to describe how they would subsequently isomerize. The increase in reactivity of IrCH_2^+ upon adding O_2 buffer gas does not distinguish among the different types of internal energy, since triplet O_2 is expected to be an effective collision partner for translational, vibrational, and spin relaxation. Additional quenching experiments are needed to identify the cause of the unusual kinetic behavior.

NbH^+ produced in the reaction of Nb^{2+} with ethane has also been shown to be internally excited.^{19b} In this case, translational excitation is quite reasonable, since the products are both cations and repel each other strongly in the exit channel.

Methane Oxidation. There is long-standing interest in oxidative coupling and direct partial oxidation of methane in order to make better use of natural gas.³³ We consider here two relevant reactions of methane, oxo-metal double bond metathesis and the conversion of methane to methanol by a metal oxide



³³ (a) Lee, J. S.; Oyama, S. T. *Catal. Rev.--Sci. Eng.* **1988**, *30*, 249-280.
 (b) Pitchai, R.; Klier, K. *Catal. Rev.--Sci. Eng.* **1986**, *28*, 13-88.



(eqs. 3 and 4). The gas phase systems may be able to provide simple models for complicated heterogeneous catalysts.

Ignoring entropic effects, reactions 3 and 4 will be spontaneous only if they are exothermic. The exothermicity requirement leads to restrictions on the bond strengths to oxygen and to methylene. Values for gas phase ions are listed in Table 5. Note that metathesis with ammonia, as observed for both ReO_2^+ and OsO_2^+ , is facilitated by the relative weakness of the N-H bonds in NH_3 . (Dehydrogenation of H_2O , CH_4 , and NH_3 requires 117, 111, and 95 kcal/mol, respectively.)

Thermochemical data and requirements are summarized graphically in Figure 6. It is clear from the figure that metal-oxo bonds weaken dramatically across a period, whereas metal-methylene bonds weaken only slightly. This is consistent with the ionic character of the oxo bond and the greater electronegativity of the later transition metals.³⁴ In the figure, the dashed horizontal line indicates the energy required to convert methanol to methane and an oxygen atom. Any metal-oxo bond that lies above this line is therefore too strong for the direct conversion of methane to methanol. The triangles indicate the calculated heat for reaction 3. Values above zero (the solid horizontal line) therefore indicate that the double bond metathesis reaction is

³⁴ Labinger, J. A.; Bercaw, J. E. *Organometallics* **1988**, *7*, 926-928.

Table 5. Transition Metal Bond Strengths $D(M^+-CH_2)$, $D(M^+-H)$, and $D(M^+-O)$.^a

M	$D(M^+-CH_2)^b$	$D(M^+-H)^b$	$D(M^+-O)^c$	M	$D(M^+-CH_2)^b$	$D(M^+-H)^b$	$D(M^+-O)^c$
Sc	99. ± 5	57. ± 2		Ru		41. ± 3	94.
Ti	94. ± 4	54. ± 3	165.	Rh	91. ± 5	36. ± 3	56.
V	80. ± 3	48.5 ± 1.5	134.	Pd		47. ± 3	50.
Cr	54. ± 4	32.5 ± 2	77.	Ag		16. ± 3	
Mn	71. ± 3	48. ± 3	59.	La	98. ± 1.5	58. ± 2	208.
Fe	83. ± 4	50. ± 1.5	75.	Hf	102. ± 9 ^g	54.9 ^f	174.
Co	78. ± 2	46.5 ± 1.5	66.	Ta	> 111. ^g	54.0 ^f	189.
Ni	75. ± 2	40. ± 2	49.	W	> 111. ^g	49.9 ^f	127.
Cu	64. ± 2	22. ± 3	33.	Re	102. ± 9 ^g	44.5 ^f	102. ± 17 ^{g,i}
Y	95. ± 3	62.5 ± 1.5	180.	Os	> 111. ^g	56.2 ^f	100. ± 12 ^j
Zr	> 111. ^d	55. ± 3	208.	Ir	> 111. ^g	65.8 ^f	60.
Nb	106. ± 4 ^{b,e}	54. ± 3	208.	Pt	> 111. ^g	62.9 ^f	60.
Mo		42. ± 3	114.	Au	> 95. ^h	33.4 ^f	
Tc		46.3 ^f					

^aIn kcal/mol. ^bFrom ref. 2 unless noted. ^cFrom data in ref. 10. ^dRef. 3. ^eRef. 5. ^fRef. 17b. ^gThis work. ^hRef. 15.

ⁱUpper limit tentative. ^jRef. 4.

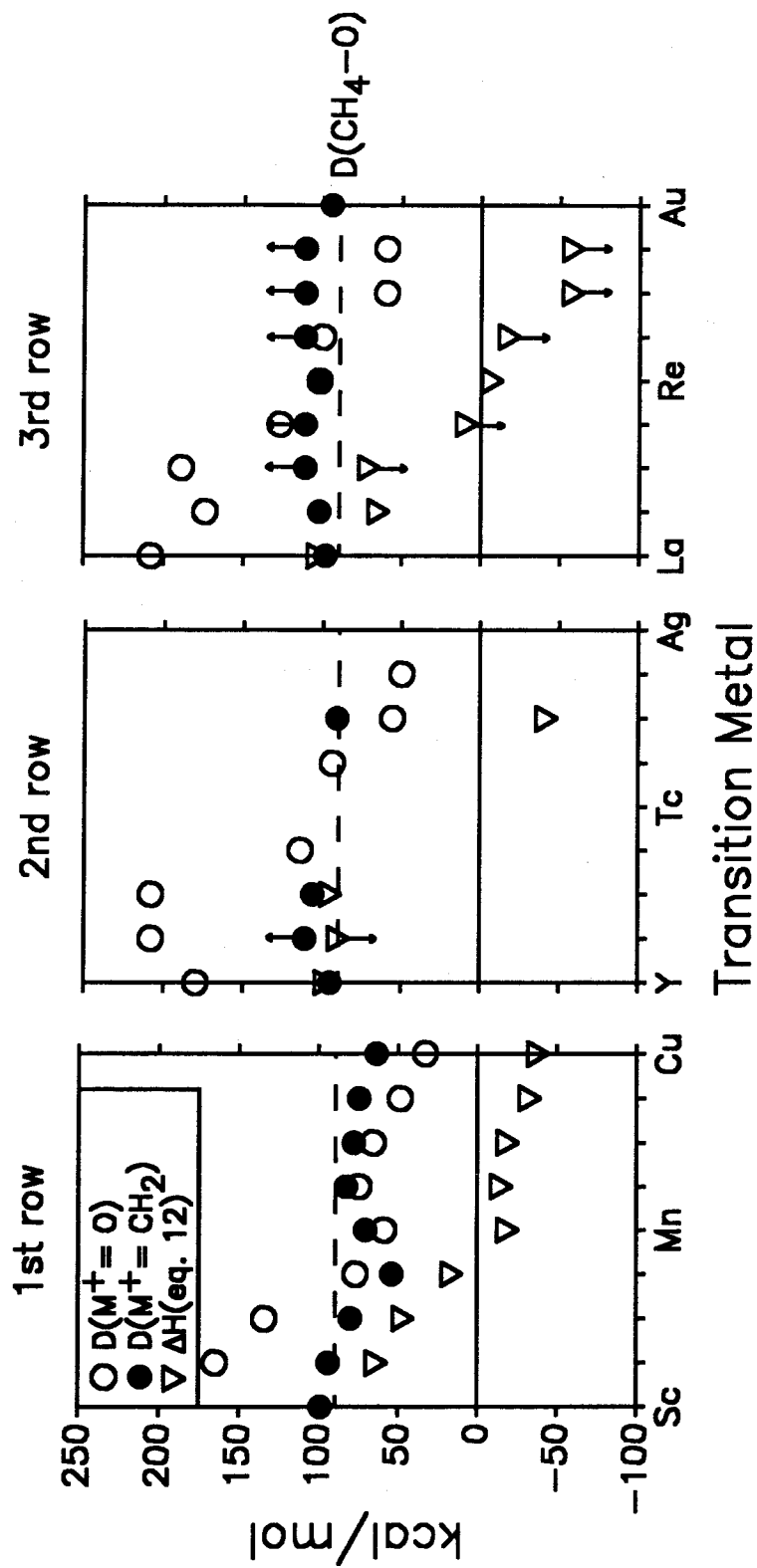
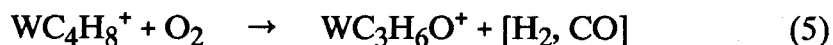


Figure 6. Energetics of metal-oxo and metal-methylene bonds. Open and solid circles represent bond strengths $D(M^+ - O)$ and $D(M^+ - CH_2)$, respectively. Triangles indicate the calculated heat of reaction 3. Bond strengths are from Table 5.

thermodynamically unfavorable. To summarize, the later metals favor both reactions 3 and 4 because their bonds to oxygen are weak.³⁵

In the present work, we have identified many ions that will activate methane. For a useful process, however, a catalytic cycle is required, and there must be some means for removing the carbon-containing ligand from the metal. No gas phase catalytic cycles have yet been found for the activation of methane. There are, however, a few reactions which lead us to believe that such cycles are indeed possible.³⁶

As noted above, $WC_4H_8^+$ reacts slowly to give products that are two, and subsequently four mass units heavier. The products are assigned as $WC_3H_6O^+$ and $WC_2H_4O_2^+$ and are presumed to occur by reaction with residual air. If the neutral reactant is O_2 , as written in equations 5 and 6, then these reactions do



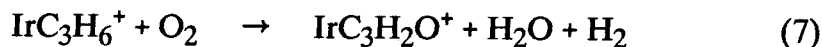
indeed involve the partial oxidation of methane. Unfortunately, the W=O bond is strong, and formation of oxo ligands will probably kill the catalytic cycle. Moreover, the neutral products may merely be synthesis gas, for which commercial processes are already available.

Another promising metal ion is Ir^+ . A number of oxygenated ions are formed in mixtures of methane and oxygen, as described in the Results section

³⁵ CrO^+ reacts with ethane to produce ethanol: Kang, H.; Beauchamp, J. L. *J. Am. Chem. Soc.* **1986**, *108*, 7502-7509.

³⁶ Although it has not been demonstrated to occur, a cycle involving OsO_2^+ is at least thermodynamically reasonable (ref. 4).

above. Although their precursors have not been carefully identified, reasonable



reaction assignments are given in equations 7 and 8. Since the bond in IrO^+ is weak (60 kcal/mol), the oxygen in the products is probably not an oxo ligand. It is likely that C-O bonds are formed instead. These products are worthy of further study both to determine their structures and to determine if the ligands can be removed as interesting products.

Conclusions.

Gas phase studies of the third row transition metal cations have extended known trends in reactivity. As one progresses from the first to the second to the third row, dehydrogenation becomes increasingly dominant and extensive, until in the third row oligomerization of methane is observed. Chemical concepts established through studies of the lighter transition metals remain applicable in the third row. Reactivity is affected by the absolute and relative sizes of the d and s orbitals. Despite the strong spin-orbit coupling, promotion and exchange energies are still helpful for understanding the pattern of reactivity across the row.

Rapid reactions of Ta^+ (ref. 5 and the present work) and of W^+ lead to MC_4H_8^+ species; we favor a metallacyclopentane structure. Some thermochemical information has been obtained, including $D(\text{M}^+-\text{CH}_2) = 102 \pm 9$ kcal/mol ($\text{M} = \text{Hf}, \text{Re}$). Reactions in mixtures of CH_4 and O_2 provide evidence for carbon-oxygen bond formation. Studies of these or similar systems

are expected to lead to gas phase models for the direct catalytic conversion of methane into useful products.

Acknowledgments.

This work is supported by the National Science Foundation (grant CHE 8711567), the Office of Naval Research (grant N00014-89-J-3198), the Caltech Consortium in Chemistry and Chemical Engineering (founding members: E. I. duPont de Nemours and Company, Inc.; Eastman Kodak Company; Minnesota Mining and Manufacturing Company; Shell Development Company), and the donors of the Petroleum Research Fund, administered by the American Chemical Society. We also thank W. H. Weinberg for donating a sample of iridium. KKI is grateful to E. H. Fowles for many helpful conversations and to the Department of Education for fellowship support.

Chapter IV

Gas-Phase Synthesis of Metalloporphyrin Ions

Karl K. Irikura and J. L. Beauchamp

*Arthur Amos Noyes Laboratory of Chemical Physics,
California Institute of Technology, Pasadena, California 91125*

Metalloporphyrins are important in biology¹ and in catalysis,² with the metal center often playing a key role in electron transfer, oxidation, or more complex chemical transformations. It is often difficult to identify the active species involved in these reactions. For example, the active intermediate in hydrocarbon activation by cytochrome P-450 is too reactive to be isolated.³ A cationic oxo-iron porphyrin complex is widely supposed to be responsible,⁴ but complexes of other metals are more tractable and are usually studied instead.⁵ In order to examine the chemistry of well-characterized metalloporphyrin ions, we are investigating methods for the generation of such species, in the gas phase, within a Fourier-transform ion cyclotron resonance spectrometer (FTICR). We report here a straightforward, fairly general procedure that we have used with success to generate a wide variety of both cationic and anionic metalloporphyrin ions.

¹ *The Porphyrins*, Dolphin, D., Ed. Academic: New York, 1979, vols. 6-7.

² (a) Meunier, B. *Bull. Soc. Chim. Fr.* **1986**, 578-594. (b) Sheldon, R. A.; Kochi, J. K. *Metal Catalyzed Oxidation of Organic Compounds*, Academic: New York, 1981, Chap. 8.

³ McMurry, T. J.; Groves, J. T. In *Cytochrome P-450: Structure, Mechanism, and Biochemistry*, Ortiz de Montellano, P. R., Ed. Plenum: New York, 1986, Chap. 1.

⁴ (a) Groves, J. T.; Watanabe, Y. *J. Am. Chem. Soc.* **1988**, *110*, 8443-52. (b) Guengerich, F. P.; Macdonald, T. L. *Acc. Chem. Res.* **1984**, *17*, 9-16. Some contrary evidence: (c) Nam, W.; Valentine, J. *J. Am. Chem. Soc.* **1990**, *112*, 4977-4979.

⁵ For example: (a) Leung, W.-H.; Che, C.-M. *J. Am. Chem. Soc.* **1989**, *111*, 8812-8818. (b) Garrison, J. M.; Bruice, T. C. *J. Am. Chem. Soc.* **1989**, *111*, 191-198. (c) Curry, M. E.; Dobson, J. C.; Seok, W. K.; Meyer, T. J. *Rec. Trav. Chim.* **1987**, *106*, 438.

Gas-phase metalloporphyrin ions, $M(P)^+$, have been known since early studies of the mass spectra of metalloporphyrins.⁶ The first reports of $M(P)^+$ in a trapped-ion spectrometer are those of Wilkins and co-workers. They identified $M(P)^+$ among the products of fast-atom bombardment or laser ablation of samples either of metalloporphyrins or of porphyrins co-deposited with metal salts.⁷ We have tested similar procedures in our search for a good source of $M(P)^+$. Pulsed CO_2 laser evaporation of dimethylated bovine hemin⁸ deposited on a stainless steel target produces a small amount of $Fe(P)^+$, but yields mostly smaller fragment ions. Excimer laser ablation of a pellet of $FeCl_2$ impregnated with porphine provides a weak and rather unstable supply of $Fe(P)^+$. While we are able to generate the species of interest, our experience indicates that these sources of $M(P)^+$ are not well-suited for further chemical studies. Subsequently, we found that many metal ions, both bare and ligated, react with porphine vapor to produce metalloporphyrin cations and anions in good yield. Porphine vapor is supplied by a small (1 mm i.d.) heated quartz tube mounted beneath the ion trap. One or two milligrams of porphine lasts for several days.

One example of $M(P)^+$ formation is illustrated in Figure 1. Fe^+ is generated by excimer laser (308 nm) ablation of an iron disk and reacts with

⁶ (a) Budzikiewicz, H. In *The Porphyrins*, Dolphin, D., Ed. Academic: New York, 1978, vol. III, Chap. 9. (b) Smith, K. W. In *Porphyrins and Metalloporphyrins*, Smith, K. M., Ed. Elsevier: Amsterdam, 1975, Chap. 9.

⁷ (a) Nuwaysir, L. M.; Wilkins, C. L. *Anal. Chem.* **1989**, *61*, 689-694. (b) Forest, E.; Marchon, J.-C.; Wilkins, C. L.; Yong, L.-C. *Org. Mass Spec.* **1989**, *24*, 197-200.

⁸ Küster, W.; Schlayer, K. *Z. Physiol. Chem.* **1927**, *168*, 294-314.

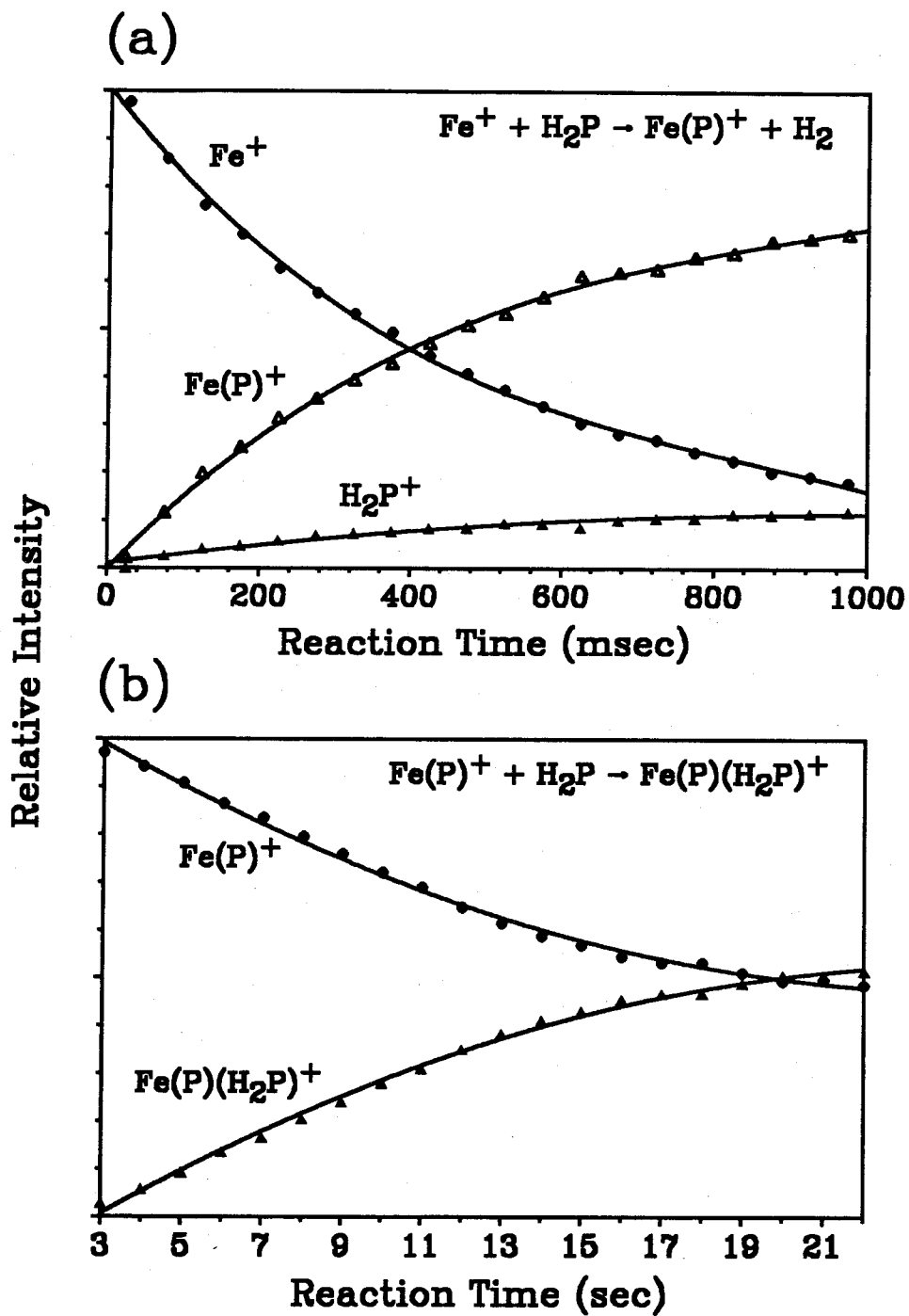
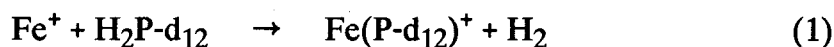


Fig. 1. (a) Laser-ablated Fe^+ reacts with H_2P by dehydrogenation to produce Fe(P)^+ , and by charge-transfer to produce H_2P^+ . (b) Fe(P)^+ slowly adds a second porphine molecule to form $\text{Fe(P)(H}_2\text{P)}^+$.

porphine⁹ to produce Fe(P)⁺ and hydrogen (Fig. 1a). Exothermic charge transfer from Fe⁺ (IP = 7.87 eV¹⁰) to porphine (IP = 6.6 eV¹⁰) generates H₂P⁺ as well. Reaction of Fe⁺ with labeled¹¹ porphine-d₁₂ yields only fully deuterated Fe(P-d₁₂)⁺, reaction 1, indicating an N,N-dehydrogenation process and therefore a metalloporphyrin structure. Although the relevant thermochemistry is not well-established, the exothermicity of reaction 1 can be used to estimate that the Fe⁺-P bond strength is greater than about 126



kcal/mol.¹² Condensation with a second H₂P molecule occurs more slowly to yield Fe(P)(H₂P)⁺ (Fig. 1b). In the presence of ligating molecules such as pyridine, complexes Fe(P)(L)⁺ are also formed. Interestingly, we have not observed any doubly-ligated metalloporphyrin ions in the systems studied thus far.

Since the porphine vapor in our vacuum system condenses before reaching the pressure gauge, we do not know the porphine pressure in our cell

⁹ Longo, F. R.; Thorne, E. J.; Adler, A. D.; Dym, S. *J. Heterocyc. Chem.* **1974**, *12*, 1305-1309.

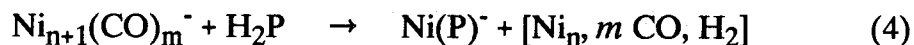
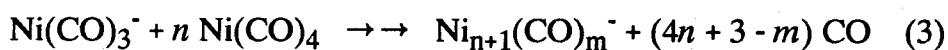
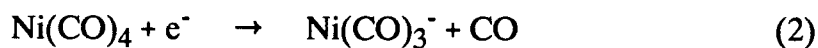
¹⁰ Lias, S. G.; Bartmess, J. E.; Liebman, J. F.; Holmes, J. L.; Levin, R. D.; Mallard, W. G. *J. Phys. Chem. Ref. Data* **1988**, *17*, Suppl. 1.

¹¹ Gladkov, L. L.; Gradyushko, A. T.; Shulga, A. M.; Solovyov, K. N.; Starukhin, A. S. *J. Mol. Struct.* **1978**, *47*, 463.

¹² We estimate $D(\text{H-PH}) = D(\text{H-P}) = D(\text{H-NC}_4\text{H}_4)$ (pyrrole), and further that $D(\text{H-NC}_4\text{H}_4) = D(\text{H-NH}_2) - D(\text{H-CH}_3) + D(\text{H-C}_6\text{H}_5)$ (benzene). Using thermochemical values from ref. 10, we reach an estimate of 115 kcal/mol for the N-H bond strength in porphine, leading to the lower limit of ~ 126 kcal/mol for removal of Fe⁺ from Fe(P)⁺.

and are unable to measure the rate of reaction 1 directly. It is, however, at least 10% as fast as proton transfer reactions that generate H_3P^+ . Since gas-phase proton transfer reactions are generally efficient, we estimate that reaction 1 occurs at least once in every 10 collisions.

Metalloporphyrin anions require a different approach, since we usually obtain no atomic anions from laser ablation of metals. Dissociative electron attachment to metal compounds often yields reactive ligated anions. For example, electron attachment to $\text{Ni}(\text{CO})_4$ yields only $\text{Ni}(\text{CO})_3^-$, which reacts with the neutral vapor to produce metal cluster ions. The cluster ions are



reactive with porphine, yielding $\text{Ni}(\text{P})^-$. This is illustrated in Figure 2. Also evident in the figure is the porphine radical anion, H_2P^- , formed by electron transfer to H_2P .¹³ Many metal-porphine and metalloporphyrin ions can be generated using these methods. Table 1 contains a list of the results obtained so far.

It is likely that the metalloporphyrin formation proceeds by sequential oxidative additive of the porphine N-H bonds to the metal center, with

¹³ $\text{Ni}(\text{P})^-$ and H_2P^- photodetachment were briefly studied using a Bausch & Lomb Xe lamp (150 W) with a monochromator. Although detachment was observed, insufficient power and lack of time resolution indicated that such experiments require a dye laser.

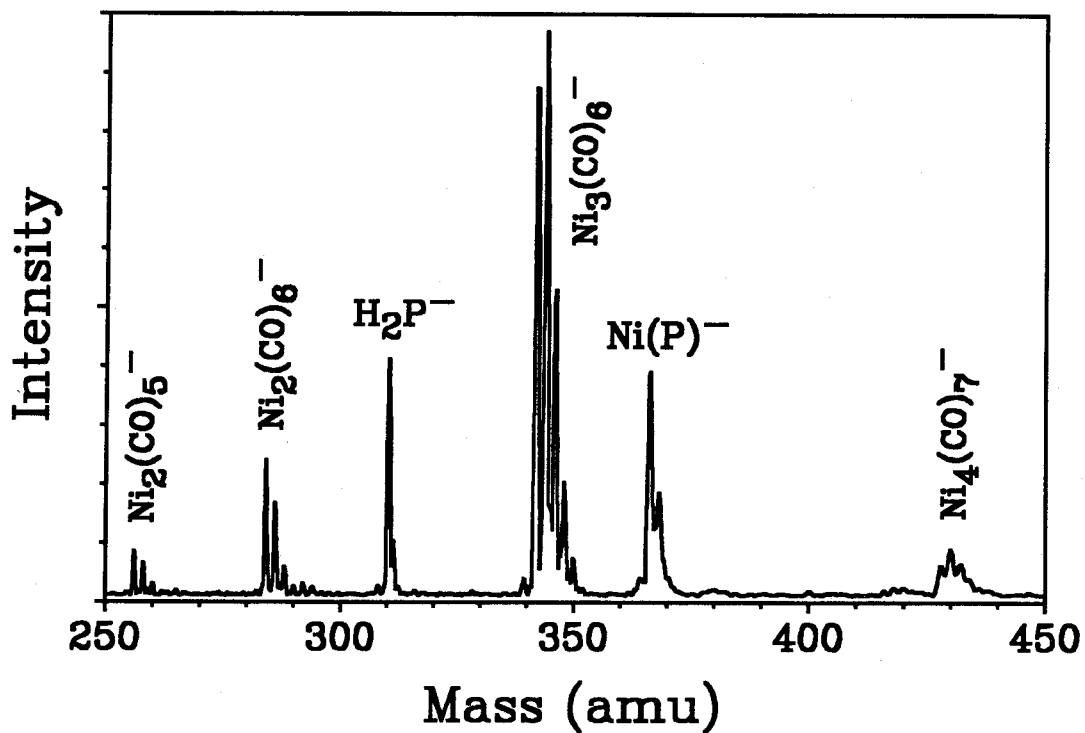


Fig. 2. Dissociative electron attachment to $\text{Ni}(\text{CO})_4$ generates $\text{Ni}(\text{CO})_3^-$, and subsequent clustering produces $\text{Ni}_n(\text{CO})_m^-$. These clusters in turn react with H_2P to yield $\text{Ni}(\text{P})^-$. Electron transfer to H_2P produces H_2P^- .

Table 1. Metal-Porphine Ions Generated

Ion	Source
Fe(P)^+	$\text{Fe}^+ + \text{H}_2\text{P}$
	$\text{Fe(CO)}_5 + \text{H}_2\text{P} + \text{e}^-$
	$\text{FeCl}_2/\text{H}_2\text{P} + \text{laser}$
$\text{Fe(P)(CH}_3\text{CN)}^+$	$\text{Fe}^+ + \text{H}_2\text{P} + \text{CH}_3\text{CN}$
Fe(P)(pyr)^+	$\text{Fe}^+ + \text{H}_2\text{P} + \text{pyridine}$
$\text{Fe(P)(H}_2\text{P)}^+$	$\text{Fe}^+ + \text{H}_2\text{P}$
Fe(P)(acetone)^+	$\text{Fe}^+ + \text{H}_2\text{P} + \text{acetone}$
Fe(P)OH^+ [minor]	$\text{Fe(P)}^+ + t\text{-BuOOH}$
Ni(P)^+	$\text{Ni(CO)}_4 + \text{H}_2\text{P} + \text{e}^-$
Ni(P)^-	
Co(P)^+	$\text{Co(CO)}_3(\text{NO}) + \text{H}_2\text{P} + \text{e}^-$
$\text{Co(H}_2\text{P)}^+$	
Co(P)^-	
$(\text{C}_5\text{H}_5)\text{Co(H}_2\text{P)}^+$	$(\text{C}_5\text{H}_5)\text{Co(CO)}_2 + \text{H}_2\text{P} + \text{e}^-$
Mn(P)^+	$\text{Mn}^+ + \text{H}_2\text{P}$
Mn(HP)^+	$\text{Mn(CO)}_5\text{CH}_3 + \text{H}_2\text{P} + \text{e}^-$
Mn(HP)^-	
Mn(P)(pyr)^+	$\text{Mn}^+ + \text{H}_2\text{P} + \text{pyridine}$
Cr(P)^+	$\text{Cr(CO)}_6 + \text{H}_2\text{P} + \text{e}^-$
Cr(P)^-	
$\text{Cu(H}_2\text{P)}^+$	$\text{Cu}^+ + \text{H}_2\text{P}$
Cu(HP)^+	
$\text{Ag(H}_2\text{P)}^+$	$\text{Ag}^+ + \text{H}_2\text{P}$

subsequent elimination of H₂ (eq. 5). Support for this mechanism comes from



the fact that Mn(HP)⁺ is the product when Mn(CO)₅CH₃ is the source of metal, while Mn(P)⁺ is formed from atomic Mn⁺. This is consistent with a methyl-containing reactant. As indicated in eq. 6,¹⁴ methane loss is expected prior to



the second oxidative addition step. The Mn(HP)⁺ product is probably better written as a hydride, MnH(P)⁺, the second insertion being driven by chelation of the metal.

We have made attempts to oxidize Fe(P)⁺ to produce Fe(P)O⁺ as a gas-phase model for the reactive centers of enzymes such as cytochrome P-450 and peroxidase. Unfortunately, we have so far been unable to get closer than Fe(P)OH⁺, formed as a minor product in the slow reaction between Fe(P)⁺ and *tert*-butyl hydroperoxide.¹⁵ Since the chemistry of the Fe(P)O⁺ moiety is strongly influenced by its environment,^{16,3} isolation in the gas phase would permit its intrinsic reactivity to be studied. We are continuing our efforts in this direction, as well as investigating other chemistry of both Fe(P)⁺ and axially-

¹⁴ The unknown number of CO ligands in eq. 6 is indicated by square brackets.

¹⁵ Reagents attempted: N₂O, ethylene oxide, O₂, NO₂, per-benzoic acid. (Per-benzoic acid: Braun, G. *Org. Synth.* 1941, *Coll. vol. I*, 431-434.) N₂O and NO₂ also failed to oxygenate Mn(P)⁺. Fe(P)⁺ is also unreactive with butane and ethyl chloride.

¹⁶ (a) Guengerich, F. P.; Macdonald, T. L. *FASEB J.* 1990, 4, 2453-2459. (b) Mandon, D.; Weiss, R.; Franke, M.; Bill, E.; Trautwein, A. X. *Angew. Chem. Int. Ed. Engl.* 1989, 28, 1709-1711. (c) Ortiz de Montellano, P. R. *Acc. Chem. Res.* 1987, 20, 289-294.

ligated Fe(P)(L)^+ . In connection with these efforts, we have prepared a table of oxygen atom affinities for reference purposes (Table 2).

Acknowledgments. We are indebted to F. R. Longo for valuable advice regarding the synthesis of porphine. This work is supported by the National Science Foundation (grant CHE 8711567), the Office of Naval Research (grant N00014-89-J-3198), and the Caltech Consortium in Chemistry and Chemical Engineering (founding members: E. I. duPont de Nemours and Company, Inc.; Eastman Kodak Company; Minnesota Mining and Manufacturing Company; Shell Development Company). KKI is grateful for fellowship support from the Department of Education.

Table 2. Oxygen Atom Affinities^a

XO	D(X-O)	XO	D(X-O)
O ₃	26	MeNO ₂	95
<i>o</i> -C ₆ H ₄ (CO ₂ H)(CO ₃ H)	32 ^b	EtOH	96
H ₂ O ₂	34.4	FeO	99. ± 5
N ₂ O	40.0	HNO ₂	103
Cl ₂ O	41	(MeO) ₂ SO	109 ^b
<i>t</i> -BuOOH	43.7 ^c	CH ₃ CHO	111.7
NO ₃	51. ± 5	Me ₂ SO ₂	112 ^b
BrO	56	H ₂ O	117.36
ClO ₂	61	O ₂	119.12
PhCH=N(O)Ph	64 ^b	MeCO ₂ H	123.3
ClO	64.2	SO	124.6
MeONO ₂	73 ^b	H ₂ CCO	125.5
NO ₂	73	CO ₂	127.19
HNO ₃	73	FeOH ⁺	132
FeO ⁺	75 ^d	SO ₂	132
PHN=N(O)Ph	77 ^b	Me ₃ PO	140
SO ₃	83.2	NO	151
CH ₂ OCH ₂	84.7	SCO	158 ^e
Me ₂ SO	86.8	H ₂ CO	179
MeOH	90.0	CO	257.3

^aThermochemical data are in kcal/mol and are from ref. 10 unless otherwise noted. ^bHolm, R. H. *Chem. Rev.* 1987, 87, 1401-1449. ^cCox, J. D.; Pilcher, G. *Thermochemistry of Organic and Organometallic Compounds*; Academic: London; 1970. ^dAlternative value = 68 ± 3: Armentrout, P. B.; Beauchamp, J. L. *J. Am. Chem. Soc.* 1981, 103, 784. ^eAlternative value = 150.: Wagman, D. D.; Evans, W. H.; Parker, V. B.; Schumm, R. H.; Halow, I.; Bailey, S. M.; Churney, K. L.; Nutall, R. L. *J. Phys. Chem. Ref. Data* 1982, 11, Suppl. 2.

Chapter V

**Prospects for the Involvement of Transition Metals in
the Chemistry of Diffuse Interstellar Clouds:
Formation of FeH^+ by Radiative Association.**

Karl K. Irikura, W. A. Goddard, III, and J. L. Beauchamp

*Arthur Amos Noyes Laboratory of Chemical Physics,
California Institute of Technology, Pasadena, California 91125*

Abstract.

Transition metals traditionally have been ignored in chemical models of interstellar clouds. Thermochemical considerations indicate that the formation of several important species can be catalyzed by transition metal ions. The importance of such chemistry depends critically upon the rate of conversion of atomic metal ions into molecular species. Potential energy curves and transition moments have been calculated and a simple model employed to determine the rate constant for the appropriate reaction of iron, FeH^+ formation by radiative association.

Introduction.

Physical processes in interstellar clouds are of general astronomical interest because of their implications for the formation of stars and planets from such clouds. Chemistry within these objects is interesting both in its own right and because of the interrelationship between chemical and physical conditions; chemical observations can lead to conclusions about cloud temperature, pressure, and history. For example, chemical considerations have led to the consensus that most clouds suffer severe mechanical shocks, and constitute important evidence that solid, granular material is present in substantial amounts.¹

The reliability of such inferences naturally depends upon the completeness of the reaction networks used to model cloud chemistry. Except for simple charge exchange, reactions of metals are given little consideration in

¹Duley, W. W.; Williams, D. A. *Interstellar Chemistry*; Academic: London, 1984. For metal abundances, see also: van Steenberg, M. E.; Shull, J. M. *Astrophys. J.* 1988, 330, 942.

such networks.^{2,3} This neglect is in general given no justification in the literature, but it probably originates in the metals' relatively low abundances and largely unknown chemistry under the exotic conditions required. Recently, however, advances have been made in understanding the chemistry of isolated, gas-phase metal ions.⁴ In addition, the low metal abundances indicate only that metal-containing species are rare, not that they are unimportant; rare elements may affect the chemistry of more abundant elements through catalytic cycles. We consider herein some possibilities for transition metal reactivity in diffuse clouds. The discussion centers on iron because it is the most abundant transition metal.

Primary Reactions of Iron. Diffuse clouds typically have temperatures of ≈ 100 K and number densities of $10^1 - 10^3 \text{ cm}^{-3}$.¹ Hydrogen comprises most of any diffuse cloud, and H atoms shield the bulk of the cloud from ultraviolet radiation at frequencies above the Lyman limit. Atoms with ionization potentials below 13.6 eV, however, are efficiently photoionized, and are present principally as ions. Discussion of metal chemistry therefore centers around ion chemistry. Only ground state ions need be considered, since the time between collisions is weeks to years, and excited states have ample time for radiative relaxation. Ternary processes can be ignored at these pressures. Although

²(a) van Dishoeck, E. F.; Black, J. H. In *Rate Coefficients in Astrochemistry*; Millar, T. J.; Williams, D. A., Eds.; Kluwer: Dordrecht, 1988; p 209.

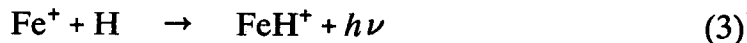
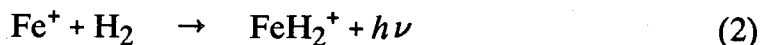
(b) Langer, W. D.; Graedel, T. E. *Astrophys. J. Suppl. Ser.* **1989**, *69*, 241-69.

³Turner, B. E. *Astrophys. J.* **1987**, *314*, 363.

⁴(a) Beauchamp, J. L. In *High Energy Processes in Organometallic Chemistry*; ACS Symposium Series 333; Suslick, K. S., Ed.; American Chemical Society: Washington, DC, 1987; Chapter 2. (b) Armentrout, P. B.; Beauchamp, J. L. *Acc. Chem. Res.* **1989**, *22*, 315.

molecules that contain transition metals could conceivably originate on grains,⁵ it is unlikely that such reactive species would be released from cold grains in substantial quantities.⁶

Relative abundances of selected species within a typical diffuse cloud are given in Table 1. Since hydrogen is by far the most abundant element in the interstellar medium,¹ we first consider reactions of Fe⁺ with H or H₂.



Reaction 1 may be dismissed immediately, since it is endothermic by 56 kcal mol⁻¹.^{7,8} The remaining two reactions are radiative associations of small molecules, which are generally slow. In addition, since the ground state of Fe⁺ is ⁶D and the sextet states of FeH₂⁺ are presumably repulsive, reaction 2 is spin-forbidden and will be exceedingly slow. Reaction 3 is probably the fastest of these processes, and we therefore consider FeH⁺ formation to be the point of entry into Fe⁺ chemistry.

⁵ Bar-Nun, A.; Litman, M.; Pasternak, M.; Rappaport, M. L. In *Interstellar Molecules*; IAU Symp. 87; Andrew, B. H., Ed.; D. Reidel: Dordrecht, 1980; p 367.

⁶ Recently, a careful search toward ζ Oph yielded no evidence for gas-phase NaH or MgH: Czarny, J.; Felenbok, P.; Roueff, E. *Astron. Astrophys.* **1987**, *188*, 155.

⁷ Elkind, J. L.; Armentrout, P. B. *J. Phys. Chem.* **1987**, *91*, 2037.

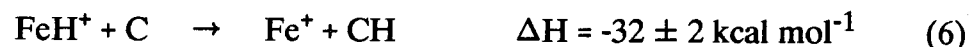
⁸ Stull, D. R.; Prophet, H. *JANAF Thermochemical Tables*, 2nd ed.; National Standards Reference Series, National Bureau of Standards 37; U. S. Govt. Printing Office: Washington, DC, 1971.

Table 1. Selected relative abundances in a typical diffuse cloud.^a

Species	Rel. Abundance
H	0.54
H ₂	0.46
O	7.2×10^{-4}
C	2.3×10^{-4}
N	1.0×10^{-4}
Mg	1.4×10^{-6}
CO	1.3×10^{-6}
Si	1.2×10^{-6}
Ar	1.2×10^{-6}
Fe	3.9×10^{-7}
Na	2.0×10^{-7}
HD	1.6×10^{-7}
OH	5.2×10^{-8}
CH	3.5×10^{-8}
Mn	2.2×10^{-8}
Ni	1.4×10^{-8}
CH ⁺	9.6×10^{-9}
CN	9.0×10^{-9}

^aLine of sight toward ζ Oph; values from ref. 1.

Secondary Reactions of Iron. Several reactions of FeH^+ with the more abundant neutral atoms (H, O, C, and N) may be envisioned. Moreover, the products are important molecules in chemical models of diffuse clouds. Reaction 4 produces H_2 , considered the "primordial" molecule. If metal-catalyzed formation of H_2 is significant, there is less need to invoke surface chemistry on grains to explain H_2 formation.



Likewise, main-group gas-phase reactions produce a lower $[\text{NH}]/[\text{OH}]$ ratio than do surface reactions, and this ratio is therefore used to gauge the importance of grain chemistry.⁹ High NH abundances do not require grains if metal ion catalysis is important.

As mentioned above, diffuse clouds are shielded from higher-frequency ultraviolet light by atomic hydrogen. Species with high ionization potentials can nevertheless be ionized by cosmic rays. The cosmic ray ionization rate is usually inferred from the abundance of either OH or HD.¹⁰ Estimates of this rate require revision if metals can generate OH or HD in significant amounts.

⁹ (a) Mann, A. P. C.; Williams, D. A. *Mon. Not. Roy. Astron. Soc.* **1984**, *209*, 33.

(b) Crutcher, R. M.; Watson, W. D. *Astrophys. J.* **1976**, *209*, 778.

¹⁰ (a) Lepp, S.; Dalgarno, A. In *Astrochemistry*; I. A. U. Symp. No. 120; Reidel: Dordrecht, 1987; p 167. (b) van Dishoeck, E. F.; Black, J. H. *Astrophys. J. Suppl. Ser.* **1986**, *62*, 109. (c) Mann, A. P. C.; Williams, D. A. *Mon. Not. Roy. Astron. Soc.* **1985**, *214*, 279. (d) O'Donnell, E. J.; Watson, W. D. *Astrophys. J.* **1974**, *191*, 89.

Reactions 4-7 are quite exothermic, and may be expected to proceed near the collision rate. Reaction 8, however, may be eliminated; laboratory experiments have demonstrated that it does not occur on the timescale of seconds at ≈ 300 K.¹¹

FeH⁺ Formation by Radiative Association. The rate of reaction 3 is essential for evaluating the expected importance of Fe⁺ chemistry. For example, if radiative association were efficient, catalysis by Fe⁺ would produce *too much* OH to be consistent with observations.¹² As one would expect, however, radiative association reactions of atoms are generally slow, and experimental rate measurements are extraordinarily difficult. Most values have therefore been calculated rather than measured.¹³ To calculate the rate of radiative association of Fe⁺ and H, we have used an approach based upon the method by Bates, as developed by Solomon and Klemperer.¹⁴ We have calibrated this method by calculating the rate of radiative association of C⁺ and H. The best current value for this latter reaction is approximately 3.5×10^{-17}

¹¹ Carlin, T. J.; Sallans, L.; Cassady, C. J.; Jacobson, D. B.; Freiser, B. S. *J. Am. Chem. Soc.* **1983**, *105*, 6320.

¹² If radiative association proceeded at the collision rate, significant contributions would be expected from reactions of iron: 1.6×10^{-5} cm⁻³ to [OH], 1.8×10^{-6} cm⁻³ to [NH], 1.7×10^{-6} cm⁻³ to [CH], and 0.042 cm⁻³ to [H₂]. The assumptions used to derive these values are described in the Results and Discussion.

¹³ (a) Bates, D. R.; Herbst, E. In *Rate Coefficients in Astrochemistry*; Millar, F. J.; Williams, D. A., Eds.; Kluwer: Dordrecht, 1988; p 17. (b) Herbst, E. *Astrophys. J.* **1985**, *291*, 226.

¹⁴ (a) Bates, D. R. *Mon. Not. Roy. Astron. Soc.* **1951**, *111*, 303. (b) Solomon, P. M.; Klemperer, W. *Astrophys. J.* **1972**, *178*, 389.

cm^3s^{-1} .¹⁵ We use this value as a benchmark for assessing the reliability of our calculation.

Calculational Details.

The rate calculation follows the method of Solomon and Klemperer with some simplifications. Essentially the same procedure has recently been applied to calculate the radiative association rates for $\text{C}^+ + \text{O}$ and $\text{C} + \text{O}$.¹⁶ In this model, the ground state atoms enter along one of the possible diabatic molecular potential energy curves. The reaction is considered to have taken place when a transition occurs to a lower electronic state. For FeH^+ , the atomic states are $\text{Fe}^+(\text{}^6\text{D})$ and $\text{H}(\text{}^2\text{S})$, and the corresponding bound molecular states are $\text{}^5\Delta$, $\text{}^5\Pi$, and $\text{}^5\Sigma$. The septet states are all repulsive (see Figure 1) and do not contribute to the reaction.

The transition probability is integrated over all classical trajectories with impact parameter b less than the classical critical value¹⁷ $b_c = (2q^2\alpha/E)^{1/4}$. The integrated probability $P(T)$ is multiplied by the Langevin collision rate¹⁷ k_L to yield a value for the temperature-dependent rate constant. Equations 9 and 10 indicate the expressions for k_L and $P(T)$.

$$k_L = 2\pi q(\alpha/\mu)^{1/2} \quad (9)$$

¹⁵ The 0 K rate was estimated by extrapolation of data from the following: Graff, M. M.; Moseley, J. T.; Roueff, E. *Astrophys. J.* **1983**, *269*, 796.

¹⁶ Dalgarno, A.; Du, M. L.; You, J. H. *Astrophys. J.* **1990**, *349*, 675.

¹⁷ Su, T.; Bowers, M. T. In *Gas Phase Ion Chemistry*; Bowers, M. T., Ed.; Academic: New York, 1979; vol. 1, Chapter 3.

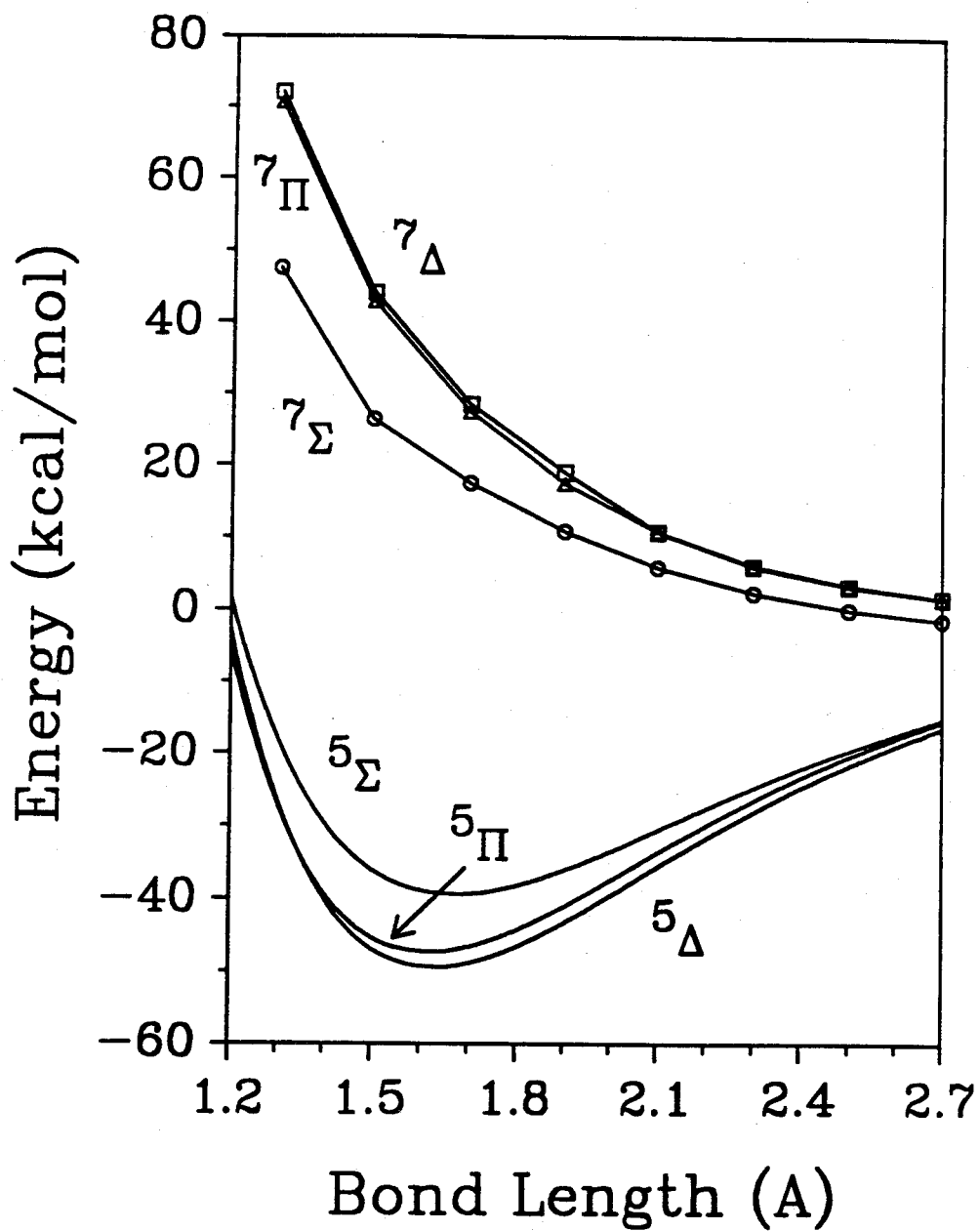


Figure 1. Calculated potential energy curves for FeH⁺. For the quintet states, best-fit Morse potentials (constrained to the D_e 's of Ref. 18) are shown.

$$P(T) \propto \int_0^\infty dv \int_0^{b_c} db \int_{r_0}^\infty dr |\mathbf{D}(r)|^2 [U_2(r) - U_1(r)]^3 \times \quad (10)$$

$$v^2 \exp(-\mu v^2/2kT) b/(b_c)^2 [v^2 - 2U_1(r)/\mu - v^2 b^2/r^2]^{-1/2}$$

In these equations, q is the elementary charge, α is the polarizability of the hydrogen atom, μ is the reduced mass of FeH^+ , and r_0 is the classical turning radius as determined from the effective potential. The potential energy functions $U_1(r)$ and $U_2(r)$ are Morse potentials generated by least-squares fits to results of *ab initio* calculations on the three lowest states of FeH^+ . The *ab initio* calculations were done at the DCCI-GEOM level as previously described by Schilling et al.¹⁸ Electric dipole moment functions $\mathbf{D}(r)$ were calculated between states at the GVB(1/2) level, and spin-orbit coupling was ignored. The potential energy and dipole moment functions are displayed in Figures 1 and 2. Fine structure and multiplicity factors are included, as discussed in Ref. 14b. An additional factor of 2 accounts for the multiplicity of the final states. No attempt is made to account for tunneling through the centrifugal barrier. At 0 K, the integrals over v and b reduce to unity, simplifying the expression for the case $P(0)$.

For comparison with the accepted rate for the radiative association of C^+ and H, the 0 K rate for CH^+ formation was calculated using the model just described. For this molecule, the Morse parameters for $U_1(r)$ and $U_2(r)$ were derived from least-squares fits to the experimental potential energy curves of

¹⁸ Schilling, J. B.; Goddard, W. A., III; Beauchamp, J. L. *J. Phys. Chem.* 1987, 91, 5616.

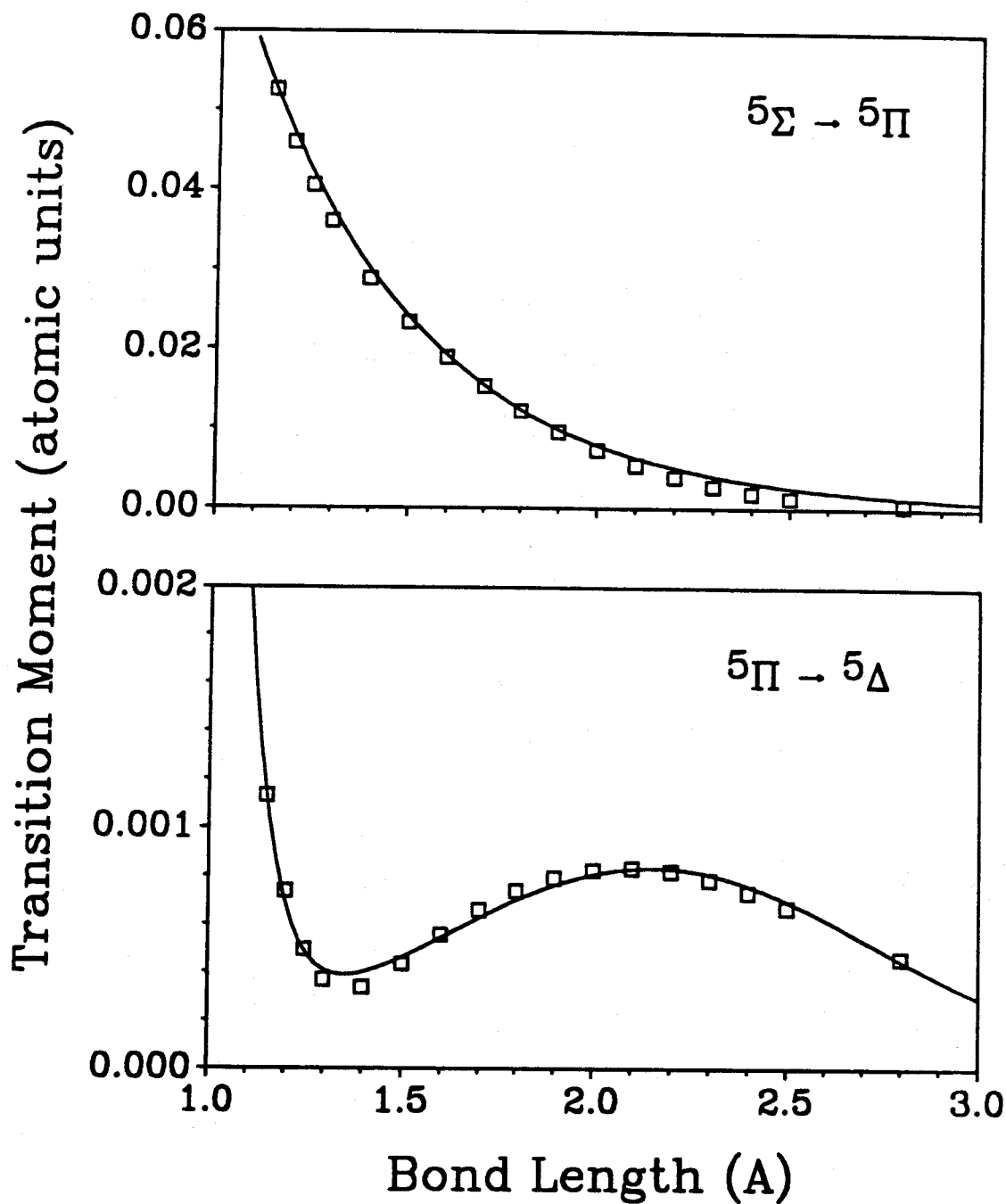


Figure 2. Calculated electric dipole moment functions for transitions in FeH^+ . Top: Transition from 5Σ to 5Π . Bottom: Transition from 5Π to 5Δ . Solid lines are fits of convenient expressions to the calculated values.

Helm et al.¹⁹, and the electric dipole moment function was a curve fit to *ab initio* results of Larsson and Siegbahn.²⁰

Techniques of much greater sophistication are necessary if accurate temperature dependence is desired.^{15,21} The simple model that we have chosen can only be expected to yield an approximate rate constant. Fortunately, this is sufficient to allow us to assess the importance of metal ion chemistry in interstellar clouds. Accurate rates are only necessary for reactions that are found to be significant.

Results and Discussion.

Potential Energy Curves. For rate calculations, the Morse potentials were fit with D_e constrained to the values of Ref. 18. This yields $D_e = 49.4, 47.3,$ and $39.4 \text{ kcal mol}^{-1}$, $r_e = 1.63, 1.62,$ and 1.67 \AA , and $a = 1.59, 1.59,$ and 1.49 \AA^{-1} for the $^5\Delta$, $^5\Pi$, and $^5\Sigma$ states, respectively. If the fit is unconstrained, we obtain instead $D_e = 61.0, 57.3,$ and $45.8 \text{ kcal mol}^{-1}$, $r_e = 1.65, 1.64,$ and 1.68 \AA , and $a = 1.39, 1.41,$ and 1.38 \AA^{-1} . These values for r_e and a are more reliable than those from the constrained fit since they describe the bonding region more accurately. The unconstrained fits lead to predictions of $\omega_e = 1690, 1650,$ and 1450 cm^{-1} (the ordering expected from the literature D_e values¹⁸) and $\omega_e x_e = 33.5, 34.0,$ and 32.8 cm^{-1} for the $^5\Delta$, $^5\Pi$, and $^5\Sigma$ states.²²

¹⁹ Helm, H.; Cosby, P.; Graff, M. M.; Moseley, J. T. *Phys. Rev. A* **1982**, *25*, 304.

²⁰ Larsson, M.; Siegbahn, P. E. M. *Chem. Phys.* **1983**, *76*, 175.

²¹ Abgrall, H.; Giusti-Suzor, A. Roueff, E. *Astrophys. J. Letters* **1976**, *207*, L69.

²² Herzberg, G. *Molecular Spectra and Molecular Structure*, 2nd ed.; Robert E. Krieger: Malabar, Florida, 1989; vol. 1, pp 100-101.

Comparison with previous calculations^{23,24} suggests that our bond lengths are too large by $\approx 0.04 \text{ \AA}$, probably because less correlation is included at the DCCI-GEOM level. For the $^5\Delta$ state, our ω_e value of 1690 cm^{-1} is probably too low; Pettersson *et al.*²³ find 1817 cm^{-1} and Sodupe *et al.*²⁴ find 1830 cm^{-1} . The latter study, however, found vibrational frequencies ranging from 1578 to 1928 cm^{-1} depending upon the level of calculation and the basis set, with no simple trends evident. It is difficult to assess the accuracy of our $\omega_e x_e$ values. We should also comment on the symmetry of the ground state of FeH^+ . A $^5\Delta$ ground state was found in two calculations^{18,23} but $^5\Pi$ was found in the third.²⁴ We favor the conclusion of the earlier calculations because of the substantially better agreement of their calculated bond energies with experiment. In addition, our DCCI-GEOM calculations indicate a $^5\Delta$ ground state.

Radiative Association Rate. For the radiative association of C^+ and H, our calculated rate at 0 K is $2.3 \times 10^{-17} \text{ cm}^3\text{s}^{-1}$, 35% less than the reference value of $3.5 \times 10^{-17} \text{ cm}^3\text{s}^{-1}$. This agreement suggests that our values for FeH^+ will also be reliable. Our corresponding 0 K rate for FeH^+ is $5.1 \times 10^{-22} \text{ cm}^3\text{s}^{-1}$. Tunneling²⁵ and vibrational relaxation are expected to increase this value only by small factors. Only a weak temperature dependence is predicted with this simple model, as illustrated in Figure 3. Essentially all reactive collisions

²³ Pettersson, L. G. M.; Bauschlicher, C. W., Jr.; Langhoff, S. R. *J. Chem. Phys.* **1987**, *87*, 481.

²⁴ Sodupe, M.; Lluch, J. M.; Oliva, A.; Illas, F.; Rubio, J. *J. Chem. Phys.* **1989**, *90*, 6436.

²⁵ Smith, I. W. M. *Astrophys. J.* **1989**, *347*, 282.

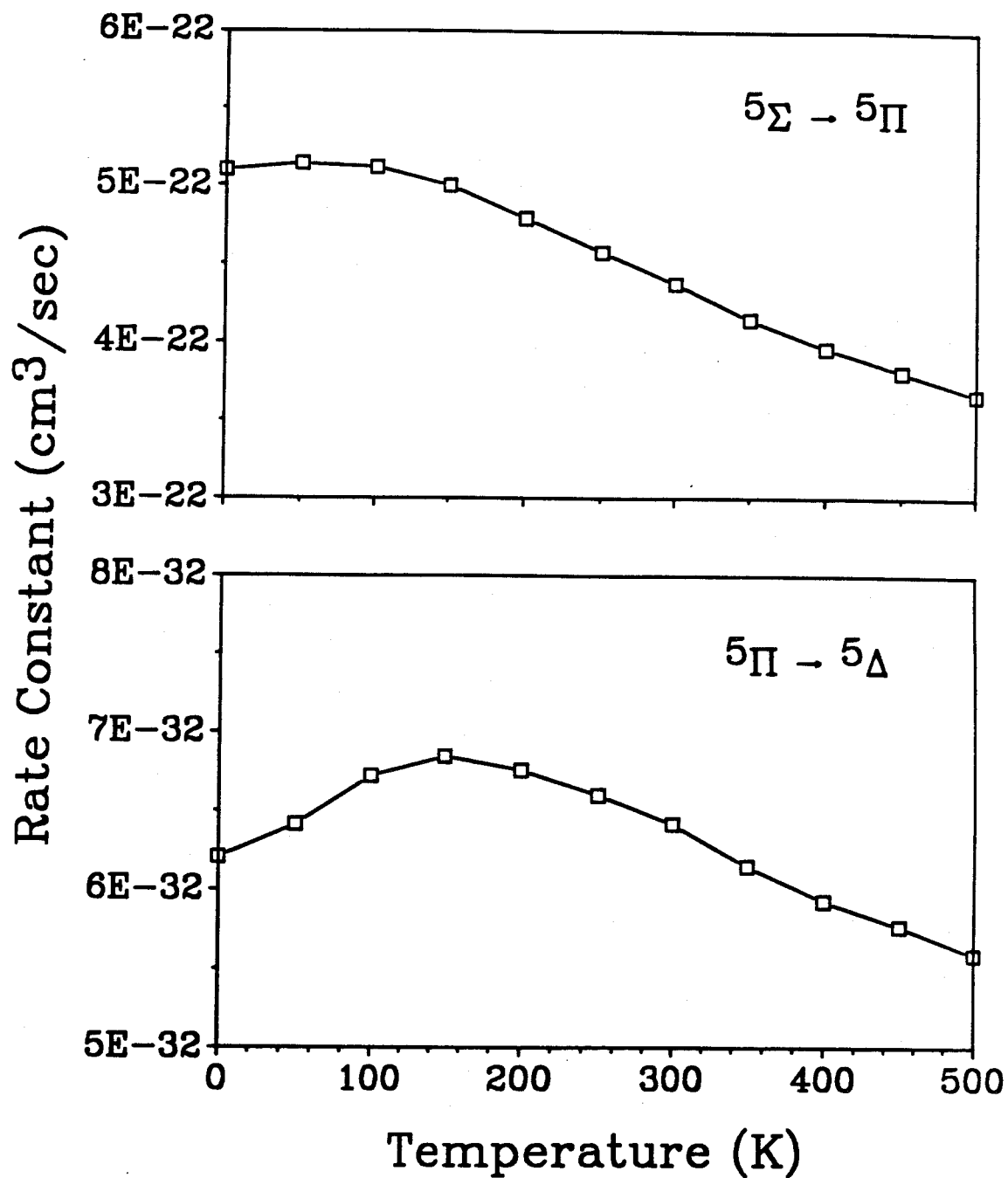


Figure 3. Contributions to the rate of radiative association of Fe^+ and H. Top: Transitions from 5Σ to 5Π . Bottom: Transitions from 5Π to 5Δ .

involve a ${}^5\Sigma \rightarrow {}^5\Pi$ transition; the 0 K contribution from ${}^5\Pi \rightarrow {}^5\Delta$ transitions is only $6.2 \times 10^{-32} \text{ cm}^3\text{s}^{-1}$, 10 orders of magnitude less.

We can estimate the chemical consequences of this rate using typical abundances¹ and considering a cloud of total density 100 cm^{-3} . Reaction 4 is assumed to account for most of the FeH^+ destruction rate ($n_{\text{H}} = 54 \text{ cm}^{-3}$), although dissociative recombination and photodissociation will also contribute. If we assume further that reaction 4 proceeds at the collision rate k_{L} (with $n_{\text{Fe}} = 3.9 \times 10^{-5} \text{ cm}^{-3}$), then we expect a steady-state FeH^+ density of $9.0 \times 10^{-18} \text{ cm}^{-3}$. Assuming that photodissociation is the major loss mechanism for the neutral products, and estimating $k = 1.0 \times 10^{-9} \text{ cm}^3\text{s}^{-1}$ for reactions 5-7, this FeH^+ density leads one to expect iron chemistry to contribute $7.7 \times 10^{-18} \text{ cm}^{-3}$ to the OH density, $8.7 \times 10^{-19} \text{ cm}^{-3}$ to [NH], $8.3 \times 10^{-19} \text{ cm}^{-3}$ to [CH], and $1.9 \times 10^{-14} \text{ cm}^{-3}$ to $[\text{H}_2]$.²⁶ It is clear from comparison with typical abundances ($n_{\text{OH}} = 5.2 \times 10^{-6} \text{ cm}^{-3}$, $n_{\text{CH}} = 3.5 \times 10^{-6} \text{ cm}^{-3}$, $n_{\text{H}_2} = 46 \text{ cm}^{-3}$) that these contributions are negligible, and that catalysis by radiatively associated FeH^+ is insignificant.

The reasons for the low radiative association rate can be gleaned from eq. 10 and a chemical comparison of FeH^+ and CH^+ . The orbitals of transition metal hydride ions MH^+ are expected to be much more diffuse than those of CH^+ . As a result, overlap between states is less and the transition moment is reduced. In addition, the energy gap between electronic states¹⁸ is expected to be much less for MH^+ than for CH^+ (for which the state splitting is 69 kcal mol^{-1}). Since the rate is proportional to the square of the transition moment and the cube of the state splitting, factors of 10^{-1} in these quantities lead to a

²⁶ Taking $A_{\text{V}} = 0.5 \text{ mag}$ and parameters (grain model 2) from the following: van Dishoeck, E. F., In *Rate Coefficients in Astrochemistry*; Millar, F. J.; Williams, D. A., Eds.; Kluwer: Dordrecht, 1988; p 49.

factor of 10^{-5} in the rate. Comparison with CH^+ thus leads to an expected rate of roughly $10^{-22} \text{ cm}^3\text{s}^{-1}$, close to the calculated value. Radiative association reactions of transition metal ions with other atoms, such as oxygen, may have larger rate constants if the corresponding molecular state splittings are greater or if charge-transfer transitions are possible, but any increase in rate constant will probably be offset by the lower abundance of the neutral reaction partner.

Although we expect the radiative association of metal ions and neutral atoms to be very slow, small molecules such as O_2 and CO_2 may be better reaction partners. Millar has investigated the consequences of rate coefficients greater than $10^{-16} \text{ cm}^3\text{s}^{-1}$ for a number of associations involving main-group metal ions. If such reactions are efficient in dense clouds, then dissociative recombination with electrons will lead to enhanced neutral metal atom abundances and probably require downward revision of estimates of the fraction of metal depleted onto grains.²⁷ In diffuse clouds, neutral metal abundances may be increased by neutralization of the ions by large molecules such as polycyclic aromatic hydrocarbons (PAHs).²⁸

We have considered only reactions involving the most abundant form of gaseous iron (Fe^+) with the most abundant neutral reaction partners (H and H_2). Since these reactions are found to be very slow, processes involving less-abundant species may be important. For example, reactions with oxygen to generate transition metal oxides such as TiO^+ , TiO ,²⁹ and

²⁷ Millar, T. J. In *Galactic and Extragalactic Infrared Spectroscopy*; Eur. Space Agency SP-192 (preprints); Kessler, M. F.; Phillips, J. P.; Guyenne, T. D., Eds.; 1982; p 33.

²⁸ Dalgarno, A. *Int. J. Mass Spec. Ion Proc.* 1987, 81, 1.

²⁹ Oppenheimer, M.; Dalgarno, A. *Astrophys. J.* 1977, 212, 683.

FeO³⁰ have previously been considered, although interstellar searches for these molecules have been unsuccessful.^{30,31} Another possibility is proton transfer to neutral Fe (eqs. 11-13). Reaction 11 has been suggested by Merer et al.³⁰



Since these proton transfer reactions are exothermic,³² they are expected to occur rapidly.

Conclusions.

Gas-phase transition metal chemistry is expected to mimic many of the reactions supposed to occur on grain surfaces. If transition metal ions can form molecules with moderate efficiency, then catalysis by metals will be important in diffuse interstellar clouds and substantial revision of chemical models will be required. However, we have calculated the rate constant for FeH⁺ formation by radiative association to be only $5 \times 10^{-22} \text{ cm}^3\text{s}^{-1}$. In general, radiative association rates of transition metal ions with atoms are probably negligibly slow. Unless faster routes into gas-phase transition metal chemistry are found, such chemistry may therefore be neglected in chemical models of diffuse interstellar clouds.

³⁰ Merer, A. J.; Walmsley, C. M.; Churchwell, E. *Astrophys. J.* **1982**, 256, 151.

³¹ Millar, T. J.; Eildér, J.; Hjalmarsen, Å.; Olofsson, H. *Astron. Astrophys.* **1987**, 182, 143.

³² Molecular proton affinities from: Lias, S. G.; Liebman, J.; Levin, R. D. *J. Phys. Chem. Ref. Data* **1984**, 13, 695.

Acknowledgments. We are indebted to J.-M. Langlois for indispensable assistance with the transition moment calculations, and to E. F. van Dishoeck and G. A. Blake for valuable comments and encouragement. We thank a referee for helpful comments, and the National Science Foundation for support under grants CHE-83-18041 (WAG) and CHE-87-11567 (JLB).

Chapter VI

Singlet-Triplet Gaps in Substituted Carbenes

CXY (X, Y = H, F, Cl, Br, I, SiH₃)

Karl K. Irikura, W. A. Goddard, III, and J. L. Beauchamp

*Arthur Amos Noyes Laboratory of Chemical Physics,
California Institute of Technology, Pasadena, California 91125*

Abstract.

Trends in carbene state-splittings have been found to be reproduced accurately using a surprisingly simple level of *ab initio* theory. The minimum balanced description (one configuration for triplets and two configurations for singlets) and basis sets of modest size yield singlet-triplet gaps that correlate linearly with available accurate values. This linear relationship is exploited to predict the state-splitting for the remaining members of the title series of carbenes. Magnitudes of splittings can be rationalized in terms of the partial charge on the carbenic carbon atom. Indeed, charges calculated using simple electronegativity equalization procedures correlate remarkably well with the predicted energy gaps. We arrive at a bonding model that reconciles the competing explanations for trends in carbene singlet-triplet gaps.

Introduction.

The spin multiplicity of substituted carbenes CXY is of prime importance in determining their reactivity.¹ Much work has been done to determine the relative stabilities of the lowest singlet and triplet states. On the theoretical front, increased accuracy from *ab initio* work has generally been obtained with large basis sets, extensive configuration-interaction (CI) calculations, or both.^{2,3} In particular, reliable state-splittings have recently

¹ Schuster, G. B. *Adv. Phys. Org. Chem.* 1986, 22, 311, and references therein.

² Bauschlicher, C. W., Jr.; Langhoff, S. R.; Taylor, P. R. *J. Chem. Phys.* 1987, 87, 387.

³ Davidson, E. R. In *Diradicals*; Borden, W. T., Ed.; Wiley: New York, 1982; chapter 2, pp 73-105.

been calculated by the dissociation-consistent CI method.⁴ When combined with available experimental results,^{5,6,7} the calculations yield reliable values for the five carbenes CH₂, CHF, CHCl, CF₂, and CCl₂. In the present work, we have found that a simple level of theory yields state-splittings that correlate linearly with the accurate values. This linear relationship is used to predict accurate values for other carbenes CXY (X, Y = H, F, Cl, Br, I, SiH₃).

The practice of scaling the results of *ab initio* calculations is well-established. Scaling of vibrational frequencies is probably the best-known example.^{8,9} For the CH₂ molecule alone, numerous workers have calibrated their energy gap results using known values for CH, for the carbon atom, or both.¹⁰⁻¹⁴ Others have used the experimental gap in CH₂ to adjust state-

⁴(a) Shin, S. K.; Goddard, W. A., III; Beauchamp, J. L. *J. Chem. Phys.* **1990**, *93*, 4986. (b) Shin, S. K.; Goddard, W. A., III; Beauchamp, J. L. *J. Phys. Chem.* **1990**, *94*, 6963.

⁵Jensen, P.; Bunker, P. R. *J. Chem. Phys.* **1988**, *89*, 1327.

⁶Murray, K. K.; Leopold, D. G.; Miller, T. M.; Lineberger, W. C. *J. Chem. Phys.* **1988**, *89*, 5442.

⁷(a) Koda, S. *Chem. Phys. Lett.* **1978**, *55*, 353. (b) Koda, S. *Chem. Phys.* **1986**, *66*, 383.

⁸Hehre, W. J.; Radom, L.; Schleyer, P. v. R.; Pople, J. A. *Ab Initio Molecular Orbital Theory*; Wiley: New York, 1986.

⁹Dykstra, C. E. *Ab Initio Calculation of the Structure and Properties of Molecules*; Elsevier: Amsterdam, 1988; chapter 6.

¹⁰Bauschlicher, C. W., Jr. *Chem. Phys. Lett.* **1980**, *74*, 273.

¹¹Bauschlicher, C. W., Jr.; Shavitt, I. *J. Am. Chem. Soc.* **1978**, *100*, 739.

¹²Shih, S.-K.; Peyerimhoff, S. D.; Buenker, R. J.; Perić, M. *Chem. Phys. Lett.* **1978**, *55*, 206.

¹³Foster, J. M.; Boys, S. F. *Rev. Mod. Phys.* **1960**, *32*, 305.

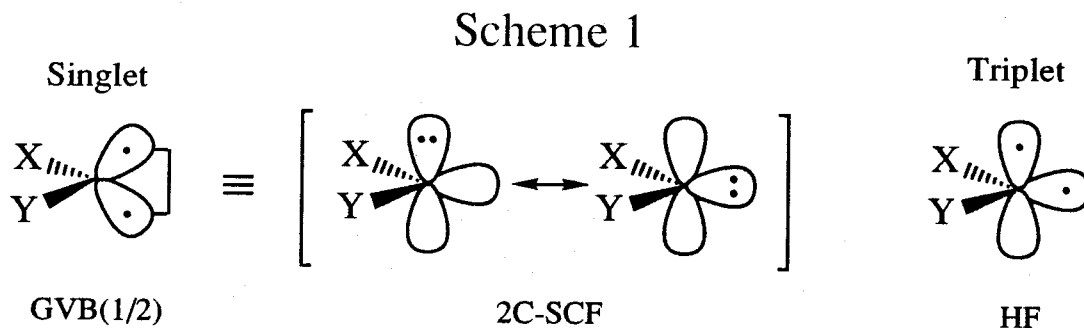
splittings calculated for substituted carbenes.¹⁵⁻¹⁷ Still others emphasize trends rather than absolute values.¹⁸⁻²⁰ We have chosen a simple combination of these approaches.

Computational Details.

For a balanced description of singlet and triplet carbenes, two configurations must be included for the singlet²¹ unless a very large CI is done.^{11,22} Since the triplet state, $\sigma^1 p^1$, uses both the σ and p orbitals, the singlet should also, requiring the two configurations $\sigma^2 p^0$ and $\sigma^0 p^2$. This description of the singlet corresponds to the simple generalized valence bond

-
- ¹⁴ Feller, D.; McMurchie, L. E.; Borden, W. T.; Davidson, E. R. *J. Chem. Phys.* **1982**, *77*, 6134.
- ¹⁵ Baird, N. C.; Taylor, K. F. *J. Am. Chem. Soc.* **1978**, *100*, 1333.
- ¹⁶ Mueller, P. H.; Rondan, N. G.; Houk, K. N.; Gano, J. E.; Platz, M. S. *Tetr. Lett.* **1983**, *24*, 485.
- ¹⁷ Pople, J. A.; Raghavachari, K.; Frisch, M. J.; Binkley, J. S.; Schleyer, P. v. R. *J. Am. Chem. Soc.* **1983**, *105*, 6389.
- ¹⁸ Harrison, J. F.; Liedtke, R. C.; Liebman, J. F. *J. Am. Chem. Soc.* **1979**, *101*, 7162.
- ¹⁹ Mueller, P. H.; Rondan, N. G.; Houk, K. N.; Harrison, J. F.; Hooper, D.; Willen, B. H.; Liebman, J. F. *J. Am. Chem. Soc.* **1981**, *103*, 5049.
- ²⁰ Hoffmann, R.; Zeiss, G. D.; Van Dine, G. W. *J. Am. Chem. Soc.* **1968**, *90*, 1485.
- ²¹ Shavitt, I. *Tetrahedron* **1985**, *41*, 1531.
- ²² Kim, S.-J.; Hamilton, T. P.; Schaefer, H. F., III *J. Chem. Phys.* **1991**, *94*, 2063-2067.

(GVB) wavefunction (with one correlated pair).²³ The triplet is treated at the Hartree-Fock (single configuration) level.



Regarding basis sets, d functions are required on the carbenic carbon to obtain accurate singlet-triplet energy separations.²¹ With our approach, however, only relative accuracy is needed. It has been observed that although the addition of d functions tends to increase $\Delta E_{st} \equiv E(\text{triplet}) - E(\text{singlet})$ substantially, it has little effect on *relative* ΔE_{st} s among carbenes.²⁴ We have therefore omitted polarization functions in our calculations. Since all-electron²⁵ and effective core potential descriptions of chlorine gave state-splittings that differed by only 0.37 kcal/mol, the economical pseudopotentials were used for Cl, Br, and I atoms.²⁶ Basis sets for fluorine²⁷ and carbon²⁸ were contracted to (3s2p) and (5s3p), respectively, and the (4s/2s) basis for

²³ Hay, P. J.; Hunt, W. J.; Goddard, W. A., III *Chem. Phys. Lett.* **1972**, *13*, 30.

²⁴ Baird, N. C.; Taylor, K. F. *J. Am. Chem. Soc.* **1978**, *100*, 1333.

²⁵ Rappé, A. K.; Goddard, W. A., III Unpublished work, 1982.

²⁶ Wadt, W. R.; Hay, P. J. *J. Chem. Phys.* **1985**, *82*, 284.

²⁷ Dunning, T. H. *J. Chem. Phys.* **1970**, *53*, 2823.

²⁸ Dunning, T. H. *J. Chem. Phys.* **1971**, *55*, 716.

hydrogen²⁹ was scaled by 1.2. All geometries were fully optimized at the restricted Hartree-Fock level (triplets) or the GVB level (singlets). The resulting bond angles θ (X-C-Y) agree well (1.5° rms) with those from ref. 4, and are listed in Table 1. Our bond lengths are consistently too long and are therefore not listed.

Results.

Figure 1 illustrates the linear relation between the five accepted carbene state-splittings and those from the present work. A least-squares fit (correlation coefficient of 0.9996) leads to eq. 1. Error estimates are twice the estimated

$$\Delta E_{\text{st}}^{\text{exp}} = A + B \times \Delta E_{\text{st}}^{\text{calc}} \quad (1)$$

$$A = 17.02 \pm 0.70 \text{ kcal/mol}$$

$$B = 1.175 \pm 0.036$$

standard deviations.³⁰ We use this relation to correct our calculated state-splittings. The resulting values, which we estimate to be accurate to ± 2 kcal/mol, are listed in Table 1 in order of decreasing energy gap.

Our predicted values are consistent with available experimental and theoretical results. For CFC1, a thermochemical estimate of $\Delta E_{\text{st}} = 39.4 \pm 4$ kcal/mol³¹ is in agreement with 37.1 from Table 1. The reactivity of CBr₂ suggests that it has a singlet ground state ($\Delta E_{\text{st}} > 0$).³² For CHBr, the

²⁹ Huzinaga, S. *J. Chem. Phys.* 1965, 42, 1293.

³⁰ Bevington, P. R. *Data Reduction and Error Analysis for the Physical Sciences*; McGraw-Hill: New York, 1969.

³¹ Carter, E. A.; Goddard, W. A., III *J. Phys. Chem.* 1986, 90, 998.

³² Skell, P. S. *Tetrahedron* 1985, 41, 1427.

Table 1. Optimized Bond Angles and Predicted Singlet-Triplet Gaps in CXY

X	Y	ΔE_{st} (kcal/mol)			θ (X-C-Y)	
		uncorr.	corr.	ref.	singlet	triplet
F	F	33.56	56.43	56.7 ^b	104.0°	118.0°
F	Cl	17.10	37.09		105.6	121.7
F	Br	12.67	31.89		106.3	122.8
F	I	7.20	25.46		107.2	124.1
Cl	Cl	2.59	20.04	20.5 ^c	109.0	126.1
Cl	Br	-0.75	16.12		110.2	127.6
H	F	-1.00	15.83	14.7 ^d	102.2	120.6
Br	Br	-3.85	12.48		111.5	129.2
Cl	I	-5.02	11.10		111.5	129.2
Br	I	-7.83	7.80		113.0	131.2
H	Cl	-9.03	6.39	6.4 ^d	101.4	123.7
H	Br	-11.04	4.03		101.8	125.4
I	I	-11.25	3.78		114.6	133.4
H	I	-13.81	0.77		102.6	127.7
F	SiH ₃	-15.58	-1.31		105.5	126.0
Cl	SiH ₃	-21.66	-8.45		108.1	130.8
H	H	-22.73	-9.71	-9.215 ^e	104.8	130.2
Br	SiH ₃	-23.49	-10.60		110.4	133.8
I	SiH ₃	-25.45	-12.90		113.1	137.3
H	SiH ₃	-30.71	-19.08		110.4	141.0
SiH ₃	SiH ₃	-31.15	-19.60		180.0	180.0

^aEstimated accurate to ± 2 kcal/mol; see text. ^bRef. 7. ^cRef. 4b. ^dRefs. 4 and 6. ^eRef. 5.

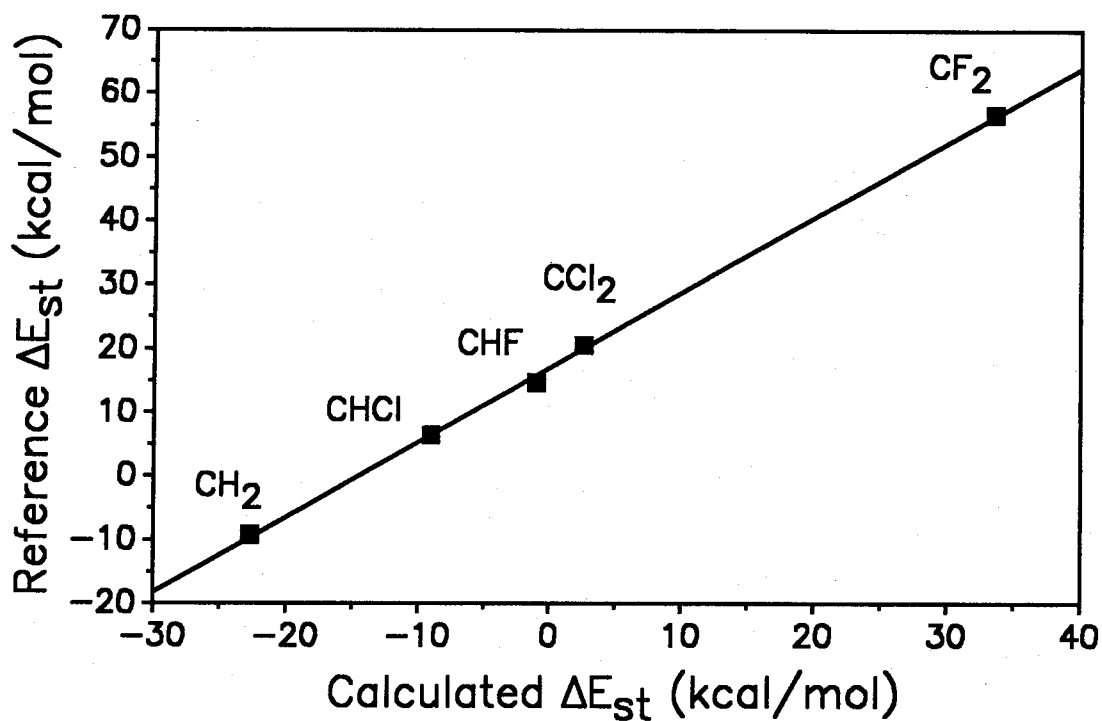


Figure 1. Singlet-triplet gaps calculated by our simple method are plotted against all five available accurate values from refs. 4-7. The least-squares line has slope 1.175 ± 0.036 , intercept 17.02 ± 0.70 kcal/mol, and correlation coefficient of 0.9996. Energy gaps predicted using this linear relation are estimated to be accurate to ± 2 kcal/mol.

experimental⁶ upper bound of 9 ± 2 and theoretical values of 1.1³³ and, more recently, 4.1³⁴ kcal/mol are also in agreement with our value of 4.0. The stereospecific addition of Cl_2 to butenes³⁵ suggests that its ground state is a singlet. Pressure and quenching studies have determined a singlet ground state for CHI as well.³⁶ For $\text{CH}(\text{SiH}_3)$, our value of -19.1 may be compared with the most recent *ab initio* values of -20.3,³⁷ -25.8,³⁸ and -18.4³⁹ kcal/mol.

Discussion.

As has often been observed, ΔE_{st} generally increases as the electronegativity of the substituents is increased. There appear to be two alternative explanations in the literature. The most popular^{2,3} is that π -donor substituents favor the singlet state by bonding with the p-orbital on the carbenic carbon, which is vacant in the singlet state and singly-occupied in the triplet.^{19,23,40,41} Many of these authors maintain that inductive effects are negligible, or even that electronegativity is irrelevant.

³³ Bauschlicher, C. W., Jr.; Schaefer, H. F., III; Bagus, P. S. *J. Am. Chem. Soc.* **1977**, *99*, 7106.

³⁴ Scuseria, G. E.; Durán, M.; Maclagan, R. G. A. R.; Schaefer, H. F., III *J. Am. Chem. Soc.* **1986**, *108*, 3248.

³⁵ Oliver, J. P.; Rao, U. V. *J. Org. Chem.* **1966**, *31*, 2696.

³⁶ Kikuchi, M.; Church, L. B. *Radiochim. Acta* **1973**, *20*, 81.

³⁷ Köhler, H. J.; Liscka, H. *J. Am. Chem. Soc.* **1982**, *104*, 5884.

³⁸ Luke, B. T.; Pople, J. A.; Krogh-Jespersen, M.-B.; Apeloig, Y.; Karni, M.; Chandrasekhar, J.; Schleyer, P. v. R. *J. Am. Chem. Soc.* **1986**, *108*, 270.

³⁹ Carter, E. A.; Goddard, W. A., III *J. Phys. Chem.* **1987**, *91*, 4651.

⁴⁰ Feller, D.; Borden, W. T.; Davidson, E. R. *Chem. Phys. Lett.* **1980**, *71*, 22.

Another explanation for the trend is that electron-withdrawing substituents inductively stabilize the σ non-bonding orbital by increasing its s-character.¹⁸ This change in hybridization leads to a larger energy gap between the σ^2p^0 (singlet) and σ^1p^1 (triplet) states. A variation on this interpretation is that electronegative groups withdraw charge from the carbenic carbon and increase its positive charge.³³ Table 2 illustrates the effect of charge on the energy gap between the 2s and 2p orbitals in an isolated carbon atom.⁴² Positive charge stabilizes the s-orbital relative to the p and hence the singlet state relative to the triplet. Each unit of charge on the atom increases the s-p energy gap by 26.8 kcal/mol.

To test the validity of the simple charge model, we examined the relationship between the predicted ΔE_{st} and the charge on the carbenic carbon. Mulliken populations were used to calculate charges; results are shown in Table 3 and Figure 2a. The energy gap does indeed depend upon the charge on the carbenic carbon atom. A least-squares fit to $\Delta E_{st} = A + B \times \delta(C)$ yields $A = 16.4$ kcal/mol, $B = 55.8$, and a correlation coefficient of 0.96.

We have investigated electronegativity equalization as a simple way to determine the partial charge on the central carbon.⁴³ Each atom's electronegativity is assumed to depend linearly upon its charge. Charge is further assumed to be distributed throughout the molecule in such a way as to

⁴¹ Hopkinson, A. C.; Lien, M. H. *Can. J. Chem.* **1985**, *63*, 3582.

⁴² Moore, C. E. *Atomic Energy Levels*; National Bureau of Standards: Washington DC, 1971.

⁴³ Huheey, J. E. *J. Phys. Chem.* **1965**, *69*, 3284. Charges were calculated using the sp^2 (tr) parameters for the central carbon; a different choice of hybridization shifts all the values by a constant.

Table 2. Orbital Ionization Energies in Carbon^a

Species	IE(2s) - IE(2p)
C ⁻	4.18 eV
C	5.34
C ⁺	6.50

^aAtomic energy levels from Ref. 42.

Table 3. Charges on Carbon and Degree of π -donation in CXY.

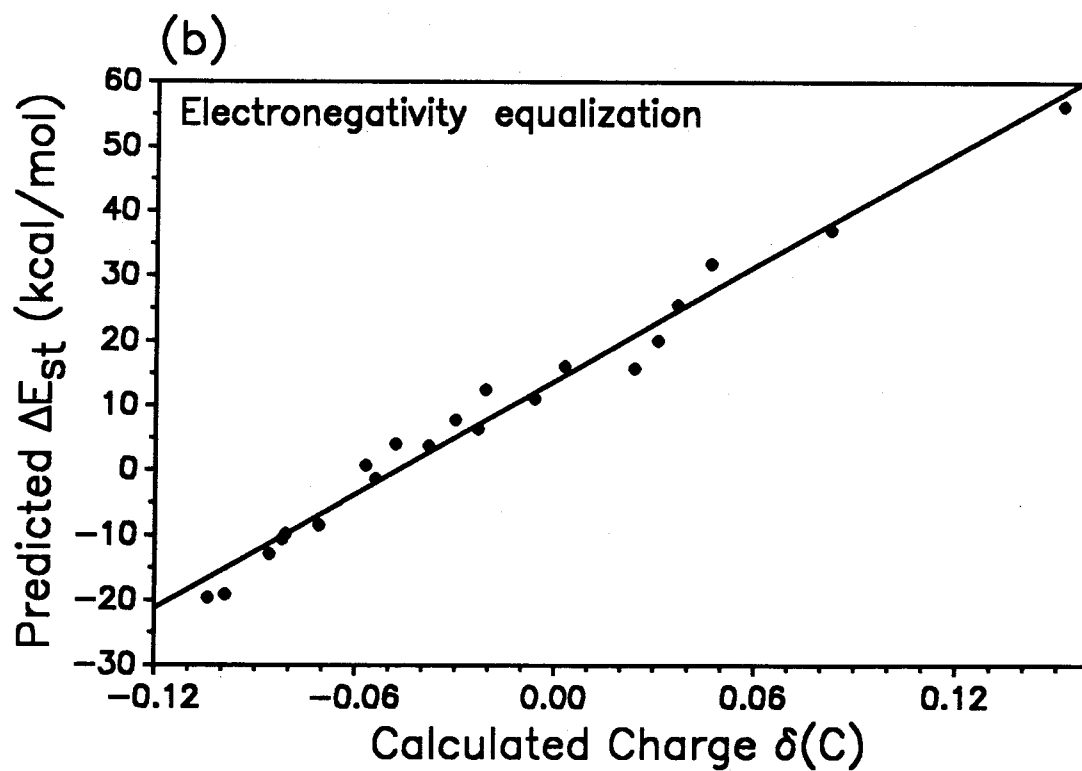
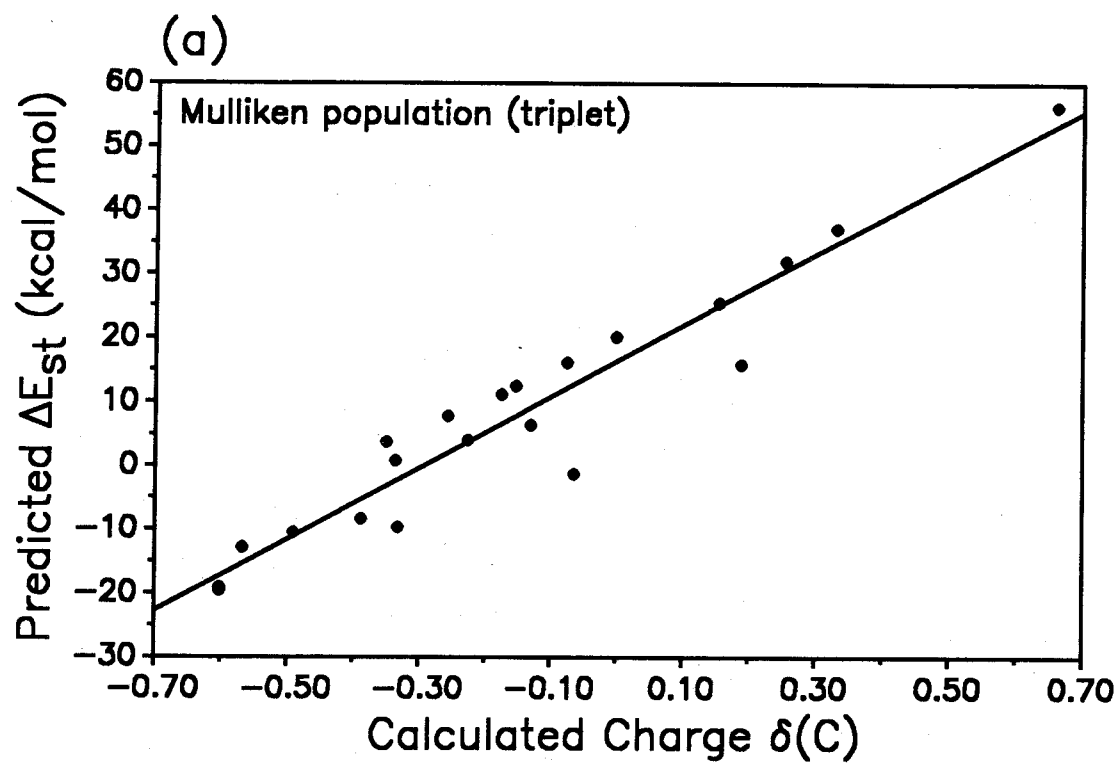
X	Y	Mulliken Pop'n ^a	EN Equal'n ^b	π -Donation ^c
H	H	-0.332	-0.081	0.0 %
H	F	0.188	0.024	12.8
H	Cl	-0.131	-0.023	9.2
H	Br	-0.226	-0.048	8.5
H	I	-0.336	-0.057	7.5
H	SiH ₃	-0.603	-0.099	1.4
F	F	0.661	0.152	22.0
F	Cl	0.332	0.083	18.8
F	Br	0.255	0.047	17.2
F	I	0.155	0.037	16.5
F	SiH ₃	-0.065	-0.054	10.7
Cl	Cl	-0.001	0.031	15.6
Cl	Br	-0.076	0.003	14.7
Cl	I	-0.175	-0.006	13.5
Cl	SiH ₃	-0.389	-0.071	9.9
Br	Br	-0.154	-0.021	13.8
Br	I	-0.257	-0.030	12.6
Br	SiH ₃	-0.492	-0.082	9.3
I	I	-0.350	-0.038	11.4
I	SiH ₃	-0.568	-0.086	8.2
SiH ₃	SiH ₃	-0.603	-0.104	3.3

^aCharge on carbenic carbon calculated from Mulliken populations in the triplet.

^bCharge calculated using electronegativity equalization procedure from ref. 43.

^cPercentage of nominal carbon p orbital (in the GVB pair in the singlet) from substituent-centered basis functions.

Figure 2. Predicted energy gaps are plotted against the charge on the carbenic carbon. Top: Charges from Mulliken population analysis of the triplets. Bottom: Charges calculated using the sp^2 parameter set and electronegativity equalization procedure of Ref. 43. The least-squares line has slope 293 ± 20 , intercept 13.9 ± 1.4 , and correlation coefficient 0.990. Energy gaps predicted using this relation are estimated to be accurate to ± 4 kcal/mol.



result in equal electronegativities for all atoms. The resulting charges calculated for the carbenic carbon are listed in Table 3 and plotted in Figure 2. The use of electronegativity equalization is appealing because it allows an easy estimate to be made for the singlet-triplet gap in any simple carbene. The linear relation (correlation coefficient of 0.990) is given in eq. 2. We estimate that energy gaps predicted using this relation are accurate to ± 4 kcal/mol.

$$\Delta E_{\text{st}} = A + B \times \delta(\text{C}) \quad (2)$$

$$A = 13.9 \pm 1.4 \text{ kcal/mol}$$

$$B = 293 \pm 20.$$

The use of eq. 2 is best illustrated by example. To predict a ΔE_{st} value for hydroxycarbene, CH(OH), parameters are taken from ref. 43 to set up the simultaneous equations 3, which have the solution $\delta(\text{H}) = 0.144$, $\delta(\text{O}) = -0.304$,

$$7.17 + 12.85 \delta(\text{H}) = 8.79 + 13.67 \delta(\text{C})$$

$$7.17 + 12.85 \delta(\text{H}) = 14.39 + 17.65 \delta(\text{O}) \quad (3)$$

$$2 \delta(\text{H}) + \delta(\text{C}) + \delta(\text{O}) = 0$$

and $\delta(\text{C}) = 0.017$. Eq. 2 then leads to $\Delta E_{\text{st}} = 19$ kcal/mol. Note that this is in excellent agreement with the most recent literature value, 19.7 kcal/mol.⁴⁴

The correlation of Figure 2 supports the view that electron-withdrawing substituents increase ΔE_{st} . The strength of the dependence upon charge, however, is too large to be explained simply by charge on the carbon atom. In the carbenes, ΔE_{st} increases by 56 kcal/mol per unit of charge on the carbon, while the s-p gap on the bare atom increases by only 26.8 kcal/mol per unit of

⁴⁴ Räsänen, M.; Raaska, T.; Kunttu, H.; Murto, J. *J. Mol. Struct.* **1990**, *208*, 79-90.

charge. This amplification of the influence of charge may be due to synergistic π -donation. Additional evidence for π -donation comes from the dependence of ΔE_{st} upon θ (X-C-Y). Opening the bond angle changes the hybridization of the central carbon. The resulting increase in p-character in the non-bonding σ orbital in turn leads to a generally lower ΔE_{st} , as shown in Figure 3. For any given angle (hybridization), however, ΔE_{st} is substantially larger when both substituents are halogens. This is presumed to reflect the substantially greater π -bonding expected for the dihalogen carbenes. Finally, we can estimate the degree of π -bonding from the calculated wavefunctions. This is taken simply as the percentage of the nominal carbon p orbital that derives from substituent-centered basis functions. Although the relationship is not monotonic, a strong correlation between ΔE_{st} and the amount of π -donation is apparent (Figure 4).

The support available for both electron-withdrawal and π -donation interpretations leads one to suspect that both are correct. Further indication that both considerations are important comes from experimental electron affinities (EAs).⁶ For X = Cl, Br, and I, the EAs increase in the series $\text{CH}_2 < \text{CHX} < \text{CX}_2$, indicating that electron-withdrawal is the major effect. For X = F, however, the EAs *decrease* sharply in the series, indicating that π -donation dominates. The switch for X = F is thought to be due to the shortness of the C-F bond, which crowds the fluorine lone pair into the carbon's π -orbital.⁶

The "competing" explanations of electron-withdrawal and π -donation are readily compatible. Electronegative substituents withdraw electron density from the carbenic carbon, making it more positively charged. The increased charge is expected to make the carbon a better π -acceptor. As a result, π -donation from substituents is enhanced. Such " π -backbonding" is

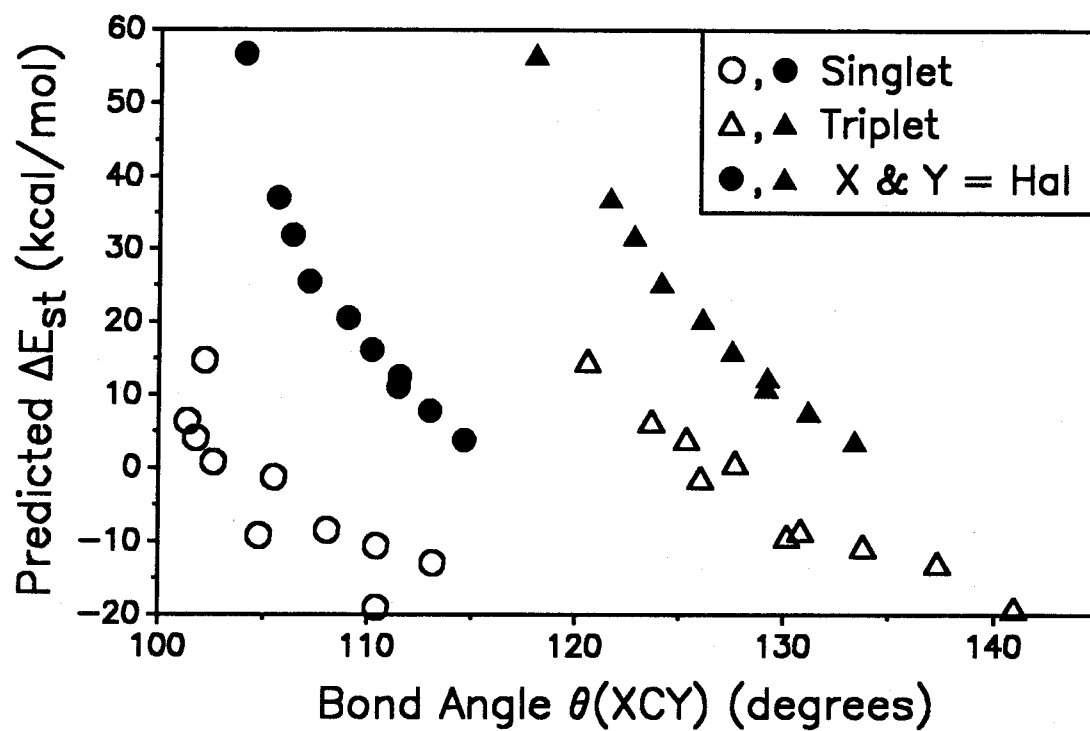


Figure 3. Predicted energy gaps are plotted against calculated bond angles for both singlet and triplet states. Dihalogen carbenes are indicated by solid symbols. $\text{C}(\text{SiH}_3)_2$ is omitted (bond angle = 180°).

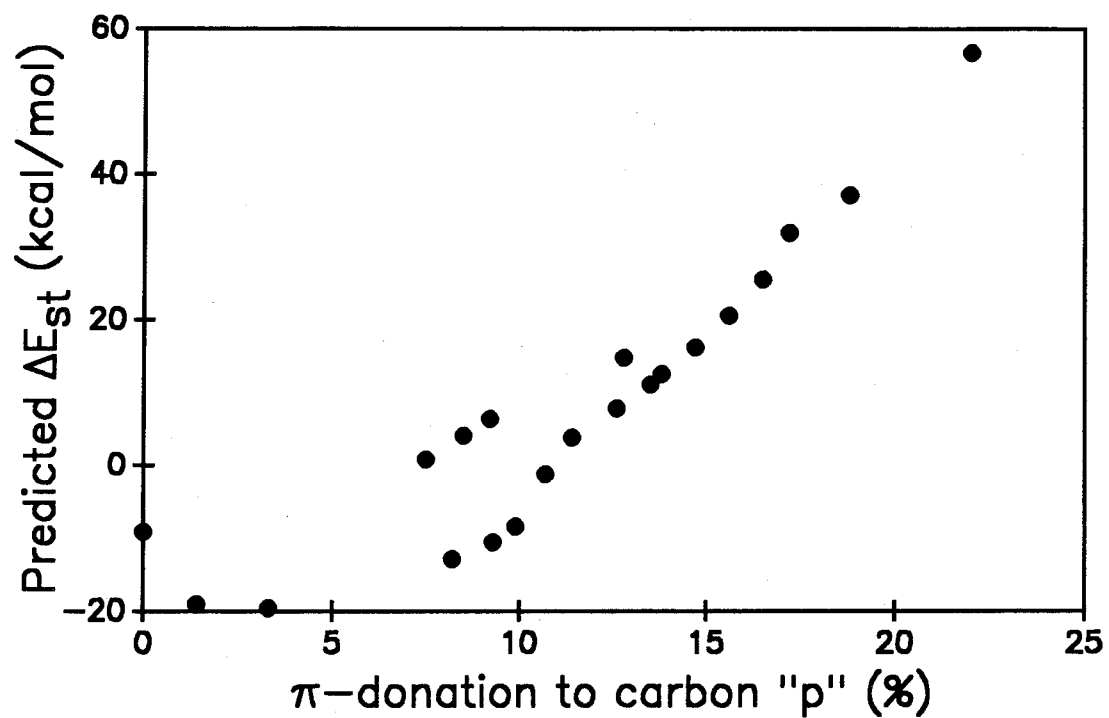


Figure 4. Predicted energy gaps are plotted against the amount of π -donation from the substituents to the central carbon "p" orbital (in the GVB singlet).

commonplace in transition metal chemistry, although the ligands are usually the σ -donors and π -acceptors in that context.

There is experimental support for a synergistic bonding model. Nuclear quadrupole coupling constants in CCl_2 indicate σ -transfer of 0.26 electron from C to Cl and π -transfer of 0.32 electron from Cl back to C.⁴⁵ In the series XCl , XCl_2 , and H_2XCl_2 ($\text{X} = \text{C}, \text{Si}$), the σ -transfer depends upon the electronegativity difference between X and Cl while the π -transfer depends upon the acceptor ability of X.⁴⁵ These observations are exactly what one would expect if the bonding is as described above. More indirect evidence comes from studies of the reactivity of substituted carbenes. It is well-established that π -donor and electron-withdrawing substituents both increase selectivity in the reaction with olefins.⁴⁶ Both types of substituent are expected to yield the same general reactivity pattern if σ -withdrawal and π -donation are strongly interdependent, as in the synergistic bonding model described here.

Conclusions.

An empirical correction to a very simple level of *ab initio* theory has been used to predict singlet-triplet energy gaps (ΔE_{st}) for a series of substituted carbenes. Energy gaps are found to correlate linearly with the charge on the carbenic carbon. Electronegativity equalization procedures permit the charge on carbon, and hence the state-splitting, to be calculated easily for any simple carbene. Although correlation with charge supports the electron-withdrawal explanation for trends in ΔE_{st} values, the strength of the charge-dependence requires an additional mechanism. This is shown to be π -donation from the

⁴⁵ Fujitake, M.; Hirota, E. *J. Chem. Phys.* 1989, 91, 3426.

⁴⁶ Moss, R. A. *Acc. Chem. Res.* 1980, 13, 58.

substituents to the empty carbon p-orbital in the singlet state. We propose a synergistic model for bonding in carbenes, in which σ -donation and π -backbonding cooperate, as consistent with experimental and theoretical observations.

Acknowledgments. We are grateful to the National Science Foundation for support under grants CHE-83-18041 (WAG) and CHE-87-11567 (JLB). KKI appreciates fellowship support from the Department of Education.

Chapter VII

Some Experimental Considerations for Fourier-Transform Ion Cyclotron Resonance Spectrometry

Karl K. Irikura

*Arthur Amos Noyes Laboratory of Chemical Physics,
California Institute of Technology, Pasadena, California 91125*

Abstract.

We consider five different issues that have arisen during FTICR studies of reactive transition metal ions. The first involves the incompatibility of ion pumps with such experiments. The second topic is the generation of ions from gaseous and solid transition metal oxides, including some discussion of the process of ion formation by laser ablation. Third, we note benefits that may be obtained through the use of rf excitation and ejection of ions in the trapping potential. Fourth, the problem of mass discrimination in FTICR is discussed, with suggestions for improvement. The fifth section deals briefly with the analysis of kinetic data (timeplots) by curve-fitting.

Chemical Synthesis by an Ion Pump.

One reason for using an ion pump instead of a diffusion pump is the reduction in heavy organic contaminants such as pump oil. Another is more economical operation; no cryogenic baffle is needed. For these reasons, a number of experiments in the study described in Chapter III were performed using an ion pump to maintain low pressures. Results were often confusing, and it was finally determined that the ion pump produces vapors (of indeterminate composition) that generally confound attempts to investigate gas phase processes. An example is provided in Figure 1, which illustrates a frustrated effort to study the reaction of Ir^+ with CD_4 . The top part of the Figure is a spectrum taken while an ion pump was in use. The lower spectrum was recorded 15 minutes later under the same conditions, except that pumping was provided by a diffusion pump with a liquid nitrogen-cooled baffle. Any oil that might escape from the diffusion pump is insignificant compared to the heavy contamination from the ion pump.

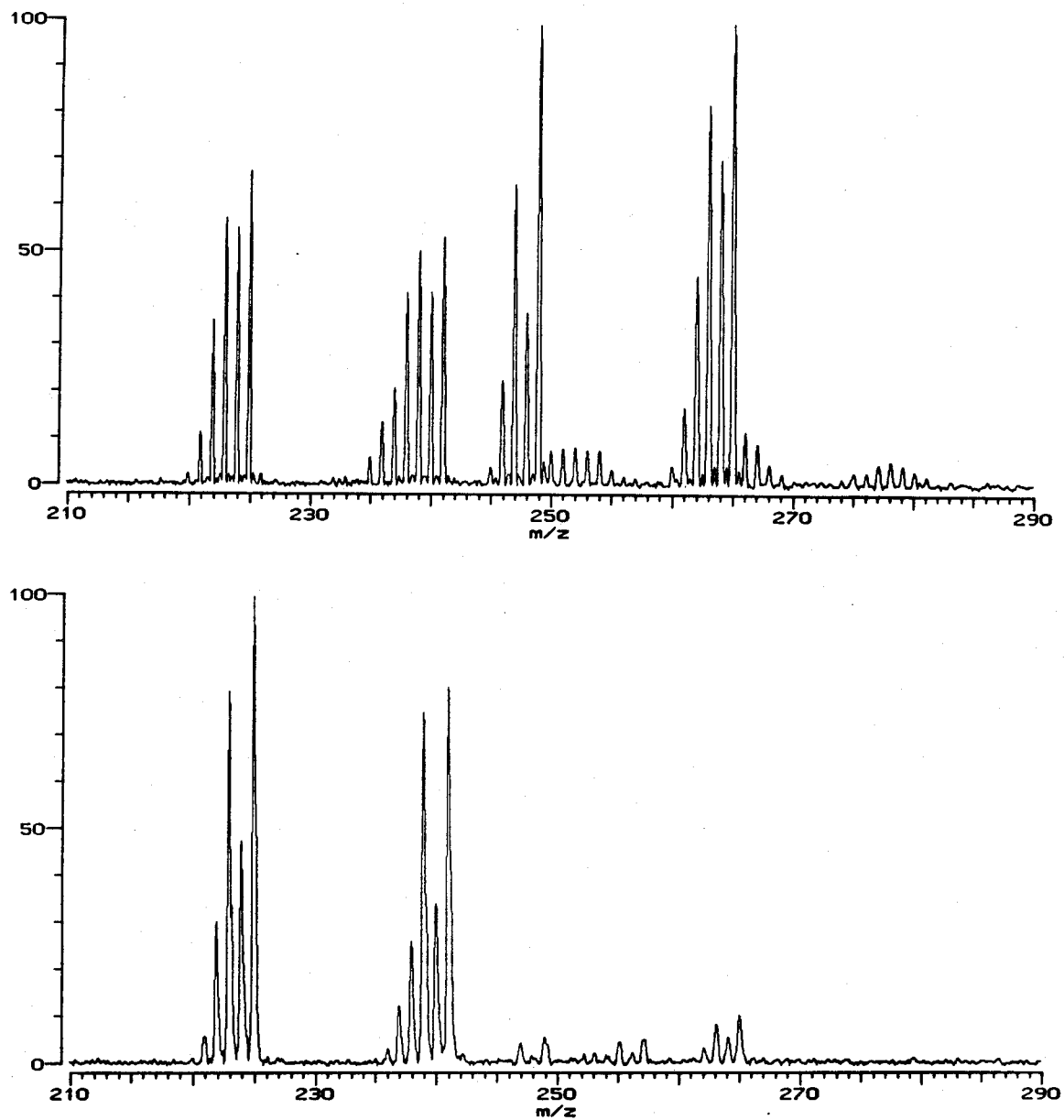


Figure 1. Reaction of Ir^+ (natural $^{193}\text{Ir}:^{191}\text{Ir} = 1.6:1$) with 1.2×10^{-6} torr of CD_4 for 1 second. Top: Pumping provided by ion pump. Bottom: Pumping provided by diffusion pump.

The contamination from the ion pump should not have been unexpected, since the pressure is determined by a dynamic equilibrium between sorption and release. The gases particularly prone to re-emission are hydrogen, methane, and noble gases.¹ The formation of partially protiated methane from CD₄, presumably by isotopic scrambling prior to re-emission, was especially problematic.

Ions From Metal Oxides.

Electron Impact Ionization of a Vapor. We have examined a number of gases in efforts to generate oxo-metal ions. A selected-ion flow tube (SIFT) study of CrO₂Cl⁺ (from CrO₂Cl₂) has revealed interesting reactions such as double bond metathesis and oxygen atom transfer with ethylene.² Our earliest attempts involved MoO₂Cl₂, which can be introduced through a leak valve. MoO_n⁺ (*n* = 0-2) are obtained from electron impact ionization. Since it was studied only briefly, the only reaction identified in this system was acetaldehyde dehydration, eq. 1 (confirmed using CD₃CDO). Exothermicity of this reaction



¹O'Hanlon, J. F. *A User's Guide to Vacuum Technology*, 2nd ed.; Wiley: New York, 1989; Chapter 14.

²Walba, D. M.; DePuy, C. H.; Grabowski, J. J.; Bierbaum, V. M. *Organometallics* 1984, 3, 498-499.

implies $D(\text{MoO}_2\text{Cl}^+-\text{H}_2\text{O}) \geq 36$ kcal/mol.³ Soon after, MoO_2Cl_2 was abandoned in favor of OsO_4 , which is easier to study and provides a larger variety of binary oxo-metal cations.⁴

Compounds with much lower vapor pressures can be introduced from a heated quartz tube mounted directly beneath the ICR cell.⁵ MoO_3 and WO_3 produce oligomeric vapors $(\text{MO}_3)_n$, $n \geq 3$, when sufficiently heated,⁶ and might be amenable to ICR study in this way. ReO_3 , however, does not require such high temperatures, and we have used it successfully as a source of ReO_n^+ ions.⁷ ReO_3 disproportionates to ReO_2 and volatile Re_2O_7 when heated.⁸ Traces of moisture react with the Re_2O_7 vapor to produce perrhenic acid,⁹ HReO_4 , which is very persistent in the vacuum system. Electron impact yields ReO_n^+ ($n = 0-3$) and Re_2O_n^+ ($n = 5-7$). After some time has been provided for ion-molecule reactions to occur, H_2ReO_4^+ , protonated perrhenic acid, becomes abundant. We have also observed clustering to lead to ions as heavy as

³ Auxiliary thermochemical data from: Lias, S. G.; Bartmess, J. E.; Liebman, J. F.; Holmes, J. L.; Levin, R. D.; Mallard, W. G. *J. Phys. Chem. Ref. Data* **1988**, *17*, Supplement No. 1.

⁴ Irikura, K. K.; Beauchamp, J. L. *J. Am. Chem. Soc.* **1989**, *111*, 75-85. (Chapter I in this thesis.)

⁵ The heated quartz tube was installed for studies involving porphine vapor; see Chapter IV in this thesis.

⁶ (a) Berkowitz, J.; Inghram, M. G.; Chupka, W. A. *J. Chem. Phys.* **1957**, *26*, 842-846. (b) Berkowitz, J.; Chupka, W. A.; Inghram, M. G. *J. Chem. Phys.* **1957**, *27*, 85-86.

⁷ Work done in collaboration with Edmund H. Fowles.

⁸ Pascal, P., Ed. *Nouveau Traité de Chimie Minérale*; Masson: Paris, 1960; Vol. 16.

⁹ Battles, J. E.; Gundersen, G. E.; Edwards, R. K. *J. Phys. Chem.* **1968**, *72*, 3963-3969.

$\text{Re}_4\text{O}_{14}^+$. Among the anions, ReO_3^- and ReO_4^- are formed initially, and clusters as heavy as for the cations are observed. Some reactions of ReO_n^+ ($n = 0-2$) with NH_3 and CH_4 were studied briefly, as described in Chapter III. Although the presence of at least two rhenium-containing vapors complicates the system somewhat, ReO_3 is a reasonable source of ReO_n^+ ions for systematic study.

Laser Ablation of Solid Binary Oxides. Laser ablation has two major advantages over electron impact (EI) as a source of ions. First, no neutral metal-containing gas is required, simplifying the interpretation of ion-molecule reactions. Second, laser ablation is a much more intense source of ions than EI. We have attempted to generate oxo-metal ions by laser ablation of solid oxides, with mixed results. Ablation of a pellet of MnO_2 ⁷ yields a very intense Mn^+ signal (more intense than ablation of metallic Mn) but no MnO_n^+ . MnO_2^- and MnO_3^- are the major anions formed. A pellet of Fe_2O_3 similarly yields no FeO_n^+ , but an Fe^+ signal much more intense than obtained by ablation of pure Fe. Among the anions, however, FeO^- and FeO_2^- (and small amounts of Fe^- and FeO_3^-) are observed (Figure 2).

Qualitatively different results are obtained from IrO_2 . Peaks due to IrO^+ and IrO_2^+ are observed in addition to an intense Ir^+ signal. As shown in Figure 3, Ir_2O_n^+ ($n = 0-4$) and tiny amounts of Ir_3O_n^+ ($n = 0-2$) are also generated. IrO_2^- is the only major anion generated. The pellet of IrO_2 is very friable, in contrast to the much harder and denser MnO_2 and Fe_2O_3 pellets. After a single day of use, the IrO_2 pellet had a large hole (~ 1 mm diameter) drilled through. This experience therefore suggests that a loose pellet will be more rapidly ablated and will yield more molecular ions from the ablation process. If more material is ablated, a greater intensity of atomic ions would

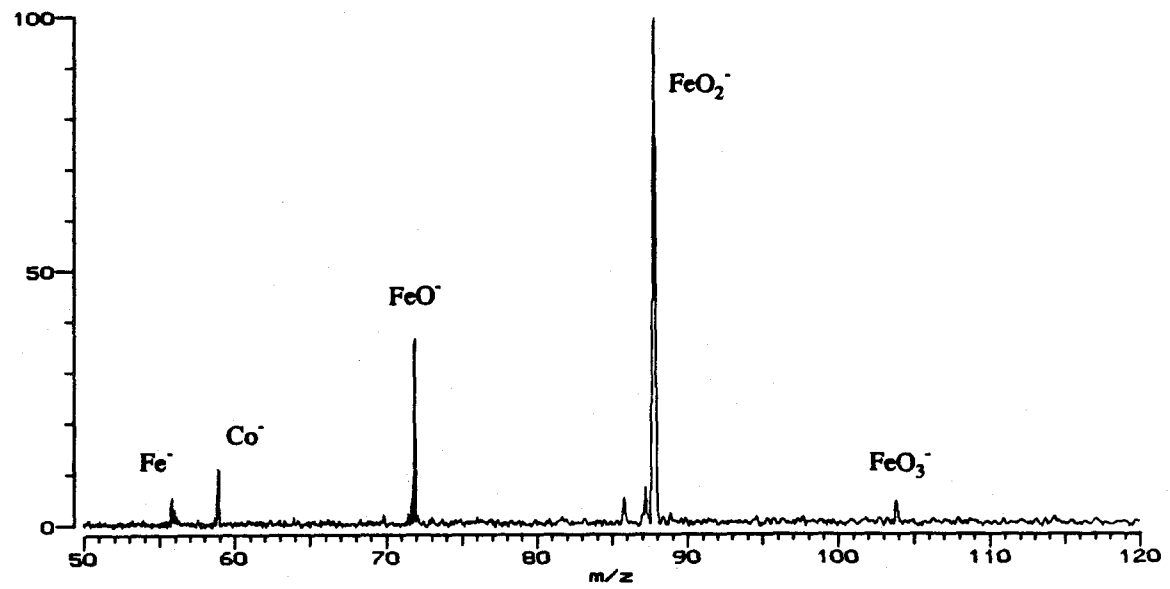


Figure 2. Anions FeO_n^- , $n = 0-3$, generated by laser ablation (308 nm) of a pressed pellet of Fe_2O_3 .

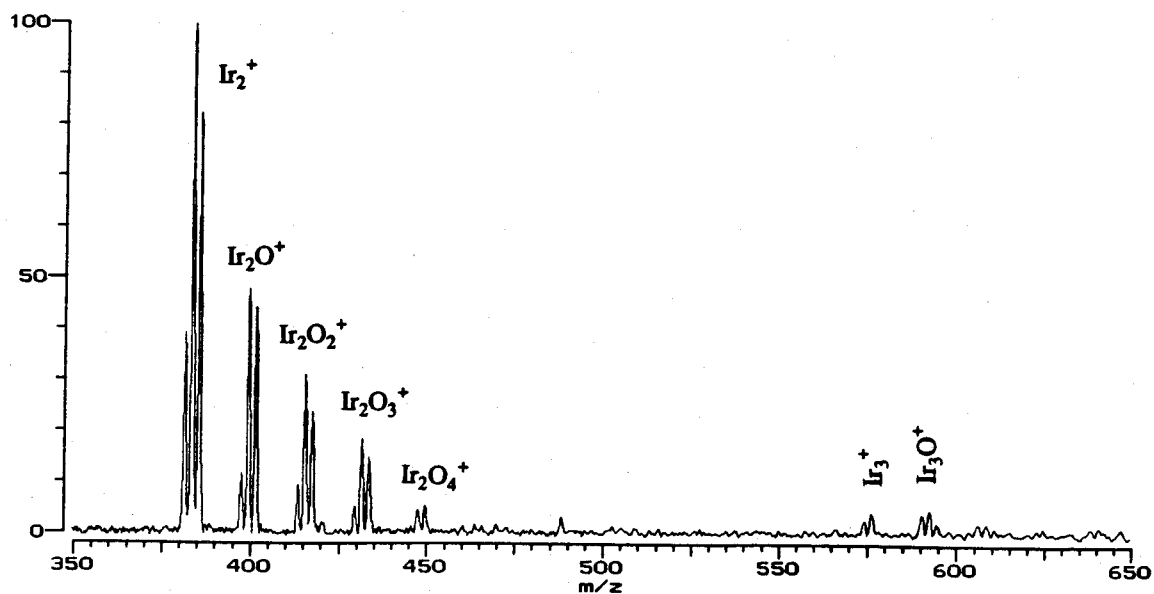


Figure 3. Ir_2O_n^+ ($n = 0-4$) and Ir_3O_n^+ ($n = 0-2$) generated by laser ablation of a loose pellet of IrO_2 . The more abundant ions IrO_n^+ ($n = 0-4$) have been ejected because of dynamic range limitations.

also be expected, consistent with the observations for the MnO_2 and Fe_2O_3 pellets.

Roughening a metal surface has been demonstrated to result in a greater yield of cluster ions upon laser ablation.¹⁰ The explanation provided is that the roughening process deposits microclusters on the surface which can then be desorbed and ionized by the laser pulse.¹⁰ This argument is inconsistent with other studies demonstrating that gas phase processes dictate the cluster distribution.^{11,12} Clustering in an FTICR is enhanced if the magnetic field is parallel to the ablating laser beam. A perpendicular field tends to separate the ions from the neutral atoms in the expanding plasma plume, thereby preventing the ion-molecule reactions responsible for clustering.¹¹ Long irradiation times lead to formation of a channel in the target, which in turn enhances cluster formation.¹¹ This may be due to confinement of the plasma, which increases its pressure and therefore the rates of gas phase reactions. Ta_nC_m^+ cluster ions result from laser ablation of pellets of mixed tantalum and carbon, although no Ta-C bonds are present in the solid.¹² Even more dramatically, most of the TaC_n^+ from ablation of a pellet containing TaC and ^{13}C (amorphous) is fully labeled with ^{13}C .¹²

A more reasonable explanation for the cluster enhancement due to surface roughening is simply that a rough surface presents a larger area to the laser beam and resulting plasma. More material is therefore ablated and the

¹⁰ Gord, J. R.; Buckner, S. W.; Freiser, B. S. *Chem. Phys. Lett.* **1988**, *153*, 577-582.

¹¹ McElvany, S. W.; Nelson, H. H.; Baronavski, A. P.; Watson, C. H.; Eyler, J. R. *Chem. Phys. Lett.* **1987**, *134*, 214-219.

¹² McElvany, S. W.; Cassady, C. J. *J. Phys. Chem.* **1990**, *94*, 2057-2062.

plasma is denser, enhancing ion-molecule reactions. This surface area argument is consistent with the observation that compressed-powder pellets of metal oxides, which have relatively large surface areas, are more intense sources of metal cations than are metal foils. The importance of gas phase ion-molecule or ion-atom reactions is consistent with the generally poor yields of $M_nO_m^+$ that we have obtained, compared with the high yields obtained by laser ablation in the absence of a magnetic field.¹³

Z-Axis Excitation and Ejection.

Ions can be translationally excited or ejected from the ICR cell by rf excitation of their trapping well motion.¹⁴ This is especially useful for ejecting light species such as electrons or protons, which have inconveniently high cyclotron frequencies. We have found that such ejection may be accompanied by tremendous increases in signal intensity as shown in Figure 4. The ejection reduces space charge effects by eliminating abundant low-mass ions. Additional signal enhancement may be due to a more even spatial distribution of ions, caused by the rf field.

Cyclotron motion can also be excited by applying the rf voltage across the trapping plates of the cell. This permits two cyclotron frequencies to be excited simultaneously, which is not normally possible with typical instruments.

¹³ Using laser microprobe time-of-flight mass spectrometry: Michiels, E.; Gijbels, R. *Anal. Chem.* **1984**, *56*, 1115-1121.

¹⁴ Beauchamp, J. L.; Armstrong, J. T. *Rev. Sci. Instrum.* **1969**, *40*, 123.

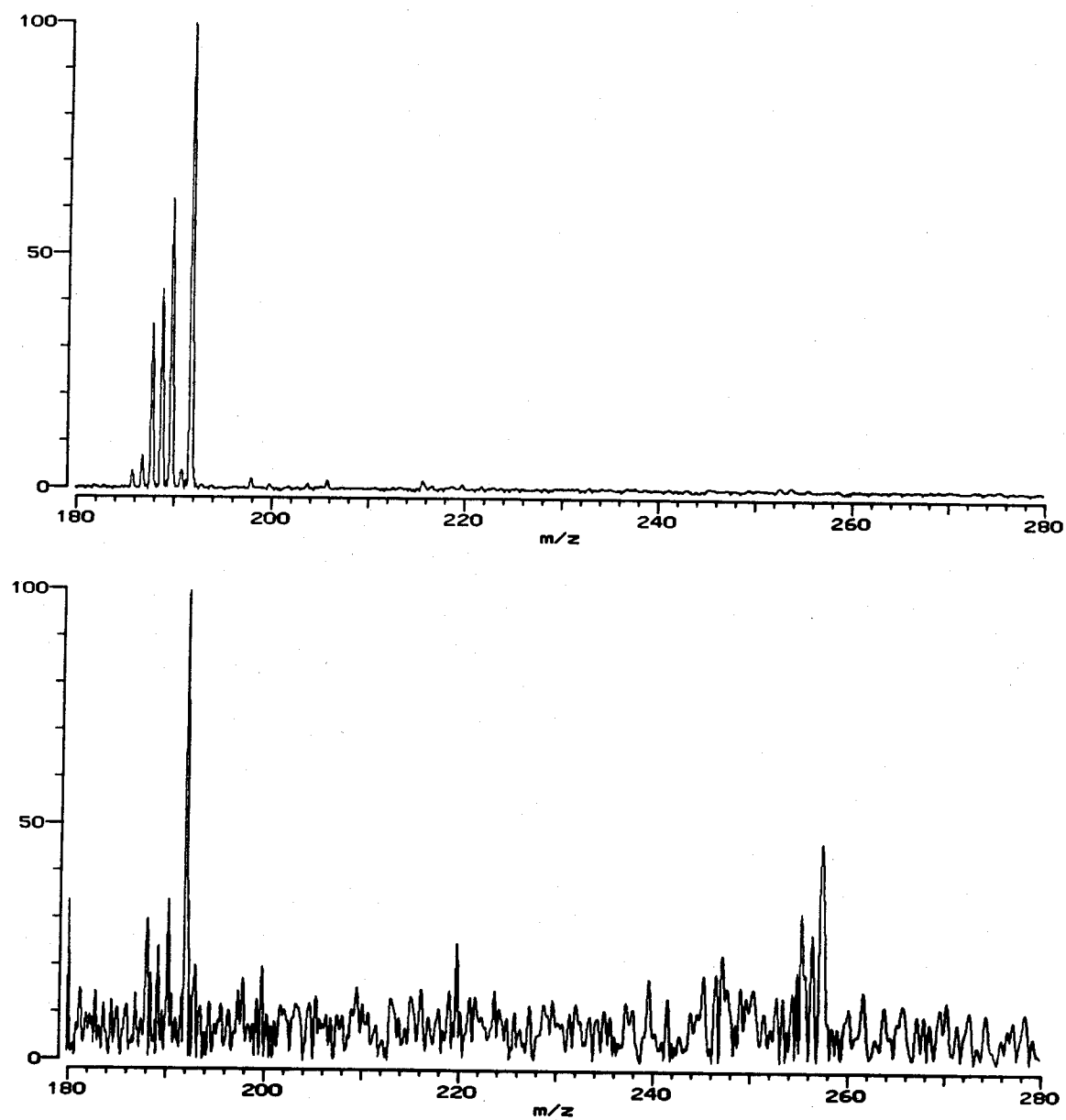


Figure 4. Os^+ , from 50 eV electron impact on OsO_4 , isolated in 6×10^{-7} torr of methane. Average of 50 scans. Top: Using z-axis rf ejection of low-mass ions. Bottom: No ejection used.

Mass Discrimination in FTICR.

FTICR suffers from generally unreliable relative intensities.¹⁵ Ideally, relative intensities should be independent of all the variable experimental parameters such as instrumental tuning and the number of trapped ions. The Caltech instrument is equipped for both chirp and impulse excitation, and we have tested both methods to determine if reliable relative intensities can be extracted.

Chirp excitation involves scanning the excitation frequency through the mass range of interest. The chirp is defined by its amplitude, frequency range, and frequency step. The length of the chirp, usually one or two milliseconds, is determined by the number of steps (1 μ s each). Figure 5 shows the effect of chirp amplitude upon both relative intensities and total signal intensity for $\text{Ni}(\text{CO})_3^-$, which is generated by dissociative electron attachment to $\text{Ni}(\text{CO})_4$. The measured $^{58}\text{Ni}/^{60}\text{Ni}$ ratio decreases monotonically by nearly three orders of magnitude as the chirp amplitude is increased. In general, stronger excitation favors peaks at higher mass. The lower part of Figure 5 indicates that approximately correct relative peak heights may be obtained by tuning for maximum total signal and then increasing the amplitude to reduce the total signal by 50%. Of course, such an adjustment is too crude for quantitative use and too tedious to be used routinely.

We have not done systematic investigations of the effects of chirp step or mass range. A smaller chirp step gives a more uniform power spectrum, but at the expense of a longer chirp. Increasing the mass range produces a wider

¹⁵ (a) Mitchell, D. W.; DeLong, S. E. *Int. J. Mass Spec. Ion. Proc.* **1990**, *96*, 1-16. (b) de Koning, L. J.; Kort, C. W. F.; Pinske, F. A.; Nibbering, N. M. M. *Int. J. Mass Spec. Ion Proc.* **1989**, *95*, 71-92.

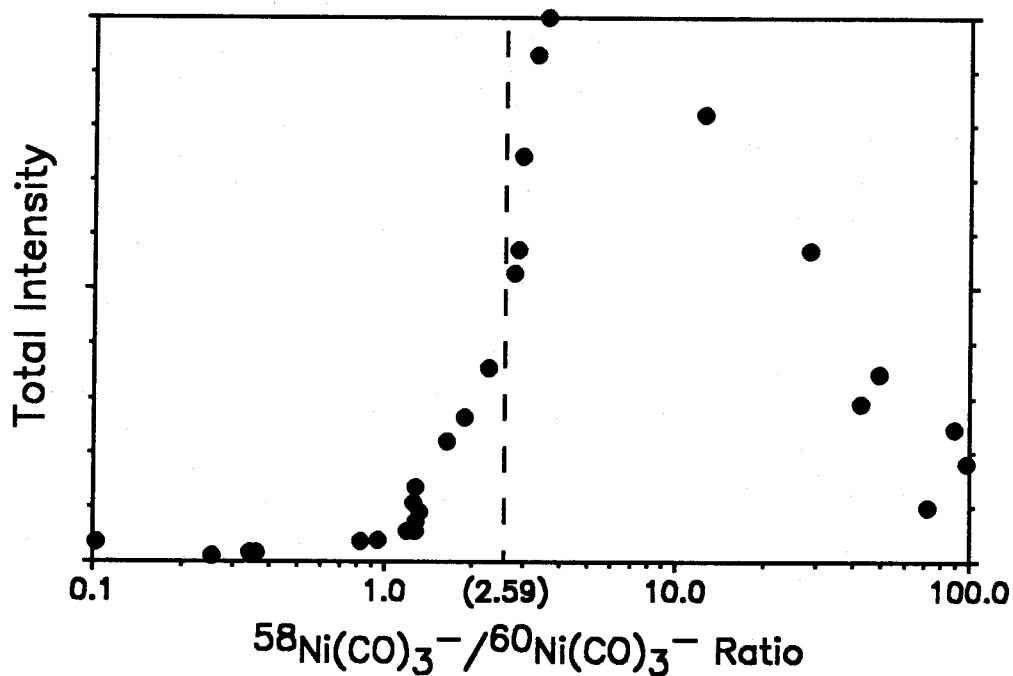
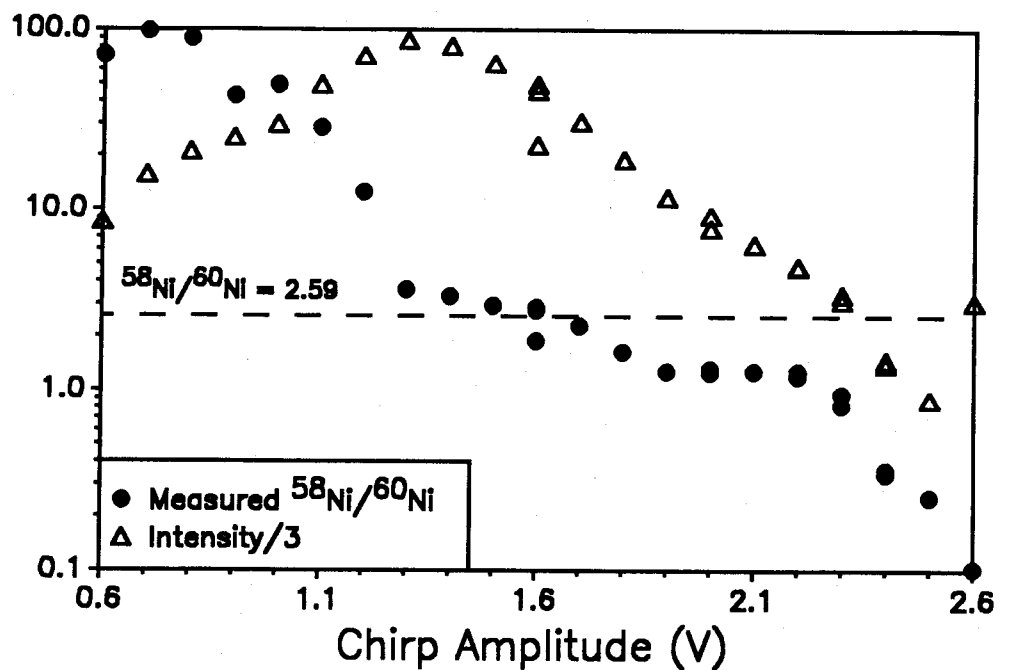


Figure 5. Tuning curve for chirp excitation of $\text{Ni}(\text{CO})_3^-$. Masses are scanned from 50 to 350 in 1313 steps ($1 \mu\text{s}$ each) of 400 Hz. Amplitude = $1.6 V_{pp}$. Top: $^{58}\text{Ni}/^{60}\text{Ni}$ ratio (circles; correct value = 2.59) and total $\text{Ni}(\text{CO})_3^-$ intensity (triangles; scaled to fit on graph). Bottom: total intensity plotted against isotope ratio.

region of uniform power, but will again make the chirp longer. If the chirp is too long, the ions that were excited at the beginning of the chirp will have dephased by the end of the chirp, leading to additional mass discrimination.

Impulse excitation involves a dc pulse about 1 μ s long and a few hundred volts in amplitude. Since all ions are excited to the same radius, less mass discrimination is expected.¹⁶ Unfortunately, we find that the measured $^{58}\text{Ni}/^{60}\text{Ni}$ ratio decreases monotonically with increasing impulse amplitude. The range is less than that for chirp excitation, but is still two orders of magnitude (Figure 6).

Both chirp and impulse excitation favor low masses at low power and high masses at high power. This is apparently caused by stronger excitation for lower masses. At large amplitudes, this leads to ejection of the low-mass ions instead of mere excitation, leading to a decrease in total signal and net discrimination *against* lower masses (Figure 5). This suggests that a deliberate shift of power to the higher masses can reduce the mass discrimination at all power levels. This chirp shaping was attempted by inserting a low-pass filter between the frequency synthesizer and the subsequent amplification and gating electronics. Several filter constants were tested. Most did not qualitatively affect the dependence of mass discrimination upon excitation amplitude. In one case, however, the dependence is actually reversed; increasing the amplitude leads to both an increase in signal and an increased bias in favor of *low* mass (Figure 7). Further work is needed to determine if some filter constant between this one (800 kHz) and the default (∞) will result in relative intensities that are independent of excitation amplitude.

¹⁶ McIver, R. T.; Baykut, G.; Hunter, R. L. *Int. J. Mass Spec. Ion Proc.* 1989, 89, 343-358.

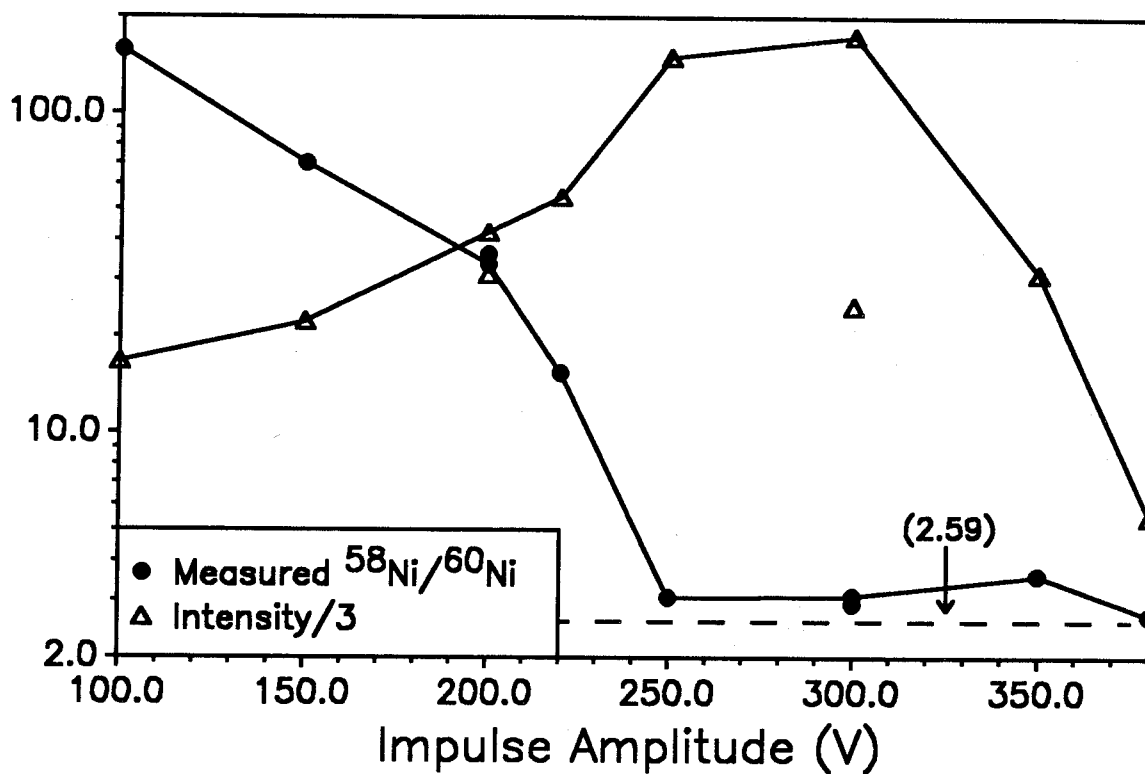


Figure 6. Tuning curve for impulse excitation of $\text{Ni}(\text{CO})_3^-$. Impulse width is $\sim 0.7 \mu\text{s}$.

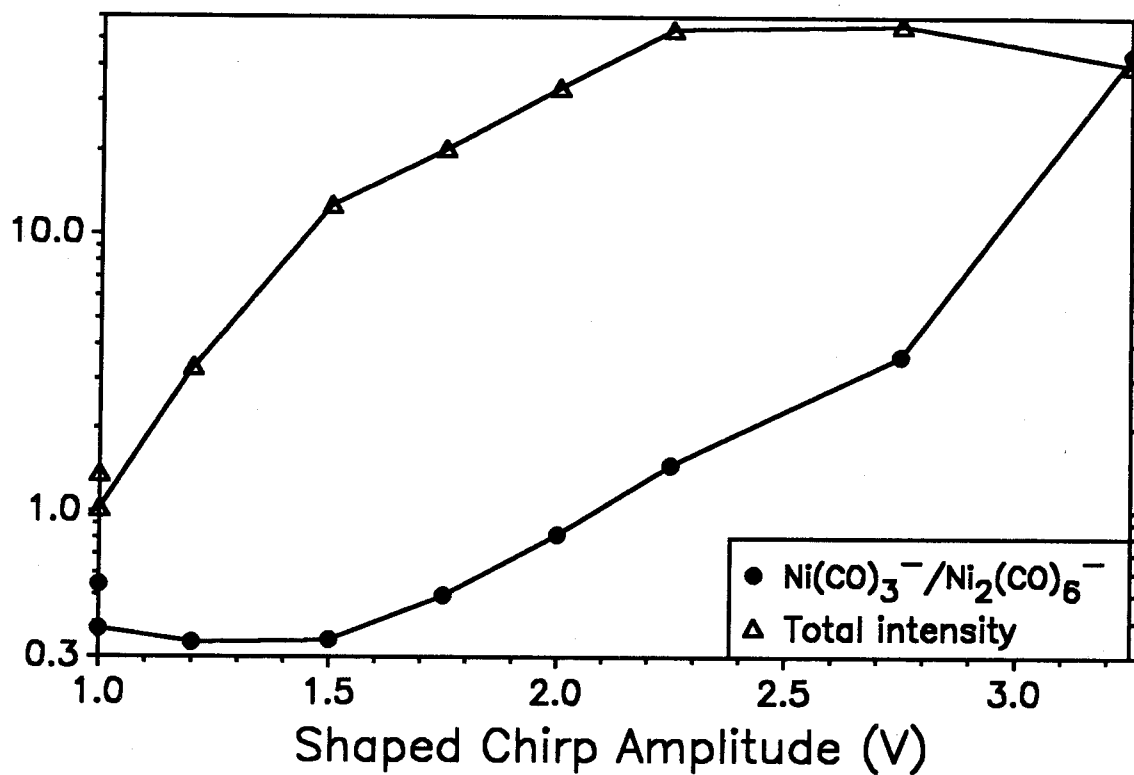


Figure 7. Tuning curve obtained using shaped chirp excitation (low-pass filter with $R = 2 \Omega$, $C = 0.1 \mu\text{F}$; $3 \text{ dB} = 800 \text{ kHz}$). Circles indicate the detected $\text{Ni}(\text{CO})_3^-/\text{Ni}_2(\text{CO})_6^-$ ratio (correct value unknown), triangles indicate the sum of the two intensities (scaled to fit on graph).

Tailored excitation (or stored waveform inverse Fourier transform, SWIFT, excitation) allows for an excitation waveform of any desired shape.¹⁷ This is therefore the best method for investigating the effects of the shape of the power spectrum upon relative intensities.

Analysis of Kinetics Data (Timeplots).

The simplest and most straightforward method for measuring a rate constant is to isolate the reactant of interest and to measure the rate of its decay (pseudo first-order kinetics). Unfortunately, ion isolation is occasionally very difficult or impossible. Such cases are encountered among the reactions between Ir^+ and methane.¹⁸ IrC_3H_6^+ is very difficult to isolate successfully because ejection of nearby peaks leads to collision-induced dissociation instead of isolation. Worse still, there appear to be two isomers or states of IrCH_2^+ , which are of course impossible to separate on the basis of mass. In difficult cases such as these, more sophisticated data analysis is necessary in order to extract rate constants. For this purpose, a computer program was written to perform least-squares fitting of model parameters (rate constants and initial intensities) to experimental timeplot data.¹⁹ Timeplot simulation is also implemented. Representative results are given in Figure 4 of Chapter III of this

¹⁷ Chen, L.; Wang, T.-C. L.; Ricca, T. L.; Marshall, A. G. *Anal. Chem.* 1987, 59, 449-454.

¹⁸ (a) Chapter III of this thesis. (b) Irikura, K. K.; Beauchamp, J. L. *J. Am. Chem. Soc.*, in press. (c) Irikura, K. K.; Beauchamp, J. L. *J. Phys. Chem.*, submitted.

¹⁹ Most algorithms are from the following: Press, W. H.; Flannery, B. P.; Teukolsky, S. A.; Vetterling, W. T. *Numerical Recipes in C*; Cambridge Univ. Press: New York, 1988.

thesis. A separate manual is available describing the detailed features and the proper use of this program (as well as a few other programs that are useful for the analysis of timeplots).

Acknowledgments.

KKI is grateful to the Department of Education and the National Science Foundation for fellowship support.

Appendix

Energy Levels of Transition Metals: Atoms and Atomic Ions

Knowledge of atomic energy levels is helpful for understanding the chemistry of transition metal ions. Since no current compilation is available in the open literature, it is worthwhile to include one here (Table 1). Transition metals in groups 3 through 11 are included.

Since the low-lying states are typically the most important chemically, high-lying states are generally omitted from Table 1. In some interesting cases, however, selected higher states have been included. Some low-lying states are absent from the table due to limited data. All values are experimental except for those from ref. 9.

Table 1 is ordered by atomic number. Elements are separated by double lines, different charge states are separated by single horizontal lines, and periods are delimited by thick lines. Energy levels of dications are included for some elements. Beneath the name of each species are listed the ionization energy (in eV, in parentheses) and the reference number (in boldface). When possible, each energy level is described using both a term symbol (L - S coupling; a superscript $^{\circ}$ indicates an odd term) and valence electron configuration. Three energies (in eV) are given for each term: (1) the energy of the lowest level of the term, with the corresponding value of J in parentheses, (2) the energy of the highest level of the term, again with J in parentheses, and (3) the weighted average energy for all the levels in the term. The reference zero of energy for each species is the lowest level of the lowest term.

For many singly- and doubly-charged ions, little or no experimental data are available. Table 2 contains the results of a brief test of *ab initio* calculations

of energy levels of Ta, Ta⁺, and Ta²⁺. The calculational level is Hartree-Fock with valence single- and double-excitation configuration interaction (HF*SDCI). Relativistic effective-core potentials are used to describe all but the valence and outer core electrons,¹⁰ and the basis set is left uncontracted. The agreement with experiment is slightly better if the lowest level of each term is used for the comparison instead of the usual $\langle E \rangle_J$. The generally good agreement suggests that such *ab initio* energy levels are reasonably accurate. The only discrepancy is for the d⁵ configuration of Ta; I have no explanation for this disagreement.

In conjunction with the orbital size argument presented in Chapter 3, the root-mean-square valence orbital sizes, $\langle r^2 \rangle^{1/2}$, for the dⁿs¹ configurations of Ta, Ta⁺, and Ta²⁺ are presented in Table 3. As above, effective-core potentials are used, and an uncontracted basis set is used for calculational consistency among the different charge states. As the charge is increased, the 6s and 5d orbitals shrink, maintaining a 3:2 size ratio. Since their size ratio is approximately constant, the two orbitals converge in absolute size.

The references for this appendix are collected after Table 3.

Table 1. Selected Energy Levels of Neutral and Ionic Transition Metal Atoms.

Species	Term	Config.	Lowest (J)	Highest (J)	$\langle E \rangle_J$
Sc (6.56154 \pm 0.00006) 1	2D	d^1s^2	0.000 (3/2)	0.021 (5/2)	0.013
	4F	d^2s^1	1.428 (3/2)	1.448 (9/2)	1.439
	2F	$d^2(^3F)s^1$	1.851 (5/2)	1.865 (7/2)	1.859
	$^4F^o$	$d^1s^1p^1$	1.943 (3/2)	1.987 (9/2)	1.968
	$^4D^o$	$d^1s^1(^1D)p^1$	1.985 (1/2)	2.010 (7/2)	2.000
	2D	$d^2(^1D)s^1$	2.109 (5/2)	2.111 (3/2)	2.110
Sc ⁺ (12.79987 \pm 0.00025) 1	3D	d^1s^1	0.000 (1)	0.022 (3)	0.013
	1D	d^1s^1	0.315 (2)	...	0.315
	3F	d^2	0.595 (2)	0.618 (4)	0.609
	1D	d^2	1.357 (2)	...	1.357
	1S	s^2	1.455 (0)	...	1.455
	3P	d^2	1.497 (0)	1.507 (2)	1.504
	1G	d^2	1.768 (4)	...	1.768
	1S	d^2	3.218 (0)	...	3.218
Ti (6.820 \pm 0.006) 1	3F	d^2s^2	0.000 (2)	0.048 (4)	0.028
	5F	d^3s^1	0.813 (1)	0.848 (5)	0.833
	1D	d^2s^2	0.900 (2)	...	0.900
	3P	d^2s^2	1.046 (0)	1.067 (2)	1.060
	3F	$d^3(^4F)s^1$	1.430 (2)	1.460 (4)	1.447
	1G	d^2s^2	1.502 (4)	...	1.502

Table 1. (continued)

Species	Term	Config.	Lowest (J)	Highest (J)	$\langle E \rangle_J$	
Ti ⁺ (13.5756 ± 0.0025)	4F	d ² s ¹	0.000 (3/2)	0.049 (9/2)	0.028	
	4F	d ³	0.113 (3/2)	0.151 (9/2)	0.135	
	2F	d ² (³ F)s ¹	0.574 (5/2)	0.607 (7/2)	0.593	
	1	2D	d ² (¹ D)s ¹	1.080 (3/2)	1.084 (5/2)	1.082
	2G	d ³	1.116 (7/2)	1.131 (9/2)	1.124	
	4P	d ³	1.161 (1/2)	1.180 (5/2)	1.172	
	2P	d ³	1.221 (1/2)	1.237 (3/2)	1.232	
Ti ²⁺ (27.4919 ± 0.0002)	3F	d ²	0.000 (2)	0.052 (4)	0.030	
	1D	d ²	1.052 (2)	...	1.052	
	3P	d ²	1.308 (0)	1.331 (2)	1.323	
	2	1G	d ²	1.787 (4)	...	1.787
	1S	d ²	4.030 (0)	...	4.030	
	3D	d ¹ s ¹	4.724 (1)	4.767 (3)	4.750	
V (6.740 ± 0.002)	4F	d ³ s ²	0.000 (3/2)	0.069 (9/2)	0.040	
	6D	d ⁴ s ¹	0.262 (1/2)	0.301 (9/2)	0.285	
	4D	d ⁴ (⁵ D)s ¹	1.043 (1/2)	1.081 (7/2)	1.066	
	1	4P	d ³ s ²	1.183 (1/2)	1.218 (5/2)	1.205
	2G	d ³ s ²	1.350 (7/2)	1.376 (9/2)	1.365	
	2P	d ³ s ²	1.711 (3/2)	1.712 (1/2)	1.712	

Table 1. (continued)

Species	Term	Config.	Lowest (J)	Highest (J)	$\langle E \rangle_J$
V ⁺ (14.66 ± 0.02) 1	⁵ D	d ⁴	0.000 (0)	0.042 (4)	0.026
	⁵ F	d ³ s ¹	0.323 (1)	0.392 (5)	0.363
	³ F	d ³ (⁴ F)s ¹	1.071 (2)	1.128 (4)	1.104
	³ P	d ⁴	1.400 (0)	1.476 (2)	1.452
	³ H	d ⁴	1.555 (4)	1.575 (6)	1.566
	³ F	d ⁴	1.673 (2)	1.687 (4)	1.681
V ²⁺ (29.311) 3	⁴ F	d ³	0.000 (3/2)	0.072 (9/2)	0.042
	⁴ P	d ³	1.429 (1/2)	1.461 (5/2)	1.448
	² G	d ³	1.485 (7/2)	1.512 (9/2)	1.500
	² P	d ³	1.930 (3/2)	1.933 (1/2)	1.931
	² D ₂	d ³			2.030
	² H	d ³			2.098
	² F	d ³			3.447
	² D ₁	d ³			5.251
	⁴ F	d ² s ¹	5.453 (3/2)	5.541 (9/2)	5.503
Cr (6.76669 ± 0.00004) 1	⁷ S	d ⁵ s ¹	0.000 (3)	...	0.000
	⁵ S	d ⁵ (⁶ S)s ¹	0.941 (2)	...	0.941
	⁵ D	d ⁴ s ²	0.961 (0)	1.030 (4)	1.003
	⁵ G	d ⁵ (⁴ G)s ¹	2.544 (2)	2.545 (4, 5)	2.544
	⁵ P	d ⁵ (⁴ P)s ¹	2.708 (3)	2.710 (1)	2.709
	³ P	d ⁴ s ²	2.872 (0)	2.987 (2)	2.950

Table 1. (continued)

Species	Term	Config.	Lowest (J)	Highest (J)	$\langle E \rangle_J$
Cr ⁺ (16.4858 ± 0.0010) 1	⁶ S	d ⁵	0.000 (5/2)	...	0.000
	⁶ D	d ⁴ s ¹	1.483 (1/2)	1.549 (9/2)	1.522
	⁴ D	d ⁴ (⁵ D)s ¹	2.421 (1/2)	2.483 (7/2)	2.458
	⁴ G	d ⁵	2.543 (5/2, 11/2)	2.544 (5/2, 7/2)	2.544
	⁴ P	d ⁵	2.706 (all)	...	2.706
	⁴ D	d ⁵	3.104 (7/2, 1/2)	3.105 (3/2, 5/2)	3.105
	⁴ P	d ⁴ (³ P)s ¹	3.714 (1/2)	3.827 (5/2)	3.785
	² I	d ⁵	3.737 (11/2)	3.738 (13/2)	3.738
	⁴ H	d ⁴ (³ H)s ¹	3.739 (7/2)	3.892 (13/2)	3.794
	⁴ F	d ⁴ (³ F)s ¹	3.854 (3/2)	3.871 (9/2)	3.864
Mn (7.43408 ± 0.00002) 1	⁶ S	d ⁵ s ²	0.000 (5/2)	...	0.000
	⁶ D	d ⁶ s ¹	2.114 (9/2)	2.187 (1/2)	2.145
	⁸ P ^o	d ⁵ s ¹ p ¹	2.282 (5/2)	2.319 (9/2)	2.303
	⁴ D	d ⁶ (⁵ D)s ¹	2.888 (7/2)	2.953 (1/2)	2.915
Mn ⁺ (15.64011 ± 0.00007) 1	⁷ S	d ⁵ s ¹	0.000 (3)	...	0.000
	⁵ S	d ⁵ (⁶ S)s ¹	1.174 (2)	...	1.174
	⁵ D	d ⁶	1.776 (4)	1.855 (0)	1.808
	⁵ G	d ⁵ (⁴ G)s ¹	3.415 (6)	3.421 (3, 2)	3.418
	³ P	d ⁶	3.703 (2)	3.846 (0)	3.753
	⁵ P	d ⁵ (⁴ P)s ¹	3.706 (3)	3.714 (1)	3.709
	³ H	d ⁶	3.784 (6)	3.818 (4)	3.800

Table 1. (continued)

Species	Term	Config.	Lowest (J)	Highest (J)	$\langle E \rangle_J$
Fe (7.9024 \pm 0.0001) 1	⁵ D	d ⁶ s ²	0.000 (4)	0.121 (0)	0.050
	⁵ F	d ⁷ s ¹	0.859 (5)	1.011 (1)	0.925
	³ F	d ⁷ (⁴ F)s ¹	1.485 (4)	1.608 (2)	1.538
	⁵ P	d ⁷ s ¹	2.176 (3)	2.223 (1)	2.193
	³ P ₂	d ⁶ s ²	2.279 (2)	2.484 (0)	2.350
	⁷ D ^o	d ⁶ (⁵ D)s ¹ p ¹	2.399 (5)	2.482 (1)	2.433
Fe ⁺ (16.1879 \pm 0.0012) 1	⁶ D	d ⁶ s ¹	0.000 (9/2)	0.121 (1/2)	0.052
	⁴ F	d ⁷	0.232 (9/2)	0.387 (3/2)	0.300
	⁴ D	d ⁶ (⁵ D)s ¹	0.986 (7/2)	1.097 (1/2)	1.032
	⁴ P	d ⁷	1.671 (5/2)	1.724 (1/2)	1.688
	² G	d ⁷	1.964 (9/2)	2.029 (7/2)	1.993
	² P	d ⁷	2.276 (3/2)	2.342 (1/2)	2.298
	² H	d ⁷	2.522 (11/2)	2.579 (9/2)	2.548
	² D ₂	d ⁷	2.544 (5/2)	2.642 (3/2)	2.583
Co (7.86 \pm 0.06) 1	⁴ F	d ⁷ s ²	0.000 (9/2)	0.224 (3/2)	0.098
	⁴ F	d ⁸ s ¹	0.432 (9/2)	0.629 (3/2)	0.515
	² F	d ⁸ (³ F)s ¹	0.923 (7/2)	1.049 (5/2)	0.977
	⁴ P	d ⁷ s ²	1.710 (5/2)	1.785 (1/2)	1.733
	⁴ P	d ⁸ s ¹	1.883 (5/2)	2.008 (1/2)	1.927
	² G	d ⁷ s ²	2.042 (9/2)	2.137 (7/2)	2.084

Table 1. (continued)

Species	Term	Config.	Lowest (J)	Highest (J)	$\langle E \rangle_J$
Co ⁺ (17.083 \pm 0.001) 1	³ F	d ⁸	0.000 (4)	0.198 (2)	0.086
	⁵ F	d ⁷ s ¹	0.415 (5)	0.645 (1)	0.515
	³ F	d ⁷ (⁴ F)s ¹	1.217 (4)	1.404 (2)	1.298
	¹ D	d ⁸	1.445 (2)	...	1.445
	³ P	d ⁸	1.644 (2)	1.685 (0)	1.655
	⁵ P	d ⁷ s ¹	2.203 (3)	2.274 (1)	2.228
	¹ G	d ⁸	2.379 (4)	...	2.379
Ni (7.6375 \pm 0.0012) 1	³ F	d ⁸ s ²	0.000 (4)	0.275 (2)	0.120
	³ D	d ⁹ s ¹	0.025 (3)	0.212 (1)	0.091
	¹ D	d ⁹ (² D)s ¹	0.423 (2)	...	0.423
	¹ D	d ⁸ s ²	1.676 (2)	...	1.676
	¹ S	d ¹⁰	1.826 (0)	...	1.826
	³ P	d ⁸ s ²	1.935 (2)	1.986 (0)	1.946
	¹ G	d ⁸ s ²	2.740 (4)	...	2.740
Ni ⁺ (18.16898 \pm 0.00005) 1	² D	d ⁹	0.000 (5/2)	0.187 (3/2)	0.075
	⁴ F	d ⁸ s ¹	1.041 (9/2)	1.322 (3/2)	1.160
	² F	d ⁸ (³ F)s ¹	1.680 (7/2)	1.859 (5/2)	1.757
	⁴ P	d ⁸ s ¹	2.865 (5/2)	3.079 (1/2)	2.970
	² D	d ⁸ (¹ D)s ¹	2.950 (3/2)	3.104 (5/2)	3.043
Cu (7.724) 4	² S	d ¹⁰ s ¹	0.000 (1/2)	...	0.000
	² D	d ⁹ s ²	1.389 (5/2)	1.642 (3/2)	1.490
	² P ^o	d ¹⁰ p ¹	3.786 (1/2)	3.817 (3/2)	3.806

Table 1. (continued)

Species	Term	Config.	Lowest (J)	Highest (J)	$\langle E \rangle_J$
Cu ⁺ (20.29) 4	¹ S	d ¹⁰	0.000 (0)	...	0.000
	³ D	d ⁹ s ¹	2.719 (3)	2.975 (1)	2.808
	¹ D	d ⁹ s ¹	3.256 (2)	...	3.256
Y (6.5) 4 (6.30, 5)	² D	d ¹ s ²	0.000 (3/2)	0.066 (5/2)	0.039
	² P ^o	s ² p ¹	1.305 (1/2)	1.408 (3/2)	1.374
	⁴ F	d ² s ¹	1.356 (3/2)	1.430 (9/2)	1.398
	⁴ F ^o	d ¹ s ¹ p ¹	1.853 (3/2)	2.013 (9/2)	1.945
	⁴ P	d ² s ¹	1.887 (1/2)	1.919 (5/2)	1.908
	² F	d ² (³ F)s ¹	1.900 (5/2)	1.967 (7/2)	1.938
Y ⁺ (12.4) 4	¹ S	s ²	0.000 (0)	...	0.000
	³ D	d ¹ s ¹	0.104 (1)	0.180 (3)	0.148
	¹ D	d ¹ s ¹	0.409 (2)	...	0.409
	³ F	d ²	0.992 (2)	1.084 (4)	1.045
	³ P	d ²	1.721 (0)	1.748 (2)	1.742
	¹ D	d ²	1.839 (2)	...	1.839
Zr (6.95) 4 (6.59, 5)	³ F	d ² s ²	0.000 (2)	0.154 (4)	0.090
	³ P	d ² s ²	0.519 (2)	0.543 (1)	0.527
	⁵ F	d ³ s ¹	0.604 (1)	0.730 (5)	0.677
	¹ D	d ² s ²	0.633 (2)	...	0.633
	¹ G	d ² s ²	0.999 (4)	...	0.999

Table 1. (continued)

Species	Term	Config.	Lowest (J)	Highest (J)	$\langle E \rangle_J$
Zr ⁺ (14.03) 4	⁴ F	d ² s ¹	0.000 (3/2)	0.164 (9/2)	0.094
	⁴ F	d ³	0.319 (3/2)	0.466 (9/2)	0.406
	² D	d ² (¹ D)s ¹	0.527 (3/2)	0.559 (5/2)	0.546
	² P	d ² (³ P)s ¹	0.710 (1/2)	0.758 (3/2)	0.742
	² F	d ² (³ F)s ¹	0.713 (5/2)	0.802 (7/2)	0.764
	⁴ P	d ² s ¹	0.931 (1/2)	0.999 (5/2)	0.974
	² G	d ³	0.972 (7/2)	1.011 (9/2)	0.993
Zr ²⁺ (24.8) 4	³ F	d ²	0.000 (2)	0.184 (4)	0.107
	¹ D	d ²	0.713 (2)	...	0.713
	³ P	d ²	1.001 (0)	1.097 (2)	1.065
	¹ G	d ²	1.371 (4)	...	1.371
	¹ S	d ²	1.717 (0)	...	1.717
	³ D	d ¹ s ¹	2.283 (1)	2.424 (3)	2.366
Nb (6.77) 4 (6.59, 5)	⁶ D	d ⁴ s ¹	0.000 (1/2)	0.130 (9/2)	0.079
	⁴ D	d ³ s ²	0.142 (3/2)	0.348 (9/2)	0.263
	⁴ P	d ³ s ²	0.620 (1/2)	0.740 (5/2)	0.692
	⁴ D	d ⁴ (⁵ D)s ¹	1.043 (1/2)	1.178 (7/2)	1.128
	² G	d ³ s ²	1.094 (7/2)	1.157 (9/2)	1.129

Table 1. (continued)

Species	Term	Config.	Lowest (J)	Highest (J)	$\langle E \rangle_J$
Nb ⁺ (~14.) 4	⁵ D	d ⁴	0.000 (0)	0.152 (4)	0.096
	⁵ F	d ³ s ¹	0.292 (1)	0.514 (5)	0.421
	³ P	d ⁴	0.690 (0)	0.900 (2)	0.833
	³ F	d ³ (⁴ F)s ¹	0.931 (2)	1.032 (4)	0.990
	³ H	d ⁴	1.179 (4)	1.263 (6)	1.225
Nb ²⁺ (28.1) 4	⁴ F	d ³	0.000 (3/2)	0.241 (9/2)	0.141
	⁴ F	d ² s ¹	3.130 (3/2)	3.397 (9/2)	3.283
Mo (7.09243 ± 0.00004) 6 (7.22, 5)	⁷ S	d ⁵ s ¹	0.000 (3)	...	0.000
	⁵ S	d ⁵ (⁶ S)s ¹	1.335 (2)	...	1.335
	⁵ D	d ⁴ s ²	1.360 (0)	1.531 (4)	1.467
	⁵ G	d ⁵ (⁴ G)s ¹	2.063 (2)	2.081 (5,6)	2.076
	⁵ P	d ⁵ (⁴ P)s ¹	2.260 (3)	2.291 (1)	2.272
	⁵ D	d ⁵ (⁴ D)s ¹	2.476 (0)	2.523 (3)	2.508
	³ P	d ⁴ s ²	2.555 (0)	2.836 (2)	2.779
	³ D	d ⁵ (⁴ D)s ¹	2.595 (1)	2.680 (3)	2.636
	³ G	d ⁵ (⁴ G)s ¹	2.597 (3)	2.646 (5)	2.626
	³ F	d ⁴ s ²	2.916 (4)	2.934 (3)	2.922

Table 1. (continued)

Species	Term	Config.	Lowest (J)	Highest (J)	$\langle E \rangle_J$
Mo ⁺ (16.16 ± 0.12) 6	⁶ S	d ⁵	0.000 (5/2)	...	0.000
	⁶ D	d ⁴ s ¹	1.461 (1/2)	1.669 (9/2)	1.587
	⁴ G	d ⁵	1.884 (5/2)	1.915 (11/2)	1.906
	⁴ P	d ⁵	1.945 (5/2, 3/2)	1.970 (1/2)	1.950
	⁴ D	d ⁵	2.082 (1/2)	2.150 (5/2)	2.120
	² D	d ⁵	2.783 (5/2)	2.835 (3/2)	2.804
	² I	d ⁵	2.849 (11/2)	2.882 (13/2)	2.867
	⁴ F	d ⁵	2.955 (9/2)	2.993 (3/2)	2.964
	⁴ D	d ⁴ (⁵ D)s ¹	3.022 (1/2)	3.142 (7/2)	3.104
	² F	d ⁵	3.039 (7/2)	3.079 (5/2)	3.056
	⁴ H	d ⁴ (³ H)s ¹	3.229 (7/2)	3.362 (13/2)	3.307
Tc (7.28) 7	⁶ S	d ⁵ s ²	0.000 (5/2)	...	0.000
	⁶ D	d ⁶ s ¹	0.319 (9/2)	0.518 (1/2)	0.406
	⁴ D	d ⁶ (⁵ D)s ¹	1.304 (7/2)	1.474 (1/2)	1.368
	⁴ P	d ⁶ (³ P)s ¹	1.643 (5/2)	1.820 (1/2)	1.711
	⁴ F	d ⁶ (³ F)s ¹	1.827 (9/2)	1.955 (3/2)	1.889
	⁴ G	d ⁶ (³ G)s ¹	1.987 (11/2)	2.035 (5/2)	2.006
	⁸ P ^o	d ⁵ s ¹ p ¹	2.037 (5/2)	2.173 (9/2)	2.112
	⁶ P ^o	d ⁵ s ¹ (⁷ S)p ¹	2.885 (7/2)	2.925 (3/2)	2.901

Table 1. (continued)

Species	Term	Config.	Lowest (J)	Highest (J)	$\langle E \rangle_J$
Tc ⁺ (15.26) 7	⁷ S	d ⁵ s ¹	0.000 (3)	...	0.000
	⁵ D	d ⁶	0.429 (4)	0.632 (0)	0.516
	⁵ S	d ⁵ (⁶ S)s ¹	1.564 (2)	...	1.564
	⁵ G	?	2.956 + x (2)	2.979 + x (5)	2.972 + x
	⁷ P ^o	d ⁵ p ¹	4.683 (2)	4.874 (4)	4.787
Ru (7.364) 7 (7.27, 5)	⁵ F	d ⁷ s ¹	0.000 (5)	0.385 (1)	0.171
	³ F	d ⁷ (⁴ F)s ¹	0.811 (4)	1.139 (2)	0.953
	⁵ D	d ⁶ s ²	0.928 (4)	1.177 (0)	1.038
	⁵ P	d ⁷ s ¹	0.997 (2)	1.193 (1)	1.078
	³ F	d ⁸	1.131 (4)	1.419 (2)	1.263
Ru ⁺ (16.76) 7	⁴ F	d ⁷	0.000 (9/2)	0.385 (3/2)	0.175
	⁴ P	d ⁷	1.024 (5/2)	1.162 (1/2)	1.056
	⁶ D	d ⁶ s ¹	1.135 (9/2)	1.439 (1/2)	1.266
	² G	d ⁷	1.347 (9/2)	1.524 (7/2)	1.426
	² P	d ⁷	1.606 (3/2)	1.835 (1/2)	1.683
	² D	d ⁷	1.808 (5/2)	2.110 (3/2)	1.929
	² H	d ⁷	1.818 (11/2)	1.999 (9/2)	1.900

Table 1. (continued)

Species	Term	Config.	Lowest (J)	Highest (J)	$\langle E \rangle_J$
Rh (7.46) 7 (7.54, 5)	4F	d^8s^1	0.000 (9/2)	0.431 (3/2)	0.149
	2D	d^9	0.410 (5/2)	0.701 (3/2)	0.527
	2F	$d^8(^3F)s^1$	0.706 (7/2)	0.966 (5/2)	0.817
	4P	d^8s^1	1.143 (5/2)	1.365 (1/2)	1.225
	2P	$d^8(^3P)s^1$	1.484 (3/2)	1.733 (1/2)	1.567
	4F	d^7s^2	1.577 (9/2)	2.101 (3/2)	1.816
	2D	$d^8(^1D)s^1$	1.676 (5/2)	1.783 (3/2)	1.719
Rh ⁺ (18.07) 7	3F	d^8	0.000 (4)	0.444 (2)	0.205
	1D	d^8	1.012 (2)	...	1.012
	3P	d^8	1.304 (1)	1.444 (2)	1.385
	1G	d^8	1.842 (4)	...	1.842
	5F	d^7s^1	2.093 (5)	2.626 (1)	2.331
Pd (8.33) 7 (8.37, 5)	1S	d^{10}	0.000 (0)	...	0.000
	3D	d^9s^1	0.814 (3)	1.257 (1)	0.951
	1D	d^9s^1	1.453 (2)	...	1.453
	3F	d^8s^2	3.112 (4)	3.684 (2)	3.377
Pd ⁺ (19.42) 7	2D	d^9	0.000 (5/2)	0.439 (3/2)	0.176
	4F	d^8s^1	3.110 (9/2)	3.713 (3/2)	3.369
Ag (7.574) 7	2S	$d^{10}s^1$	0.000 (1/2)	...	0.000
	$^2P^0$	$d^{10}p^1$	3.664 (1/2)	3.778 (3/2)	3.740
	2D	d^9s^2	3.750 (5/2)	4.304 (3/2)	3.971

Table 1. (continued)

Species	Term	Config.	Lowest (J)	Highest (J)	$\langle E \rangle_J$
Ag ⁺ (21.48) 7	¹ S	d ¹⁰	0.000 (0)	...	0.000
	³ D	d ⁹ s ¹	4.856 (3)	5.423 (1)	5.034
	¹ D	d ⁹ s ¹	5.709 (2)	...	5.709
La (5.61 ± 0.03) 7 (5.55, 5)	² D	d ¹ s ²	0.000 (3/2)	0.131 (5/2)	0.078
	⁴ F	d ² s ¹	0.331 (3/2)	0.511 (9/2)	0.434
	² F	d ² (³ F)s ¹	0.869 (5/2)	0.998 (7/2)	0.943
	⁴ P	d ² s ¹	0.897 (1/2)	0.952 (5/2)	0.935
	² D	d ² (¹ D)s ¹	1.047 (3/2)	1.139 (5/2)	1.102
	² P	d ² (³ P)s ¹	1.121 (1/2)	1.205 (3/2)	1.177
La ⁺ (11.43 ± 0.07) 7	³ F	d ²	0.000 (2)	0.244 (4)	0.147
	¹ D	d ¹ s ¹	0.173 (2)	...	0.173
	³ D	d ¹ s ¹	0.235 (1)	0.403 (3)	0.342
	³ P	d ²	0.651 (0)	0.772 (2)	0.738
	¹ S	s ²	0.917 (0)	...	0.917
	¹ G	d ²	0.927 (4)	...	0.927
	¹ D	d ²	1.252 (2)	...	1.252
	³ F ^o	f ¹ s ¹	1.754 (2)	1.946 (4)	1.846
	¹ F ^o	f ¹ s ¹	1.956 (3)	...	1.956

Table 1. (continued)

Species	Term	Config.	Lowest (J)	Highest (J)	$\langle E \rangle_J$
Hf (near 7.) 7 (6.52, 5)	3F	d^2s^2	0.000 (2)	0.566 (4)	0.340
	3P	d^2s^2	0.685 (0)	1.114 (2)	0.967
	1D	d^2s^2	0.699 (2)	...	0.699
	1G	d^2s^2	1.306 (4)	...	1.306
	$^3D^o$	$d^2s^1(^2D)p^1$	1.738 (1)	2.279 (3)	2.079
	5F	d^3s^1	1.747 (1)	2.219 (5)	2.032
	$^3F^o$	$d^2s^1(^2D)p^1$	1.790 (2)	2.260 (4)	1.996
Hf ⁺ (14.9) 7	2D	d^1s^2	0.000 (3/2)	0.378 (5/2)	0.227
	4F	d^2s^1	0.452 (3/2)	1.037 (9/2)	0.790
	4P	d^2s^1	1.482 (1/2)	1.672 (5/2)	1.617
	2F	$d^2(^3F)s^1$	1.497 (5/2)	1.870 (7/2)	1.710
	2D	$d^2(^1D)s^1$	1.780 (3/2)	2.153 (5/2)	2.004
	2P	$d^2(^3P)s^1$	1.891 (1/2)	2.211 (3/1)	2.104
	2G	$d^2(^1G)s^1$	2.156 (9/2)	2.196 (7/2)	2.174
	4F	d^3	2.343 (3/2)	2.870 (9/2)	2.661
Ta (7.88) 7 (7.40, 5)	4F	d^3s^2	0.000 (3/2)	0.697 (9/2)	0.443
	4P	d^3s^2	0.750 (1/2)	1.147 (5/2)	0.949
	2G	d^3s^2	1.203 (7/2)	1.325 (9/2)	1.271
	6D	d^4s^1	1.210 (1/2)	1.655 (9/2)	1.481
	2P	d^3s^2	1.358 (3/2)	1.462 (1/2)	1.392
	6S	d^5	1.463 (5/2)	...	1.463

Table 1. (continued)

Species	Term	Config.	Lowest (J)	Highest (J)	$\langle E \rangle_J$
Ta ⁺ (16.2 ± 0.5) 7	⁵ F	d ³ s ¹	0.000 (1)	0.767 (5)	0.466
	³ F	d ² s ²	0.394 (2)	1.208 (4)	0.894
	³ P	d ² s ²	0.511 (0)	0.702 (2)	0.667
	³ F	d ³ (⁴ F)s ¹	1.201 (2)	2.293 (4)	1.871
	⁵ P	d ³ s ¹	1.328 (1)	1.542 (3)	1.476
	³ G	d ³ (² G)s ¹	1.459 (3)	1.591 (5)	1.551
	⁵ D	d ⁴	1.562 (0)	2.136 (4)	1.937
	¹ D	d ² s ²	1.681 (2)	...	1.681
	¹ G	d ² s ²	1.761 (4)	...	1.761
³ D	d ³ (² D)s ¹	1.814 (1)	2.300 (3)	2.146	
W (7.98) 7 (7.60, 5)	⁵ D	d ⁴ s ²	0.000 (0)	0.771 (4)	0.553
	⁷ S	d ⁵ s ¹	0.366 (3)	...	0.366
	³ P	d ⁴ s ²	1.181 (0)	2.387 (2)	2.007
	³ H	d ⁴ s ²	1.508 (4)	2.109 (6)	1.865
	³ G	d ⁴ s ²	1.655 (3)	2.458 (5)	2.110
	³ F	d ⁴ s ²	1.708 (2)	2.121 (4)	2.047
	³ D	d ⁴ s ²	1.857 (2)	2.242 (1)	1.962
	⁵ G	d ⁵ (⁴ G)s ¹	2.246 (2)	2.436 (6)	2.389
	⁵ S	d ⁵ (⁶ S)s ¹	2.266 (2)	...	2.266

Table 1. (continued)

Species	Term	Config.	Lowest (J)	Highest (J)	$\langle E \rangle_J$
W ⁺ (17.7 ± 0.5) 7	⁶ D	d ⁴ s ¹	0.000 (1/2)	0.762 (9/2)	0.514
	⁶ S	d ⁵	0.920 (5/2)	...	0.920
	⁴ F	d ⁴ (³ F)s ¹	1.080 (3/2)	1.842 (9/2)	1.588
	⁴ P	d ⁴ (³ P)s ¹	1.095 (1/2)	1.666 (5/2)	1.453
	⁴ D	d ⁴ (⁵ D)s ¹	1.633 (1/2)	1.878 (7/2)	1.834
	⁴ G	d ⁴ (³ G)s ¹	2.013 (5/2)	2.162 (11/2)	2.083
	⁴ H _{7/2}	d ⁴ (³ H)s ¹			2.232
	² D _{3/2}	d ⁵			2.355
Re (7.87) 7 (7.76, 5)	⁶ S	d ⁵ s ²	0.000 (5/2)	...	0.000
	⁴ P	d ⁵ s ²	1.436 (5/2)	1.880 (1/2)	1.603
	⁶ D	d ⁶ s ¹	1.457 (9/2)	2.137 (1/2)	1.759
	⁴ G	d ⁵ s ²	1.813 (5/2)	2.061 (9/2)	1.963
	⁴ D	d ⁵ s ²	2.149 (7/2)	2.539 (3/2)	2.336
	⁸ P ⁰	d ⁵ s ¹ (⁷ S)p ¹	2.350 (5/2)	2.930 (9/2)	2.653
	² F	d ⁵ s ²	2.700 (7/2)	3.028 (5/2)	2.841
	² G	d ⁵ s ²	2.747 (9/2)	3.065 (7/2)	2.889
	² D	d ⁵ s ²	2.780 (3/2)	2.871 (5/2)	2.835
Re ⁺ (16.6 ± 0.5) 7	⁷ S	d ⁵ s ¹	0.000 (3)	...	0.000
	⁵ D	d ⁴ s ²	1.708 (0)	1.851 (3)	1.827
	⁵ S	d ⁵ (⁶ S)s ¹	2.135 (2)	...	2.135
	⁵ G	d ⁵ (⁴ G)s ¹	2.337 (2)	2.732 (6)	2.561
	⁵ P	d ⁵ (⁴ P)s ¹	2.682 (3)	2.941 (1)	2.804

Table 1. (continued)

Species	Term	Config.	Lowest (J)	Highest (J)	$\langle E \rangle_J$
Os (8.7) 7 (8.3 ± 0.1, 8)	5D	d^6s^2	0.000 (4)	0.755 (0)	0.328
	5F	d^7s^1	0.638 (5)	1.614 (1)	1.080
	3F	$d^7(^4F)s^1$	1.368 (4)	1.747 (3)	1.546
	$J = 2$				1.657
	3H	d^6s^2	1.778 (5)	1.841 (6)	1.820
	$J = 2$				1.887
Os ⁺ (17 ± 1) 7	6D	d^6s^1	0.000 (9/2)	0.823 (1/2)	0.364
	$J = 5/2$				0.978
	$J = 7/2$				1.421
	$J = 5/2$				1.445
	$J = 3/2$				1.629
	$J = 7/2$				1.637
	$J = 5/2$				1.663
	$J = 9/2$				1.935
	$J = 7/2$				2.138
	$J = 3/2$				2.160
	$J = 5/2$				2.178
	$J = 11/2$				2.193
	9	4F	d^7	0.918 (9/2)	

Table 1. (continued)

Species	Term	Config.	Lowest (J)	Highest (J)	$\langle E \rangle_J$
Ir (9) 7 (9.02, 5)	4F	d^7s^2	0.000 (9/2)	0.784 (7/2)	0.450
	4F	d^8s^1	0.351 (9/2)	1.467 (3/2)	0.849
	2P	$d^8(^3P)s^1$	1.312 (3/2)	1.551 (1/2)	1.391
	2F	$d^8(^3F)s^1$	1.515 (5/2)	1.623 (7/2)	1.576
	4P	d^8s^1	1.606 (5/2)	2.068 (1/2)	1.832
	2G	d^7s^2	1.728 (9/2)	2.204 (7/2)	1.940
	4P	d^7s^2	1.997 (5/2)	2.509 (1/2)	2.183
Ir ⁺ (?) 9	5F	d^7s^1	0.000 (5)		
	3F	d^8	0.281 (4)		
	5D	d^6s^2	2.136 (4)		
Pt (9.0) 7 (8.61, 5)	3D	d^9s^1	0.000 (3)	1.256 (1)	0.283
	3F	d^8s^2	0.102 (4)	1.922 (2)	0.919
	1S	d^{10}	0.761 (0)	...	0.761
	3P_2	d^8s^2			0.814
	3P_1	d^8s^2			2.302
	1D	d^9s^1	1.673 (2)	...	1.673
	1G	d^8s^2	2.724 (4)	...	2.724
Pt ⁺ (18.56) 7	2D	d^9	0.000 (5/2)	1.044 (3/2)	0.418
	4F	d^8s^1	0.593 (9/2)	1.958 (3/2)	1.177
	4P	d^8s^1	2.086 (5/2)	2.693 (1/2)	2.366
	2D	$d^8(^1D)s^1$	2.960 (3/2)	4.081 (5/2)	3.633
	4F	d^7s^2	3.085 (9/2)	4.696 (3/2)	3.969

Table 1. (continued)

Species	Term	Config.	Lowest (J)	Highest (J)	$\langle E \rangle_J$
Au (9.22) 7	2S	$d^{10}s^1$	0.000 (1/2)	...	0.000
	2D	d^9s^2	1.136 (5/2)	2.658 (3/2)	1.745
	$^2P^o$	$d^{10}p^1$	4.632 (1/2)	5.105 (3/2)	4.947
Au ⁺ (20.5) 7	1S	d^{10}	0.000 (0)	...	0.000
	3D	d^9s^1	1.865 (3)	3.442 (1)	2.288
	1D	d^9s^1	3.673 (2)	...	3.673

Table 2. *Ab Initio* Energy Levels of Ta, Ta⁺, and Ta²⁺.

Species	Config.	E (eV) ^a	exptl ^b $\langle E \rangle_J$	exptl ^b lowest level
Ta	d ³ s ²	0.00	0.000	0.000
	d ⁴ s ¹	1.19	1.038	1.210
	d ⁵	3.86	1.020	1.463
Ta ⁺	d ³ s ¹	0.00	0.000	0.000
	d ² s ²	0.40	0.428	0.394
	d ⁴	1.58	1.471	1.562
Ta ²⁺	d ³	0.00		
	d ² s ¹	0.62		
	d ¹ s ²	3.62		

^a*Ab initio* HF*SDCI values (see text). ^bFrom Table 1.

Table 3. *Ab Initio* Orbital Sizes, $R \equiv \langle r^2 \rangle^{1/2}$, of Ta, Ta⁺, and Ta²⁺.^a

Species	Config.	R(6s)	R(5d)	R(6s)/R(5d)	R(6s) - R(5d)
Ta	d ⁴ s ¹	1.98 Å	1.34 Å	1.48	0.64 Å
Ta ⁺	d ³ s ¹	1.80	1.19	1.51	0.60
Ta ²⁺	d ² s ¹	1.62	1.09	1.49	0.53

^aFrom Hartree-Fock *ab initio* calculations (see text).

References

1. Sugar, J.; Corliss, C. *J. Phys. Chem. Ref. Data* **1985**, *14*, Suppl. 2.
2. Sugar, J.; Corliss, C. *J. Phys. Chem. Ref. Data* **1979**, *8*, 1-62.
3. Sugar, J.; Corliss, C. *J. Phys. Chem. Ref. Data* **1978**, *7*, 1191-1262.
4. Moore, C. E. *Atomic Energy Levels*; NSRDS-NBS 35 (reprint of NBS circular 467); U. S. Government Printing Office: Washington, D.C., 1971, vol. 2.
5. Rauh, E. G.; Ackermann, R. J. *J. Chem. Phys.* **1979**, *70*, 1004-1007.
6. Sugar, J.; Musgrove, A. *J. Phys. Chem. Ref. Data* **1988**, *17*, 155-239.
7. Moore, C. E. *Atomic Energy Levels*; NSRDS-NBS 35 (reprint of NBS circular 467); U. S. Government Printing Office: Washington, D.C., 1971, vol. 3.
8. $IP(Os) = 8.3 \pm 0.1$ eV recommended in the appendix to the following: Irikura, K. K.; Beauchamp, J. L. *J. Am. Chem. Soc.* **1989**, *111*, 75-85. (Chapter 1 in this thesis).
9. van Kleef, Th. A. M.; Metsch, B. C. *Physica C* **1978**, *95*, 251-265. The configurations of Ir^+ are "strongly intermingled." In particular, 5F_5 is 89% d^7s^1 , 3F_4 is 90% d^8 , and 5D_4 is only 38% d^6s^2 . They obtained average configuration energies, calculated from fitted parameters, as follow: $E(d^8) = 1.903$, $E(d^7s^1) = 3.059$, and $E(d^6s^2) = 5.678$ eV.
10. Hay, P. J.; Wadt, W. R. *J. Chem. Phys.* **1985**, *82*, 299-310.